UNIVERSITY OF BERGEN

Investigations on the External Forcings acting on the Convective Boundary Layer during the BLLAST Campaign by the CLASS Model

---

Submitted by

Andrew Walter Seidl

To the

Geophysical Institute,

Faculty of Mathematics and Natural Sciences

In partial fulfilment of the requirements

for achieving the Degree of

Master of Science in

Meteorology and Oceanography

With a specialisation in

Meteorology

June 2017

Bergen, Norway

Supervisor:
Joachim Reuder
Geophysical Institute
University of Bergen, Norway

Co-Supervisor:
Jordi Vilà-Guerau de Arellano
Department of Environmental Sciences
Wageningen University & Research Centre, Netherlands

Abstract

Using both observed and modelled datasets from the 2011 Boundary Layer Late Afternoon and Sunset Turbulence (BLLAST) campaign, the influence of large-scale forcings and surface heterogeneity is investigated for ten out of twelve Intensive Observational Periods (IOPs) in order to assist and facilitate future research on this unique data set. This includes a categorisation of the individual IOPs according to the importance of horizontal advection and subsidence, as well as the sensitivity of the Boundary Layer (BL) development during those days to the time of initialisation. This is accomplished through the use of the Chemistry Land-surface Atmosphere Soil Slab (CLASS) model which is based on Mixed Layer theory.

The study shows that neglecting large-scale forcings leads to considerable deviations between observed and modelled key parameters, such as BL height or average values of temperature and humidity, in nearly all of the investigated IOPs. In this context, only the simulations for IOP08 provided comparable results. In addition, for six out of the twelve IOPs, meso-scale simulations with MesoNH are available, with a horizontal resolution of 400 m. It is found that upon incorporation of those large-scale forcings from MesoNH, the Mixed Layer Model (MLM) simulations for IOPs 05 & 06 capture the observed trends closely. Furthermore, a novel concept of an averaging "box" domain is introduced for the treatment of surface heterogeneity in MLM theory. Using this concept, it is discovered that the BLLAST campaign area

exhibits a "MLM blending length-scale" of approximately 5 km. Horizontally averaged surface fluxes on smaller scales depend on both the chosen domain size and the selected location (e.g. Site #1 or Site #2), whereby areal flux averages on larger scales become independent on the domain size.

Acknowledgements

The realisation of this thesis is thanks to many individuals, more than I can name here, but below I will try to name a few. Firstly, my supervisors Joachim Reuder and Jordi Vilà-Guerau de Arellano: for helping me to build this thesis from the ground up; and no matter the crisis (and there were more than a few), the patience and assistance demonstrated always motivated me to redouble my efforts. Omar El Guernaoui and Line Båserud: for all the brainstorming sessions and ideas, especially at the start. All the other staff and students at the GFI: for helping me return to academic life and making this a truly amazing experience. Natasha: for convincing me to come to Bergen in the first place. Ryan: for providing sound thesis writing assistance, and for making me realize that 100 pages aren't that many. My family: for the support they gave when I decided to move halfway around the world, and the encouragement they continue to give. And, of course, Henni: for always believing in me, even when I didn't. You spent hour after hour listening to my convoluted thought process; an ever-present smile on your face, and always ready with a warm cup of tea for me in your hand. I could not have done this without you.

Additionally, thesis progress would have stalled early on without the MesoNH dataset from Maria Antonia Jiménez Cortes at the Universitat de les Illes Balears. It was a fundamental building block of this work, and helped to kick-start the main ideas of this thesis. Once the "ball was rolling",

the comprehensive surface heat flux maps from Oscar Hartogenesis at the Wageningen University & Research Centre allowed for the fulfilment of Experiments 1-2, and the further expansion into Experiment 3. Both these datasets have been invaluable tools in the construction of my thesis. And in general, the BLLAST field experiment itself was made possible thanks to the contribution of several institutions and supports : INSU-CNRS (Institut National des Sciences de l'Univers, Centre national de la Recherche Scientifique, LEFE-IDAO program), Météo-France, Observatoire Midi-Pyrénées (University of Toulouse), EUFAR (EUropean Facility for Airborne Research) and COST ES0802 (European Cooperation in the field of Scientific and Technical). The field experiment would not have occurred without the contribution of all participating European and American research groups, which all have contributed in a significant amount[1]. BLLAST field experiment was hosted by the instrumented site of Centre de Recherches Atmosphériques, Lannemezan, France (Observatoire Midi-Pyrénées, Laboratoire d'Aérologie). BLLAST data are managed by SEDOO, from Observatoire Midi-Pyrénées.

Remember: keep your stick on the ice.

[1] http://bllast.sedoo.fr/supports/

Contents

List of Figures

List of Tables

Acronyms

BL Boundary Layer

BLLAST Boundary Layer Late Afternoon and Sunset Turbulence

CLASS Chemistry Land-surface Atmosphere Soil Slab

EF Evaporative Fraction

EZ Entrainment Zone

FA Free Atmosphere

IOP Intensive Observational Period

ML Mixed Layer (aka. Convective Boundary Layer)

MLM Mixed Layer Model

RL Residual Layer

SBL Stable Boundary Layer

SL Surface Layer

SUMO Small Unmanned Meteorological Observer

Notation

z_i Boundary Layer Height	[m] or [km]
c_p Specific heat capacity at constant pressure	$[1004\,\mathrm{J\,kg^{-1}\,K^{-1}}]$
L_w Latent heat of vaporization of water	$[2.264 \times 10^6\,\mathrm{J\,kg^{-1}}]$
LE Latent heat flux	$[\mathrm{g_{water}\,kg_{air}^{-1}\,m\,s^{-1}}]$ or $[\mathrm{W\,m^{-2}}]$
p Pressure	[Pa]
ψ Generic turbulent variable	[-]
q Specific humidity	$[\mathrm{g_{water}\,kg_{air}^{-1}}]$
R Specific gas constant of dry air	$[287\,\mathrm{J\,kg^{-1}\,K^{-1}}]$
ρ Density	$[\mathrm{kg\,m^{-3}}]$
SH Sensible heat flux	$[\mathrm{K\,m\,s^{-1}}]$ or $[\mathrm{W\,m^{-2}}]$
T Temperature	[K] or [°C]
θ Potential temperature	[K] or [°C]
θ_v Virtual Potential temperature	[K] or [°C]

$\mathbf{v}$	Meridional wind component	$[\mathrm{m\,s^{-1}}]$
$\mathbf{u}$	Zonal wind component	$[\mathrm{m\,s^{-1}}]$

1 Introduction

Considering that every person spends the vast majority of their lives in the Atmospheric Boundary Layer (BL), the study of how it works is particularly important. BL properties, such as height, can have far-reaching impacts on air quality indices, cloud conditions, and surface temperature and humidity. Convective BL development under "textbook" conditions (Stull 1988, Vilà-Guerau de Arellano et al. 2015) is relatively well understood, however there do exist forcings for which direct observation is difficult to obtain. These include advections of heat and moisture, as well as large-scale vertical motion of the atmosphere above the BL, all of which entail challenging measurement regimes. And though processes acting over any one individual type of surface are generally understood, measuring how these processes evolve over real-world patchwork land use can be a logistical feat.

These forcings can, instead be studied through the use of numerical models, such as Direct Numerical Simulations (DNSs) (e.g. Rai & Moin 1993, Moin & Mahesh 1998), Large-Eddy Simulations (LESs) (e.g. Moeng 1984, Moeng & Sullivan 2015), and Mixed Layer Models (MLMs) (e.g. Tennekes 1973, Tennekes & Driedonks 1981), all having varying degrees of complexity. And such modelling is nothing new in meteorology. LESs have been around since the late 1960's, albeit with limited grid size (Moeng & Sullivan 2015, p.232). Since then, tremendous progress in computational capability has allowed for much finer resolutions. But though the capability is there,

limitations still exist. LESs can still take significant amounts of time, as they are crunching numbers in a three dimensional space, and even then, only focus computations on the most dominant scales: the "Large Eddies". Smaller scale turbulent processes, must still be parametrized. Even with these parametrizations, in order to properly utilize them, simulations must be run on powerful machines, the likes of which may not be accessible to some atmospheric scientists. Nowadays, however, access to a personal computer (a veritable supercomputer by 1960's standards) is a necessity for daily life. It is on these machines that MLMs can easily be run.

Though both LESs and MLMs are based on laws of conservation of energy, mass and momentum (Moeng & Sullivan 2015, Vilà-Guerau de Arellano et al. 2015, p.24), the implementation of these laws differ. Whereas LESs allow for horizontal gradients to develop and interact, MLMs forego computations of these interior turbulent processes, focusing instead on processes occurring at the top and bottom BL boundaries. A simplified analogy would be adding cream to a cup of coffee. An LES would describe some of the complicated whirls and swirls one sees as pouring the cream, before it eventually spreads to all parts of the mug. Alternatively, a MLM merely recognizes that cream was added, and assumes the pourer is stirring. Though this analogy is an *over*-simplification of MLMs dynamics (in actuality the processes are occurring simultaneously at the top and bottom of "the mug" and are turbulent fluxes of "cream" rather than an advection like "pouring"), the core conceptual difference is valid. The end result of changing the overall concentration of coffee in the mug is the same, but the MLM was computationally cheaper. However, these savings come with the caveat of only being valid under well-developed convective conditions (i.e. stirring, albeit not mechanical, as with a spoon).

The Chemistry Land-surface Atmosphere Soil Slab (CLASS) model (Vilà-Guerau de Arellano et al. 2015) is based upon MLM theory. The decrease in

computational requirements comes by acting only on one spatial dimension, the vertical. This is achieved by assuming a well-mixed (stirred), homogeneous BL, where horizontal gradients are non-existent. And therein lies one of the inherent drawbacks of MLMs; properly representing surface heterogeneity. As surface heterogeneity is a common feature in the real-world, this may lead one to believe that MLMs have no place in modelling it. It is one of the ambitions of this project to test a conceptual "box" domain over which the BL will evolve, essentially imposing limitations to the horizontal extent of homogeneous mixing. To accomplish this end, the influence that advection and subsidence exert on the BL must first be investigated.

The subject of this investigation will be the Boundary Layer Late Afternoon and Sunset Turbulence (BLLAST) campaign, conducted in southern France in 2011. Individual days of this campaign have previously been subject to study with CLASS (Blay-Carreras et al. 2014, Pietersen et al. 2015), however these studies also involved LESs and focus on in-depth analysis for a single Intensive Observational Period (IOP). In contrast, this study will use observed and modelled data from the campaign to initialize and initiate CLASS under various conditions, and then apply a common set of methods and analyses to ten of the twelve IOPs. By comparing CLASS outputs with large-scale forcing free runs, or actual BL evolution observed during BLLAST, individual campaign days will be classified with respect to the impact of external forcings. It is the intention of this work, that the characterisation and grouping of particular days will make targeted research based on the BLLAST dataset in the future more effective. The IOPs will also be subject to tests of how sensitive the BL development for each day is, to the choice of initial conditions, whereby CLASS is initiated using profiles measured at different times. Finally, the "box" domain concept will be applied for each studied IOP, to determine the effects of averaging surface heat fluxes as a method to resolve surface heterogeneity in MLMs.

This thesis is divided into eight chapters: Chapter 2 reviews information about the BLLAST campaign and presents the datasets used in this study. Chapter 3 provides theoretical background on the convective BL and a description of the CLASS model physics, as well as the developed and applied modifications implemented into the pre-existing CLASS model coding. Chapter 4 describes steps taken to initialize CLASS with BLLAST data, in addition to outlining the cases for each round of experiments. Chapters 5, 6, and 7 present the outcomes of the experiments, and discusses their implications. Finally, Chapter 8 summarizes project findings, discusses challenges encountered during the study and suggests directions of further research.

(Note: In an effort to facilitate navigation ease, hyperlinks have been created in Chapters 5, 6, and 7 to quickly navigate between figures, appendices, and particular IOP sections. When viewing as a PDF, clicking on underlined figure numbers, appendix letters, or IOP numbers will lead to the indicated object.)

2 BLLAST

2.1 Campaign Overview

The BLLAST campaign took place in Southern France near the "Plateau de Lannemezan" from 14 June to 8 July 2011, in an effort to better study and understand the afternoon transition of the BL (Lothon et al. 2014). For the campaign, several institutions and organizations came together to facilitate a comprehensive set of observations of the BL, utilizing a wide range of in-situ and remote sensing instrumentation and measurement methods. A total of twelve IOPs were designated during the overall experimental period, with coordinated flight strategies involving two manned research aircraft and different Remotely Piloted Aircraft Systems (RPAS), as well as tethered and untethered balloon launches (Lothon et al. 2014). The area itself (purple circle in Figure 2.1), is characterized by a heterogeneous mix of agricultural fields, forest, moor, and urban development. This layout was specifically chosen, as BL development over mixed land use was a main aspect of interest for the study (Lothon et al. 2014). Several eddy-covariance stations were also deployed to monitor, among other things, surface fluxes above mostly uniform land types (Lothon et al. 2014).

Further details about the campaign can be found in Lothon et al. (2014) and the associated now freely available data set is accessible on the BLLAST website at: http://bllast.sedoo.fr/database/.

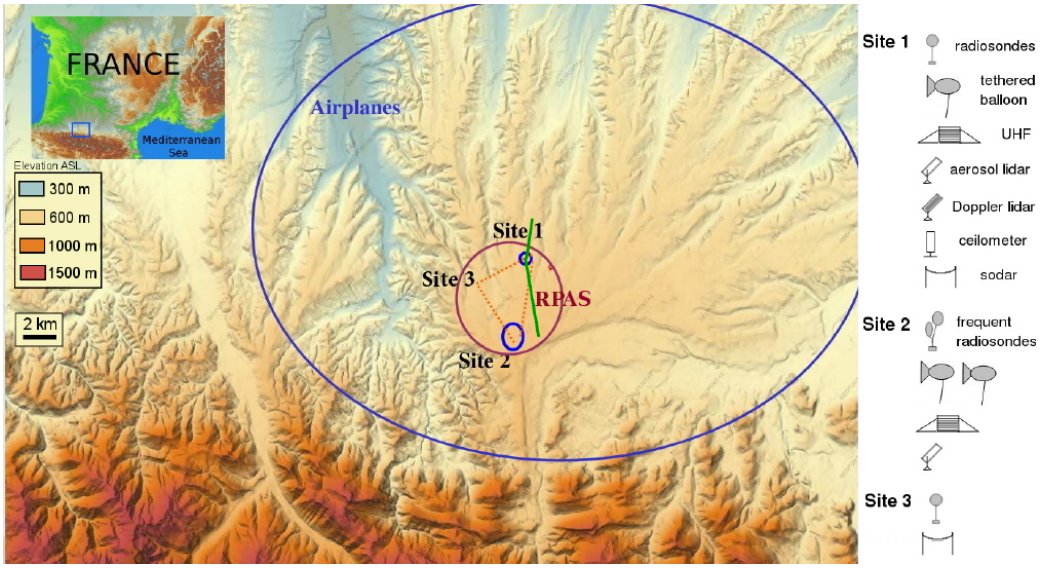

Figure 2.1: Location of BLLAST experimental area (Lothon et al. 2014, p.10938)

2.2 Datasets

2.2.1 SUMO profiles

One such RPAS is the Small Unmanned Meteorological Observer (SUMO) (Reuder et al. 2009, 2016). On IOPs 02-11, SUMO flights were launched from either Site #1 or Site #2, providing profiles of pressure, temperature, and relative humidity in the BL. These parameters could then be combined to calculate potential temperature (θ) and specific humidity (q). Wind speed and wind direction, or the zonal (u) and meridional (v) wind components, are derived from the variation of the SUMO ground speed during ascent (with constant throttle) and descent (motor off) in a helical pattern (Mayer et al. 2012). The vertical resolutions of temperature and humidity is on the order of 5 m for the ascent and 1 m for the descent. Due to airspace

restrictions, the flights could only be performed to a maximum altitude of 1.6 km above ground level, with one flight typically lasting between 10 to 15 minutes (Reuder et al. 2016). Ascent and descent profiles were then processed into a single, corrected profile, with 20 m vertical resolution to correct for sensor time lag, in particular for the temperature and humidity sensors (Jonassen 2008). The u and v profiles have a much coarser resolution, with gaps in the data, sometimes exceeding 100 m. Reliable wind data from SUMO are only available in fully automatic flight mode which has typically been established at a height of 150 m after manual take off (Mayer et al. 2012). Wind data below 200 m have therefore been omitted from further analysis. Otherwise, these profiles were the primary source of data for model

Table 2.1: Number of SUMO profiles flown for each IOP, as well as from which site they were launched

IOP number	Calendar date	Number of profiles flown	Launch site
IOP00	14Jun	0	N/A
IOP01	15Jun	0	
IOP02	19Jun	11	#1
IOP03	20Jun	11	
IOP04	24Jun	10	
IOP05	25Jun	10	#2
IOP06	26Jun	11	
IOP07	27Jun	12	
IOP08	30Jun	12	#1
IOP09	01Jul	6	
IOP10	02Jul	9	
IOP11	05Jul	10	

initialisation, as will be discussed in Chapter 4. The number of flights per day and their location can be found in Table 2.1 (Lothon et al. 2014).

Further details regarding SUMO specifications and its use in BLLAST can be found in Båserud (2013) and Reuder et al. (2012, 2016).

2.2.2 MesoNH modelling

Contributions of large-scale advection and subsidence from simulations with the MesoNH model by Jiménez (2016) were vital for this study. This data set included both horizontal and vertical advection of potential temperature and moisture, presented as vertical profiles. Also included were profiles of vertical velocities, used to estimate the large-scale divergence in the Free Atmosphere (FA). These modelled profiles started at 06:30 UTC, and are available with 30 minute resolution until 00:00 UTC of the next day (Jiménez 2016).

The lowermost point is 1.5 m above ground level, with the next being 3 m above that, and then ever increasing distances between higher points. For instance, model levels 39 and 40 are separated by 145 m, while the uppermost point of 8.5 km (model level 85) is 700 m above the second highest. The horizontal resolution is 400 m, and the available profiles are averaged over a 10 km × 10 km domain, centred at Site #1, representing an average of 625 horizontal grid points. Zonal advections are calculated as the difference between ψ_E and ψ_W at the same latitude, over the width of the domain, 10 km, and multiplied by the average zonal wind, $\overline{u}$. ψ is a generic variable that can represent potential temperature or specific humidity. These results are then averaged across all latitudes to obtain a value for the entire domain (Equation 2.1) (Jiménez 2016).

$$adv(x) = \overline{u \times \frac{\Delta\psi}{\Delta x}} = \overline{u} \times \overline{\frac{\psi_E - \psi_W}{10km}} \tag{2.1}$$

A similar process is done for $adv(y)$ with $\overline{v}$, ψ_N and ψ_S along all longitudes.

Vertical advections required slightly different treatment. At each model level, k, the vertical advection is computed as the centred difference of the vertical ψ gradient, multiplied by the vertical velocity at that model level (Equation 2.2) (Jiménez 2016).

$$adv(z) = \overline{w_k \times \frac{\Delta\psi}{\Delta z}} = \overline{w_k \times \frac{\psi_{k+1} - \psi_{k-1}}{z_{k+1} - z_{k-1}}} \tag{2.2}$$

This is done for each gridpoint in the domain, over which the spatial average is then taken to find a mean value for the entire domain at level k.

The calculation of vertical advection requires the knowledge of w at all heights and gridpoints, and it is the horizontal mean over all gridpoints that is available for use in the MesoNH dataset. This mean is used to calculate subsidence values from heights in the FA (see Section 4.1.5). Variability of w over the domain is embedded in the dataset as the standard deviation across all gridpoints at a given height level. Unfortunately, this standard deviation be can quite high, on the order of 10^2 greater than the magnitude of the mean itself. This reveals that individual updrafts and downdrafts exist within the domain, and while operating over a smaller area, can be 100 times stronger than the mean. These values would reflect measurements taken at a particular point, whereas the mean represents the overall vertical motion of the FA over the domain. This is what is desired for subsidence values. The model set-up is described in further detail, in Jiménez & Cuxart (2014). With limitations of this MesoNH dataset in mind, conceptual progress in this study is hinged upon these outputs matching with reality.

2.2.3 Surface heat flux maps

Land use maps and corresponding surface heat flux maps by Hartogensis (2015*b*) were instrumental for investigating the sensitivity of BL evolution to surface inhomogeneity. These 30 m resolution maps, averaged over a

30 min period, formed a time-series spanning each entire IOP (Hartogensis 2015*a*). Their creation involved the eddy-covariance stations deployed across the BLLAST experimental area. As each of these stations was deployed over mostly uniform land type, the surface heat fluxes observed were assumed to be representative of the fluxes for the corresponding land surface over the whole domain. For land uses not monitored during the campaign (urban and bare soil), a simple energy-balance model was used (Hartogensis 2015*a*), to estimate the fluxes for these surface types. Further details regarding surface heat flux map creation can be found in (Hartogensis 2015*a*).

2.2.4 Radiation

Additionally, minutely radiation information was obtained from the energy balance station operated by the University of Bergen, at the small-scale heterogeneity field at Site #1. This dataset provides direct measurements of the four components of the radiation balance (incoming solar radiation, reflected solar radiation, downwelling longwave radiation, and longwave radiation emitted by the surface) that can be used to calculate the surface radiation balance. Measurements were taken with a Kipp and Zonen CNR1 Net Radiometer and were assumed to be representative for the entire experimental area.

3 Theory

3.1 Boundary Layer Physics

Stull (1988, p.2) defines the BL as "that part of the troposphere that is directly influenced by the presence of the earth's surface, and responds to surface forcings with a timescale of about an hour or less". So by his definition, the BL is a rapidly evolving environment, with surface and near-surface processes playing key roles in its development. The energy these processes need is overwhelmingly driven by the effect of incoming solar radiation has on the surface itself. Therefore, the properties and characteristics of the ground and how it responds to solar forcings make major contributions to BL development.

Sensible (SH) and latent (LE) heat fluxes are two such processes, relating to potential temperature and specific humidity, respectively. Depending on the type of surface, more energy may be allocated towards SH or LE. Dry desert sand has very little water to be evaporated, especially if compared to a damp tropical rainforest. Therefore the rainforest has a larger ratio of LE to the total amount of SH and LE, a ratio known as the Evaporative Fraction (EF) (Vilà-Guerau de Arellano et al. 2015, p.151) The value of the EF is an indication of how much of the total energy is being partitioned into LE, which will affect BL height, and temperature and humidity evolutions. These last two, along with momentum, are usually distributed uniformly throughout a

subdivision of the BL known as the Mixed Layer (aka. Convective Boundary Layer) (ML) (Stull 1988, p.12). Growth of this layer is typically convectively driven, and is related to the strength of the fluxes at the surface (Stull 1988, p.452).

This growth can be inhibited by the stable stratification of potentially warmer air aloft, a feature known as an inversion layer. The presence of this inversion layer, also known as the Entrainment Zone (EZ), will enhance diurnal warming of the ML, up until such time as the potential temperature of the ML is the same as the potential temperature of the lowest part of the FA, at which point the height of the ML will begin to increase. This growth occurs via downwards entrainment of the less turbulent, but potentially warmer air of the FA (Stull 1988, p.12). This air is also typically drier, thereby decreasing the mean specific humidity of the ML, further impacting surface SH and LE.

One other hitherto unspoken of mechanism for BL development is the large scale synoptic condition. As Stull (1988) points out, a low pressure system is characterized by large scale upward vertical motion, so the presence of a cyclone can drastically lift the BL. Conversely, a high pressure system, with FA convergence and corresponding large scale subsidence, will repress growth and provide a more well-defined BL top (Stull 1988, p.10).

3.2 CLASS Physics

The Chemistry Land-surface Atmosphere Soil Slab (CLASS) model is a one dimensional (in space), zeroth-order-jump MLM, meaning that the EZ is treated as an infinitesimally thin layer, where uniformly blended variables in the ML abruptly jump to FA values. Though this is a simple approximation, it has been shown that zeroth-order-jump models can accurately represent the evolution of the ML variables (Pino et al. 2006, e.g.). Figure 3.1 shows a textbook vertical profile of potential temperature along-side a zeroth-order-

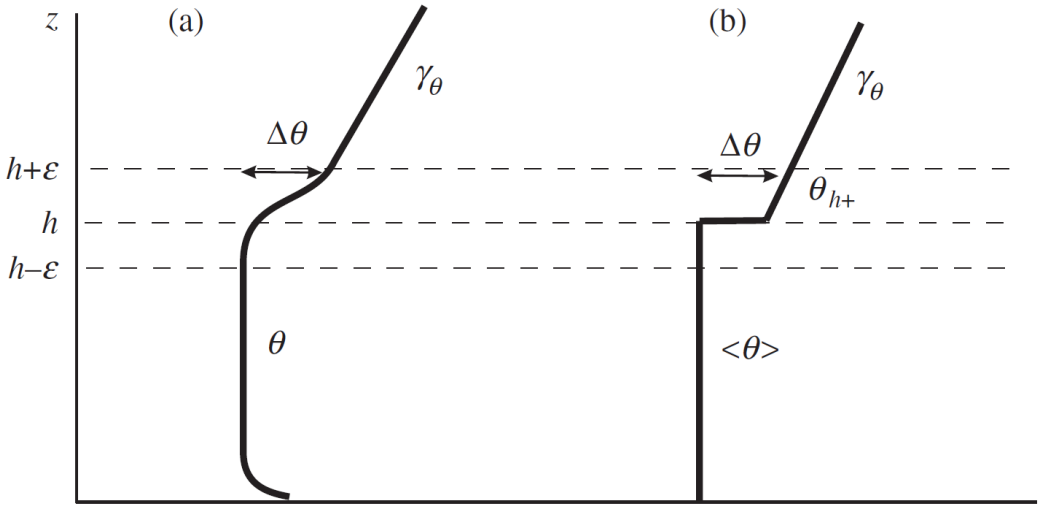

Figure 3.1: (a) Typical vertical potential temperature (θ) profile of the BL. (b) The same profile approximated using a zeroth-order-jump. "h" is the BL height. (Vilà-Guerau de Arellano et al. 2015, p.27)

jump profile.

In order to represent the evolution of these ML variables, CLASS employs the generalized Equation set 3.1 (Vilà-Guerau de Arellano et al. 2015, p. 29).

$$\frac{\partial\langle\psi\rangle}{\partial t} = \frac{1}{z_i}\left[(\overline{w'\psi'})_s - (\overline{w'\psi'})_e\right] \tag{3.1a}$$

$$(\overline{w'\psi'})_e = -\Delta\psi_{z_i}\left(\frac{\partial z_i}{\partial t} - w_s\right) \tag{3.1b}$$

$$\frac{\partial\Delta\psi_{z_i}}{\partial t} = \gamma_\psi\frac{1}{z_i}\left[(\overline{w'\psi'})_s - (\overline{w'\psi'})_e - \frac{\partial\langle\psi\rangle}{\partial t}\right] \tag{3.1c}$$

In Equations 3.1, ψ is a generic turbulent variable, that can represent a ML variable such as potential temperature, or specific humidity. ψ can also represent u or v, although Equation set 3.1 requires then the addition of pressure gradient and coriolis terms (Vilà-Guerau de Arellano et al. 2015,

p.70).

Potential temperature and specific humidity can also be affected by the addition of an advective term in Equation 3.1a, using a constant value over the entire simulation time. Subsidence is parametrized by FA horizontal divergence and BL height (Equation 3.2) (Vilà-Guerau de Arellano et al. 2015, p.47), and can similarly be set to a constant input.

$$w_s = -Div(U_{FA})z_i \tag{3.2}$$

SH and LE maximums are prescribed and can be fit to a sinusoidal curve beginning and ending, by default at sunrise/sunset, or explicitly stated times (see Section 4.1.3). Though these surface fluxes, specifically SH, can become negative in the real world, CLASS values will not decrease below a value of zero during the afternoon transition.

Incoming solar radiation can be calculated using a set latitude, longitude, and the day of the year, and further modified with a cloud-cover factor expressed as percentage of the sky covered.

CLASS thermodynamics can be coupled to the land surface, effectively bringing the surface fluxes "online" and interactive with changes in the land-atmosphere system. However, the activation of this aspect of CLASS involves the prescription of surface characteristics, such as water content and temperature of soil layers across different depths, as well as various ecological parameters. As the surface flux maps provided by Hartogensis (2015*b*) represent the evolution of the observed surface forcings of the day, the inclusion of this CLASS module was deemed outside of the scope of this study, and subsequently, SH and LE were left "offline" and prescribed.

3.3 CLASS modifications

CLASS is a powerful and efficient tool, however the code required specific and precise adaptation to suit the needs of this study. Most importantly, advection and subsidence forcings needed to be time-dependent, rather than constant, as the base version of CLASS allows. With the availability of advection and subsidence data from the MesoNH model (Jiménez 2016), it was possible to create evolutions of these large-scale forcings (see Section 4.1.4). CLASS was then customized to accept these evolutions as variables in the model code (coding details can be found in Appendix A). Therefore, CLASS would be updated every timestep (1 s) with new values of subsidence and

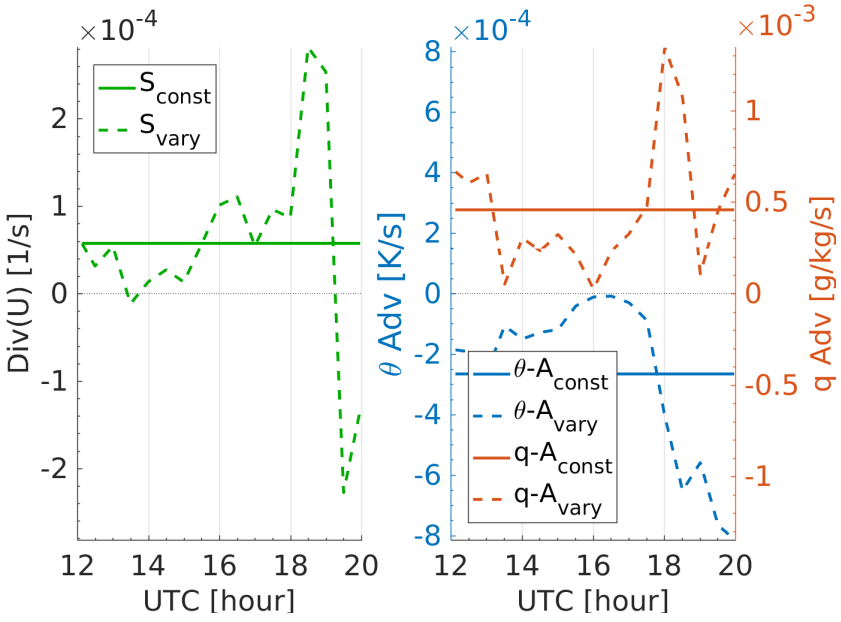

Figure 3.2: Comparisons between constant and time-dependent divergence (i.e. subsidence) (left) and potential temperature and specific humidity advections (right), from the MesoNH outputs, for IOP06 (26 June 2011)

advection to influence the ML. This same procedure was also made possible to be implemented for radiation values, using data from the University of Bergen's MicroSite at Site #1, to account for changing sky conditions.

The change in value from one second to the next may seem minor, and it's implementation involves a non-trivial increase in complexity as compared to simply applying an average across the simulation time. However, this setup culminates to allow for predominantly monotonic motions (as in Figure 3.2) to assert their maximum influence at the appropriate times. This creates the potential for noticeably different outcomes from situations where a constant average is applied to the entire simulation.

4 CLASS Modelling

4.1 Initialisation

4.1.1 SUMO and ML profiles

The primary basis for the CLASS model initial profiles came from the official SUMO BLLAST dataset consisting of multiple vertical flights for each IOP day. For this reason, only ten of the twelve IOP days were studied, since SUMO profiles were not flown on IOP00 nor IOP01. For the remaining IOPs, flights measured various atmospheric conditions, such as temperature, and relative humidity to generate a profile of the vertical structure of the BL. As MesoNH advection and subsidence data was only available after 06:30 UTC, interpolations of large-scale forcings for flights earlier than this were impossible (see Section 4.1.4), and all flights earlier than 06:30 UTC were removed from further analyses. Additionally, four other SUMO profiles were removed due to various issues, as detailed in Table 4.1.

A MATLAB® script (hereafter referred to as "the program") was written to compile and organize each profile, and then from each profile, analyse and derive all BL and FA properties required by CLASS. Additionally, the program was configured to automatically initiate the CLASS model and afterwards import model outputs, while extracting and storing meta-data relating to model run generation and statistical measures for each. The first step to

Table 4.1: SUMO runs removed from analyses

Day	Date	Runtime [UTC]	Reason for removal
IOP02	19Jun	05:56	Earlier than 06:30UTC
IOP03	20Jun	05:28	
IOP03	20Jun	05:50	
IOP05	25Jun	06:28	
IOP06	26Jun	06:04	
IOP11	05Jul	06:20	
IOP06	26Jun	14:31	Low flight <750m
IOP07	27Jun	15:59	
IOP11	05Jul	13:01	Pressure sensor failure
IOP11	05Jul	13:24	

this process was the generation of ML, zeroth-order profiles. To accomplish this end, appropriate BL heights had to be estimated and passed to the program. Pre-existing height estimates, gathered by a variety of measurement methods, are available in the BLLAST dataset[1], however upon their incorporation into the program, it was found that their use did not always provide satisfactory results when imposed on the SUMO profiles. This is especially poignant in regards to the calculation of ML profiles, which can be sensitive to differences as small as 20 m (one height interval in the profiles). Therefore, BL heights deemed "Best", and used for this study, were estimated on a visual basis.

To assist with the visual evaluation, coding for four automatic criteria was implemented into the program, based on potential temperature, virtual potential temperature, specific humidity, and relative humidity (Couvreux 2012), and were used to guide estimates. Figure 4.1 shows potential tem-

[1] http://bllast.sedoo.fr/database/source/metadata_list.php

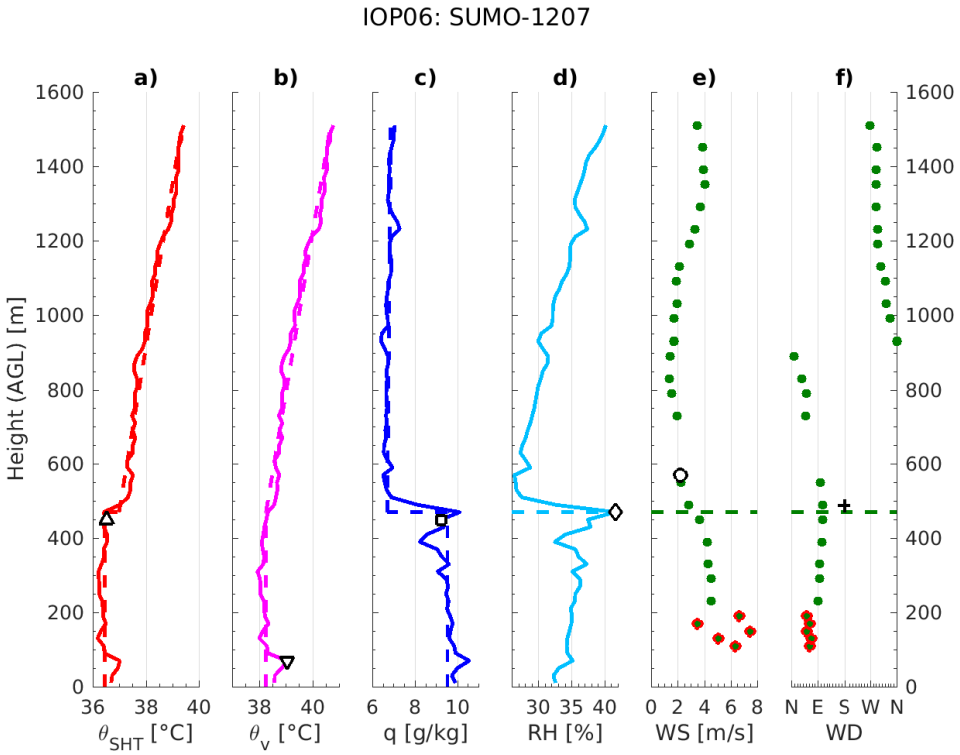

Figure 4.1: SUMO profiles of IOP06 (26 June 2011) at 12:07 UTC for (a) Potential temperature (θ), (b) Virtual potential Temperature (θ_v), (c) Specific humidity (q), (d) Relative humidity, (e) Wind speed, and (f) Wind direction. Solid lines correspond to observed measurements, with approximated ML profiles overlaid in dashed lines. Black symbols indicate automatically estimated BL height from the five criteria, with the modified average of the first four appearing in (f). Red circled points for WS and WD, are those below 200 m, and are therefore deemed unreliable and not considered in the mean of the ML.

perature, virtual potential temperature, specific humidity, relative humidity, wind speed, and wind direction profiles for 12:07 UTC on IOP06 (26 June 2011), as well as corresponding automatic criteria and manually estimated heights. Criteria (Couvreux 2012) were determined by:

- Criteria 1, uses the height of the maximum of the second derivative of potential temperature. In order to emphasize the BL transition and minimize small irregularities in the FA and ML, a 5-point moving average was applied to the potential temperature and specific humidity profiles. After which, a centered differencing numerical scheme was implemented to approximate the first and second derivatives. Unfortunately, while the smoothing generally improved automatic estimates, it did also occasionally differ by 20 m from the placement that would have occurred if smoothing was not applied (see Figure 4.1a,c).

- Criteria 2, is the altitude where virtual potential temperature becomes greater than the mean of all levels below, +0.25 K. Similarly to Criteria 1 & 3, a 5-point moving average smoothing function helped to eliminate small distortions in the ML profile, which may have otherwise lead to grossly inaccurate BL heights.

- Criteria 3 is analogous to Criteria 1, however it uses the **minimum** of the second derivative of specific humidity.

- Criteria 4 places the BL height at the same altitude as the maximum of the relative humidity profile. As this maximum would occasionally be at the very top or bottom point of the profile, with clear visual indications that the true relative humidity maximum (BL height estimate) was at an intermediate altitude, these points were dealt with using a linear detrending algorithm. This algorithm identifies linear

FA and Surface Layer (SL) relative humidity lapse rates and removes them from consideration of the relative humidity maximum.

Additionally, a fifth criteria using the bulk Richardson number method (Zhang et al. 2014) was implemented into the program. The critical Richardson number was made dependent on the stability of the BL, with the values recommended by Zhang et al. (2014) (0.24, 0.31, or 0.39) for stable, weakly stable, or unstable regimes, respectively. However, due to gaps in wind data sometimes exceeding 100 m, this criteria was not used as a guide, but moreso as a potential affirmation of the best BL height after the fact. In a similar capacity, the average of the first four criteria was determined, so that it might be compared with the visually determined height. In order to prevent clearly spurious criteria (as in Figure 4.1b) from influencing this average, any criteria point further than one standard deviation from the mean of all four was neglected, and the average recalculated with those remaining. Ultimately, the final height passed to CLASS was qualitatively decided.

Once the appropriate BL heights were loaded, mean values for ML potential temperature, specific humidity, and u & v wind components could be calculated. As all SUMO data points below 200 m were deemed unreliable, they were neglected in mean calculations. An unfortunate side effect of this quality control, was the inability to find averages for u and v if the BL was deemed to be below 200 m. Fortunately, this caveat impacted few flights, as the treatments of morning and afternoon transitions were different. BL heights for morning flights, which were more likely to be used for initialisation, were taken to be the top of the Stable Boundary Layer (SBL). This is in contrast to afternoon transition flights being less used for initialisations and moreso for comparisons of BL development. For these times, the top of the Residual Layer (RL), if present, was deemed a more accurate representation of the BL height.

FA lapse rates were approximated as a linear trend of all data points above

the BL height. The zeroth-order jumps required by CLASS were calculated as the difference between ML mean value and the intersection of the lapse trend and the BL height. Figure 4.2 gives a visual representation of the process for finding the required ML properties.

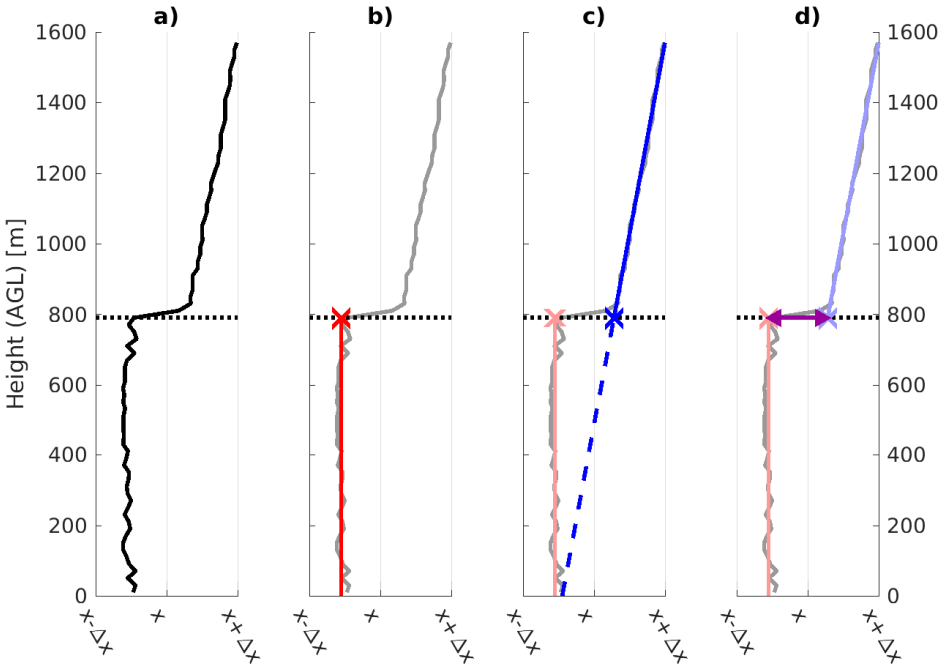

Figure 4.2: Visualization of finding ML properties: (a) A vertical profile (solid black line), with pre-determined BL height (dotted) (b) From BL height (red X) to ground, values are averaged to find ML mean (solid red) (c) Linear lapse trend determined of all points above BL height, blue X is the intersection of that trend line with the BL height (d) Zeroth-order jump (purple) is determined to be blue X minus red X.

4.1.2 Surface fluxes

Instantaneous surface momentum fluxes for u and v required calculation for each initialization run. Utilizing the assumption of a SL that is one tenth of the total height of the BL (z_i), the friction velocity (u_*) can be found using Equation 4.1 (Vilà-Guerau de Arellano et al. 2015, p.67).

$$u_* = k|u| \ln^{-1}\left(\frac{z_i}{10 z_{om}}\right) \tag{4.1}$$

where, $|u| = \sqrt{\langle u\rangle^2 + \langle v\rangle^2}$, k is von Karmen's constant (0.4), and z_{om} is the surface momentum roughness length. Once u_* is calculated, Equation 4.2 can be substituted into Equations 4.3 and 4.4, to give the instantaneous surface momentum fluxes (Vilà-Guerau de Arellano et al. 2015, p.69).

$$C_M = \left(\frac{u_*}{|u|}\right)^2 \tag{4.2}$$

$$(\overline{w'u'})_s = -C_M|u|\langle u\rangle \tag{4.3}$$

$$(\overline{w'v'})_s = -C_M|u|\langle v\rangle \tag{4.4}$$

4.1.3 Sensible and Latent Heat Fluxes

As the influence of surface heterogeneity was of particular interest in the BLLAST campaign (Lothon et al. 2014, p.10936) and also this study, SH and LE fluxes were taken as areal averages over a square of variable size, centered on the launch site of the daily SUMO profiles (see Figure 4.3).

Pre-generated surface flux maps (Hartogensis 2015*b*) were used as the basis for these averages, based off of a 30 m resolution land use map. Using eddy-covariance data from the various surface stations, or modelled fluxes for 'Urban' and 'Baresoil' surface types (Hartogensis 2015*a*, p.11), each surface type was assigned a flux evolution. The proportion of a particular land type within a given domain would influence how substantially that surface's flux

magnitudes affected the average flux, for that domain (Equation 4.5).

$$Flux_{avg,t} = \frac{1}{N}\Big(\sum_{surface=1}^{8} n_{surface} Flux_{surface,t} \Big) \tag{4.5}$$

where $surface$ cycles through the eight surface type classifications used by Hartogensis (2015*b*), n is the number of 30 m $\times$ 30 m gridpoints of that surface type inside the domain, and $Flux$ is the SH or LE value at time, t. Finally, N is the total number of gridpoints contained within the given domain, resulting in a mean $Flux$ value.

These averages were calculated every 30 minutes, leading to a timeseries

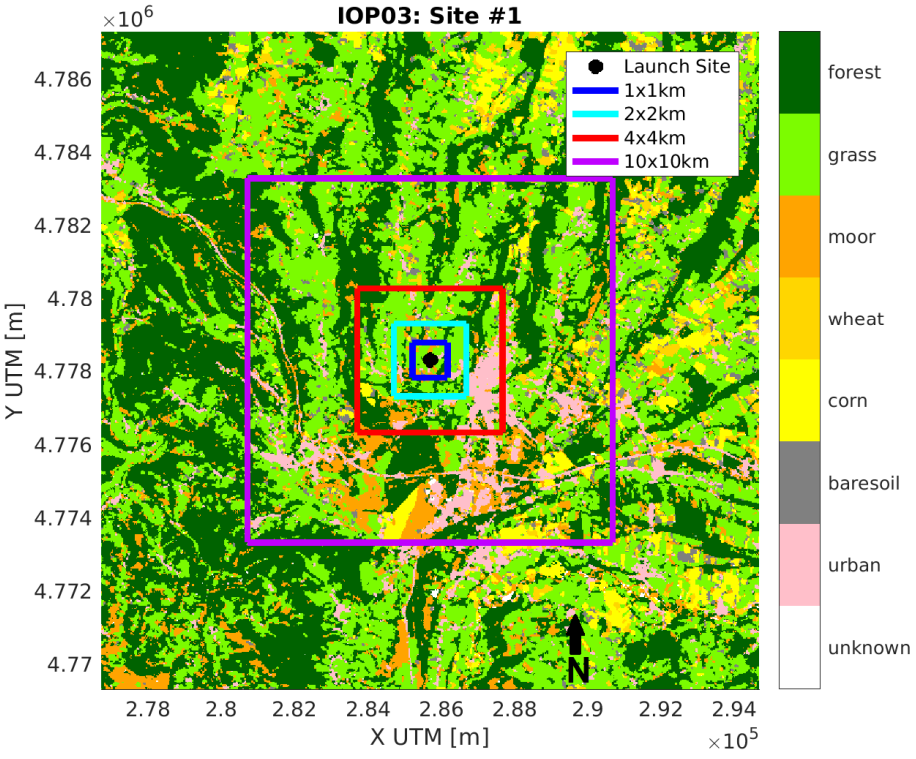

Figure 4.3: Heat flux and roughness areal averages of IOP03 (20 June 2011).

of mean surface fluxes. A sinusoidal approximation was then fit to positive SH values, with the same being done to LE for the same time period. The peak of each approximation was prescribed as the diurnal maximum of a sinusoidal curve to CLASS, for both SH and LE. Start and endtimes for these curves (see `starttime_wt` & `starttime_wq` and `endtime_wt` & `endtime_wq` in Appendix B) were determined to be the time when the fitted SH and LE approximations intersected 0 in the morning and afternoon. However, as data for both SH and LE were embedded in the flux maps in units of $\mathrm{W\,m^{-2}}$, they first had to be converted and passed to CLASS in units of $\mathrm{K\,m\,s^{-1}}$ and $\mathrm{g_{water}\,kg_{air}^{-1}\,m\,s^{-1}}$, respectively. This was done via Equations 4.6 and 4.7

$$SH_{CLASS} = \frac{SH_{fluxmap}}{c_p \rho} \tag{4.6}$$

$$LE_{CLASS} = \frac{LE_{fluxmap}}{L_w \rho} \tag{4.7}$$

where L_w is the latent heat of vaporisation of water, c_p is the specific heat capacity of air at constant pressure, and ρ is the density of the air. As ρ was not explicitly recorded in the SUMO profiles, the ideal gas law ($\rho = pR^{-1}T^{-1}$) was applied to pressure and temperature values at the lowest point in the profile (10 m), where R is the specific gas constant for dry air. The average of densities found from each profile was used as ρ in the ideal gas law, representing a density for the day.

Utilizing the same land use maps used by Hartogensis (2015*b*) to generate the surface flux maps, typical roughness lengths were assigned to each surface type (see Table 4.2). Over the same area of interest as the surface heat fluxes, an average across all roughness lengths was calculated to find a value representative for the area. Having heat fluxes and roughness length dependent on area was motivated by the aim to produce more realistic ratios of buoyancy and shear production.

Table 4.2: Surface roughness lengths (Hansen 1993, p.25-30). Unknown surfaces were assigned a value of NaN and not considered in the average.

Surface Type	z_o [m]
Urban	0.4
Baresoil	0.001
Corn	0.25
Wheat	0.2
Moor	0.007
Grass	0.01
Forest	1
Unknown	NaN

4.1.4 Time-dependent variables

In order to assess the impact changing subsidence and advection has on BL properties, CLASS required modifications to the FORTRAN code. These modifications can be read about in detail in Appendix A. For these modifications to function properly, large text files had to be generated and passed into CLASS. These text files consist of a single line of numerical entries, with as many entries as timesteps in the appropriate CLASS run. Each entry corresponds to an instantaneous value, which has been interpolated between two advection/subsidence output files from the MesoNH model. As each model output file is also an instantaneous value, a linear interpolation is done over the time difference between the files, with the number of discrete intervals dependent on the CLASS timestep. The example code block below, though not written in a specific programming language, demonstrates the interpolation described above.

```
CLASS_timestep_size(dtime)   = 1 second
Model_file_1_time            = 13:00 UTC
Model_file_2_time            = 13:30 UTC
Model_time_difference        = (13:30 - 13:00)*60
                             = 1800 seconds
Model_file_1_value           = 100 units
Model_file_2_value           = 200 units

value(i)   = (200 - 100)*i/(1800/1) + 100,
    where i = 0,1,...,1800
So,
value(180) = 110 units
    where 180 is 13:03 UTC
```

To obtain a high-resolution evolution of advection/subsidence, this interpolation was performed between all model output files, starting from the file just before the simulation start time and ending with the file just after the simulation end time.

A similar interpolation was done with the minutely radiation timeseries for the University of Bergen's instrumentation at Site #1.

4.1.5 Large-scale forcings

With semi-hourly advection and subsidence profiles, average values across the ML and FA needed to be extracted from each profile (represented by the "units" in the Section 4.1.4 example). As SUMO flights were attempted on a mostly hourly basis during IOPs, linear interpolation between best deemed BL height estimates was required to differentiate BL and FA in MesoNH profiles. The black dotted line in Figure 4.4 represents this interpolation between observations ($\times$). Once layers were appropriately identified, vertical profiles at each time and within the confines of a particular layer could be created. Figure 4.4(right) shows the vertical profile for ML potential temperature advection at 18:30 UTC on IOP09. The lowermost 300 m has warm air

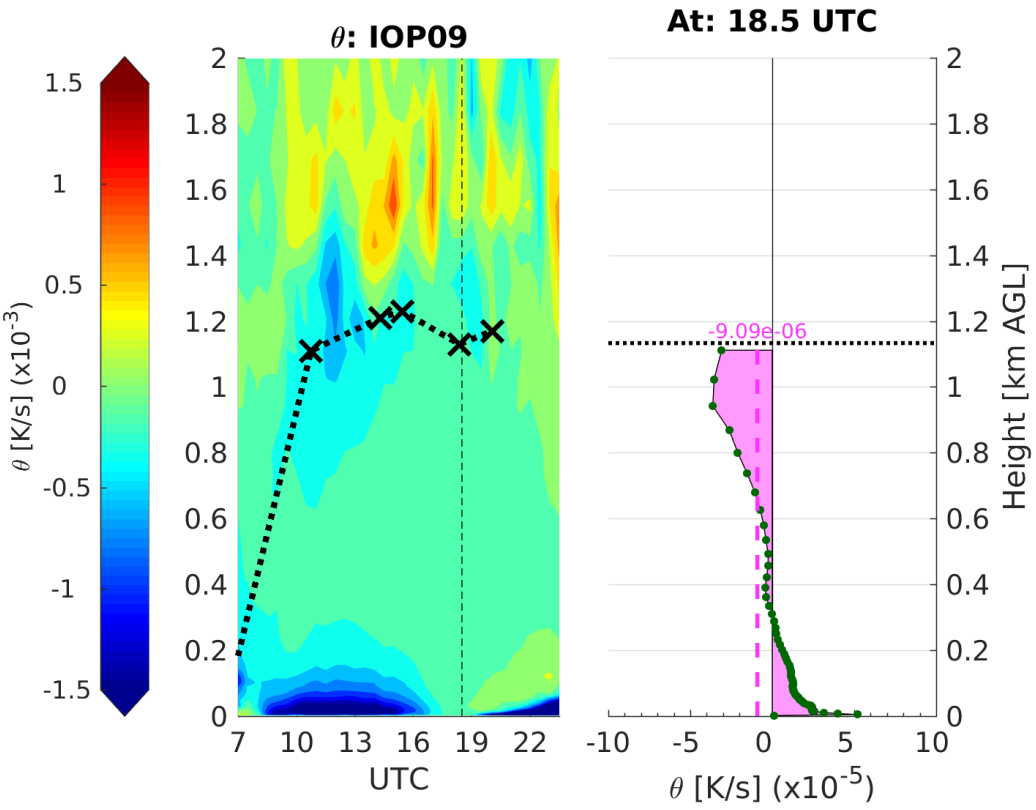

Figure 4.4: 3D Potential temperature advection evolution of IOP09 (01 July 2011) (left). Observed BL heights are indicated with ×, with linear interpolations between as dotted lines. Dashed line indicates time of vertical profile (right). Green dots are MesoNH model levels, and pink dashed line is the spatial average of the pink shaded area, over the model depth.

advection, while from 300 m to the BL height, has cooling. These positive and negative areas were calculated, summed, and the remainder distributed evenly throughout the model depth. Thus, the sign of the remainder indicates warming or cooling, and the value indicates the strength. In cases where interpolated heights did not match exactly with MesoNH height levels, the determined value was seen to be representative of the whole ML. A similar process can be done for the moistening or drying of the ML.

The calculation of w_s is analogous to advections, though it operates from the BL height, up to just below 2.5 km. Once an average FA vertical velocity was found, it was then converted to horizontal divergence via Equation 3.2. This was done to maintain consistency with the unmodified version of CLASS, which can only accept a constant divergence, rather than a constant vertical velocity.

4.2 Numerical Experiments

4.2.1 Experiment 1: Advection & Subsidence Influence

In order to investigate how significant advection and subsidence effects were to daily BL development, Experiment 1 was built upon a control simulation with both set to zero, otherwise referred to as "A-Off/S-Off". This was then compared to a situation with the time-dependency explained in Section 4.1.4 only activated for advections, and subsidence absent ("A-Vary/S-Off"), and the corresponding scenario of vice versa ("A-Off/S-Vary"). Finally, time-dependency was triggered for both advections and subsidence ("A-Vary/S-Vary"). For the three set-ups with time-dependency, advections of potential temperature and specific humidity were only applied within the BL. Large scale forcings data from the MesoNH model, provided by Jiménez (2016),

were used. Where this large-scale data was unavailable (such as IOPs 02, 04, 07, & 08), model performance was considered equivalent to "A-Off/S-Off".

As the MesoNH dataset was averaged over a 10 km × 10 km square centered over Site #1 (see Figure 4.3), the equivalent size was used for the areal averages of SH, LE, and roughness length. Since the same area, and therefore the same average flux, was used for all three runs, the ending times for SH and LE across the runs were identical. Time-dependent radiation information was provided by the University of Bergen's set-up at Site #1, and overrode the default radiation settings that CLASS normally obtains from latitude, longitude and day of the year. As the assumption of a SL is critical for the calculation of instantaneous surface momentum fluxes, this assumption was passed to CLASS for all situations, with identical roughness lengths.

4.2.2 Experiment 2: Sensitivity to Initial Conditions

As CLASS is initialized at an exact moment in time, determining the impact of initializing run choice on BL development was important. Using visual aides such as Figure 4.1, the three best SUMO runs from any given IOP were chosen. This was done almost entirely on a qualitative basis, with contributing factors such as EZ distinctness and sharpness, vertical structure of ML profiles, and linearity of FA lapse rates. To provide as many data points as possible for comparison to CLASS output later, only runs earlier than 14:00UTC were selected. An exception to this rule was IOP09, since due to a limited number of runs, especially runs prior to noon, the third profile of the day was conducted at 14:18UTC, and was selected to be the second best initialization run. Table 4.3 lists three model initialisation times, with time used in Experiment 1 listed as "#1-Control", and two additional test runs, as well as the number of valid flights for each day.

Experiment 2 was only implemented for IOPs 03, 05, 06, 09, 10, & 11,

Table 4.3: Best run choice and the number of valid profiles flown each day. In this context, valid refers to the total number of profiles flown on each day, minus any removed for reasons listed in Table 4.1)

Day	Initialization Runtime [UTC]			Number of
	1st-Control	2nd-Test	3rd-Test	valid profiles flown
IOP03	12:11	09:43	11:16	9
IOP05	11:02	12:29	13:58	9
IOP06	12:07	11:11	12:54	10
IOP09	10:45	14:18	06:52	6
IOP10	09:19	10:01	10:58	9
IOP11	09:17	12:08	08:54	7

as approximate convergence given time-dependent advection and subsidence information was the primary objective of the Experiment. Areal averages and surface layer assumptions for Experiment 2 were also consistent with Experiment 1.

4.2.3 Experiment 3: Areal Averaging Effects

To assess the impacts that extent of surrounding area differences have on BL development, Experiment 3 focuses on changing the length-scale of this averaging. For continuity, included in this Experiment is a CLASS model run already introduced in both Experiments 1 and 2. Specifically, the 1st choice run inside the 10 km $\times$ 10 km domain, with advection, subsidence, and radiation all varying in time.

Experiment 3a: Coarse Areal Averaging Effects

Firstly, this model run was analysed alongside three others of decreasing domains: $4\,\text{km} \times 4\,\text{km}$, $2\,\text{km} \times 2\,\text{km}$, and $1\,\text{km} \times 1\,\text{km}$, all centred around the launch site of the day (see Figure 4.3 for Site #1). Due to the nature of this Experiment, results for all ten IOPs could be obtained. For IOPs 03, 05, 06, 09, 10, & 11 variation about domain was done with time-dependent advection and subsidence, whereas for IOPs 02, 04, 07, & 08, advection and subsidence were forced to be "Off".

Experiment 3b: Fine Areal Averaging Effects

Expanding upon the preliminary results from Experiment 3a, a more detailed analysis was implemented, under all the same conditions. However, domain changes were much finer, increasing by 0.25 km from 0.25 km up to 10 km.

5 Experiment 1: Advection & Subsidence Influence

5.1 Results

Advection and subsidence are both processes that can impact BL development, depending on the synoptic conditions of the day. While advections can influence ML means and change the strength of the overlying inversion (zeroth-order jump), the presence of a strong high-pressure system will inhibit the rate of BL growth by large/scale subsidence, impacting the height (i.e. volume) over which ML means can spread. It is therefore the conclusion of Stull (1988) that advection and subsidence cannot be neglected for modelling BL development (Stull 1988, pp.483-484). However, synoptic and mesoscale conditions govern the influence these forcings can have on any particular day. The effect on the BL height for the different IOPs during the BLLAST campaign is summarized in Figures 5.1 and 5.2. Each Subfigure displays the automatically generated criteria (as described in Section 4.1.1), having symbology consistent with that introduced in Figure 4.1. The corresponding time series for ML means of potential temperature and specific humidity can be found in Appendix C, though only markers representing ML means derived from "BLH_{best}" are presented. These two ML means, along with BL height, will be used as the primary variables to gauge model

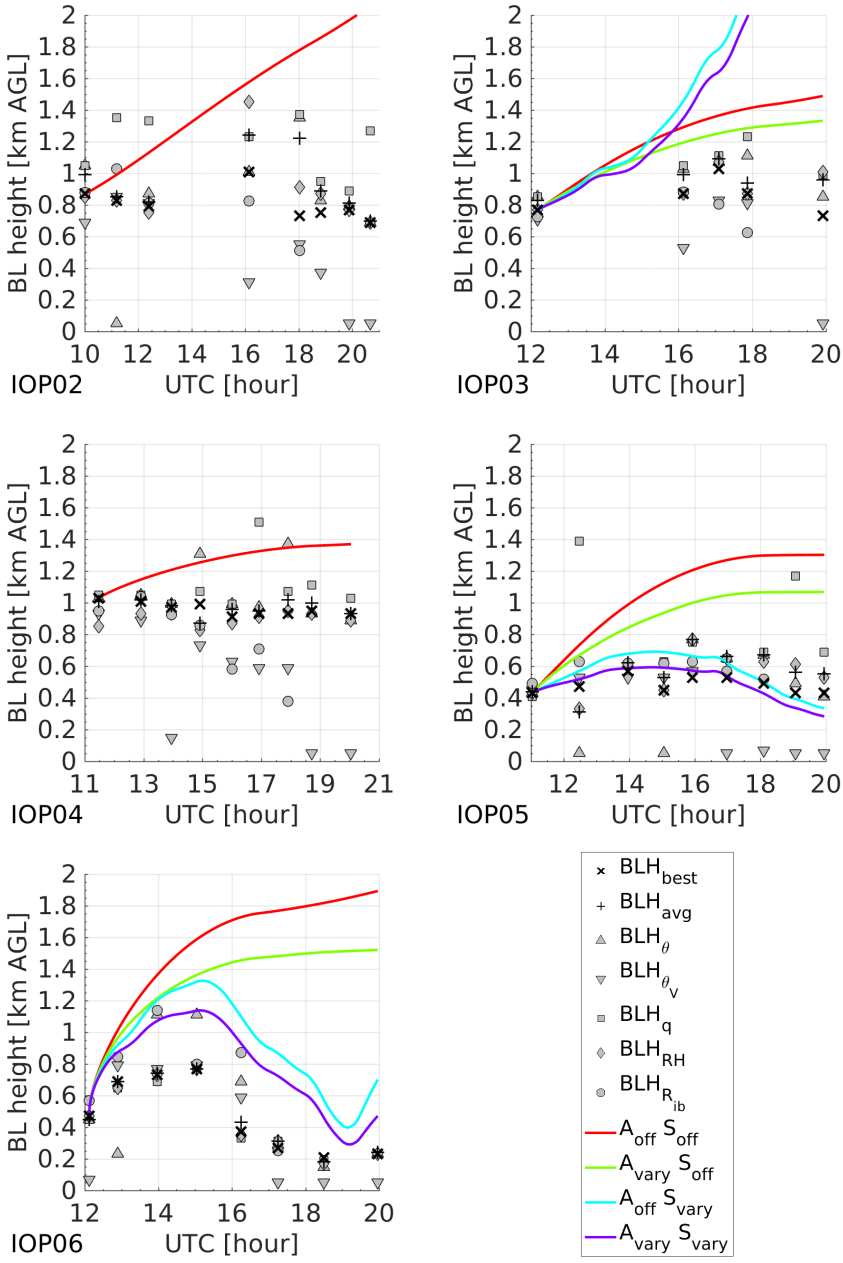

Figure 5.1: CLASS model runs for Experiment 1, IOPs 02-06. Later IOPs and description continued in Figure 5.2. (Jump to: IOP02, IOP03, IOP04, IOP05, IOP06)

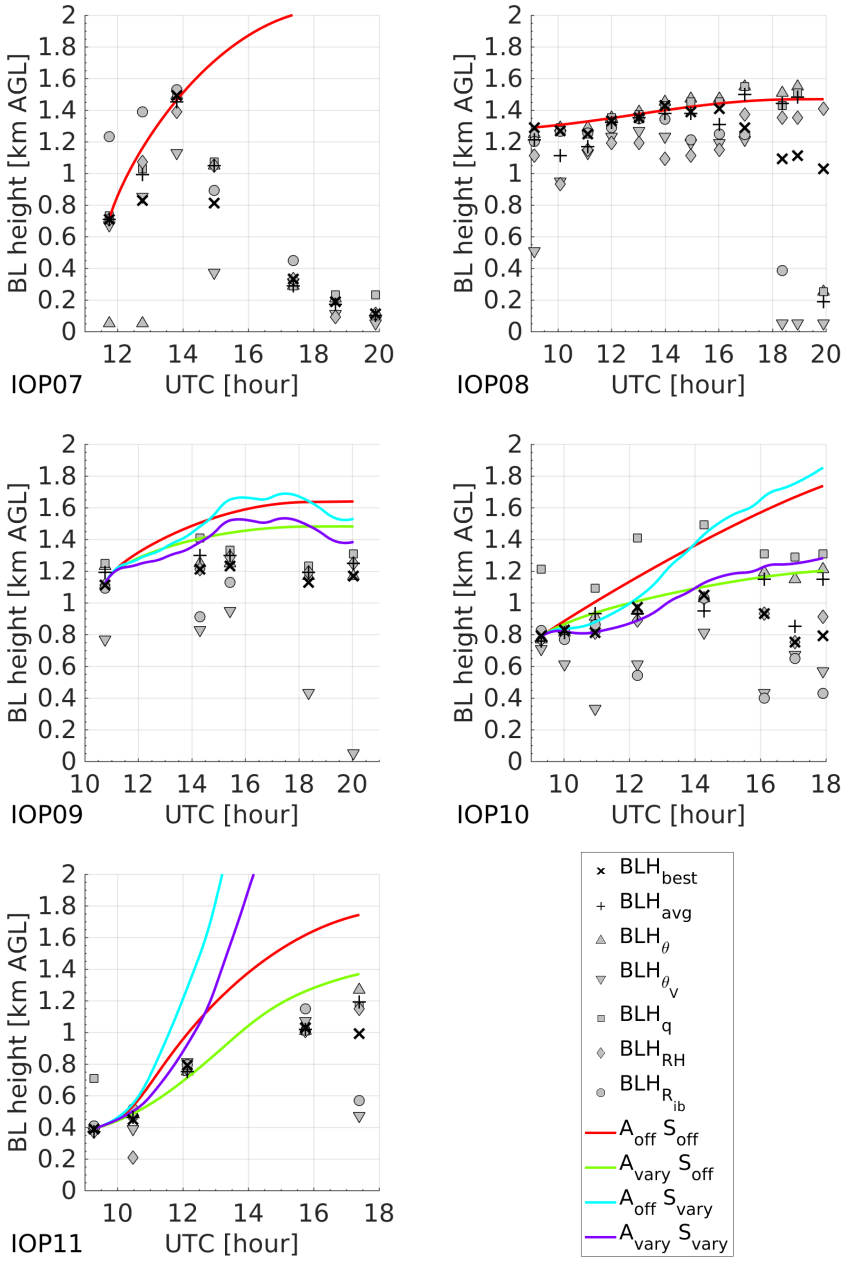

Figure 5.2: CLASS model runs for Experiment 1, IOPs 07-11. Red lines correspond to model runs without advection or subsidence (A-Off/S-Off), green with time-varying advections (A-Vary/S-Off), cyan with time-varying subsidence (A-Off/S-Vary), and purple with both varying in time (A-Vary/S-Vary). (Jump to: IOP07, IOP08, IOP09, IOP10, IOP11)

performance. The four results of the CLASS model runs overlie these points: "A-Off/S-Off" represents the model run with large-scale forcings set to zero; "A-Vary/S-Off" introduces time-variant advection, while remaining subsidence free; "A-Off/S-Vary" is the converse of "A-Vary/S-Off"; and finally, "A-Vary/S-Vary" activates both advection and subsidence.

Though large-scale data was not available for IOPs 02, 04, 07, & 08, a CLASS simulation without advection or subsidence was still possible, the equivalent of an "A-Off/S-Off" situation. Therefore, information pertaining to the importance of large-scale external forcings for these days could still be inferred, albeit to a lesser extent than for IOPs 03, 05, 06, 09, 10, & 11.

In regards to the automatically generated BL heights based on the five criteria described in Section 4.1.1, depending on the day, estimates can be mostly constrained (IOP08 in Figure 5.2) or with a good deal of scattering (IOP02 in Figure 5.1). It is important to note, that while tight agreement of criteria with each other and the best deemed height ($\times$ in Figures 5.1 and 5.2) does give an indication of a well-defined BL top, the opposite is not necessarily true. Wide spread in criteria heights could point to "messy" profiles, ones lacking smooth curves in either the ML or FA lapse rate, generating spurious estimates. Or it could indeed imply as intuition would conclude: a poorly-defined BL top with an extensive EZ. These considerations are important to keep in mind when scrutinizing CLASS model performance to observations.

5.2 Discussion

As it is available for all ten IOP days, the "A-Off/S-Off" set-up is an ideal standard to use in the analysis of this Experiment. For all but one of the studied days, IOP08, the red curve rises well above the best deemed BL heights, and even above most criteria heights in some cases. Aside from

IOP08, two other dates, IOPs 04 & 09 exhibit advection and subsidence free runs that moderately approximate observed BL heights. For all other days, however, these runs do a poor job of simulating observed BL heights. Even for these three days, model runs have difficulty capturing the shape of the observed heights.

As the terms "poor" and "shape" are subjective, objective methods can be introduced, to better assess model performance. One such method, the Root Mean Squared Error (RMSE) is a measure of model accuracy: the larger the RMSE, the less accurate the model. It is a quantification for "poor", and it is described by Equation 5.1.

$$RMSE = \sqrt{\frac{1}{N}\sum_{n=1}^{N}(M_n - O_n)^2} \tag{5.1}$$

where O_n is the observed value of a particular flight, n, while M_n is the corresponding CLASS output value at the same time, and N is the number of observations made. As differences between model output and observation at the initialisation time of the model were zero, RMSE calculations were applied only to flights post-initialisation.

While RMSE can give an indication of how accurate a model run is, the Mean Error (ME) (Equation 5.2), reveals whether the run is under or overestimating observations, otherwise known as its bias.

$$ME = \frac{1}{N}\sum_{n=1}^{N}(M_n - O_n) = \bar{M} - \bar{O} \tag{5.2}$$

It is the signage of ME that signals the direction of bias, while its magnitude represents the strength of the bias. Similarly to RMSE, only measurements post-initialisation were used.

The final statistical measure used to quantify model performance is the Correlation Coefficient (CORR) (Equation 5.3).

$$CORR = \frac{cov(M, O)}{\sigma_M \sigma_O} \tag{5.3}$$

where $cov(M, O)$ is the covariance of M and O, while σ is the standard deviation of the same. It provides an indication of how alike the shapes of two curves are, regardless of magnitude, though as sample size (N) becomes smaller, CORR becomes less reliable. It should also be noted that quantitative comparisons between curve shapes is an extremely nuanced field of study, and though CORR may not be the most robust measure of shape similarity, its use was deemed adequate.

Unfortunately, as SUMO observations form discrete evolutions, CLASS outputs could only be evaluated at corresponding times. Therefore, undulations in CLASS outputs occurring between flights cannot be assessed for any of these three methods. Additionally, it is through the combination of these measures that pertinent information can be derived, as any one measure does not communicate all of "the big picture". With these statistical tools, model results from each IOP day can be evaluated and weighed against the others.

5.2.1 IOP08 (Figure 5.2; Appendix C.3)

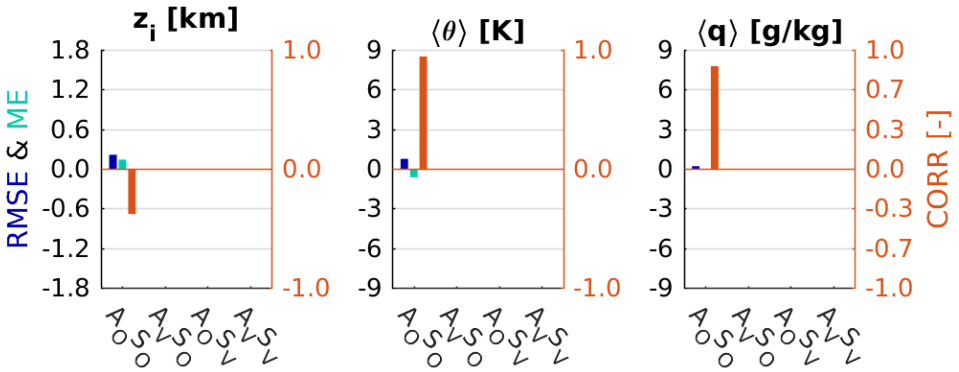

Figure 5.3: Statistical metrics for Experiment 1: IOP08

IOP08, for instance, has the smallest RMSE and ME (see Figure 5.3) for "A-Off/S-Off" of all IOPs (Appendix D has numerical tables of statistical

metrics of all IOPs). Therefore, it can be said that this day had the best performing "Off" run of all the IOPs. Although, this run also has a negative CORR of -0.380, hinting that the shape of the observed BL height, z_i, is not captured by CLASS. Indeed, late afternoon BL decay appears to go undetected. However, as it is at this time that the automatic criteria begin to spread, it may be the opinion of others that the best deemed height would be higher and much closer to the CLASS simulation height, thereby removing any need for explanation of negative CORR value and improving RMSE and ME. Figure 5.4 showcases the subjectivity of pin-pointing exact heights for these late afternoon flights. It is worth repeating that late afternoon BL

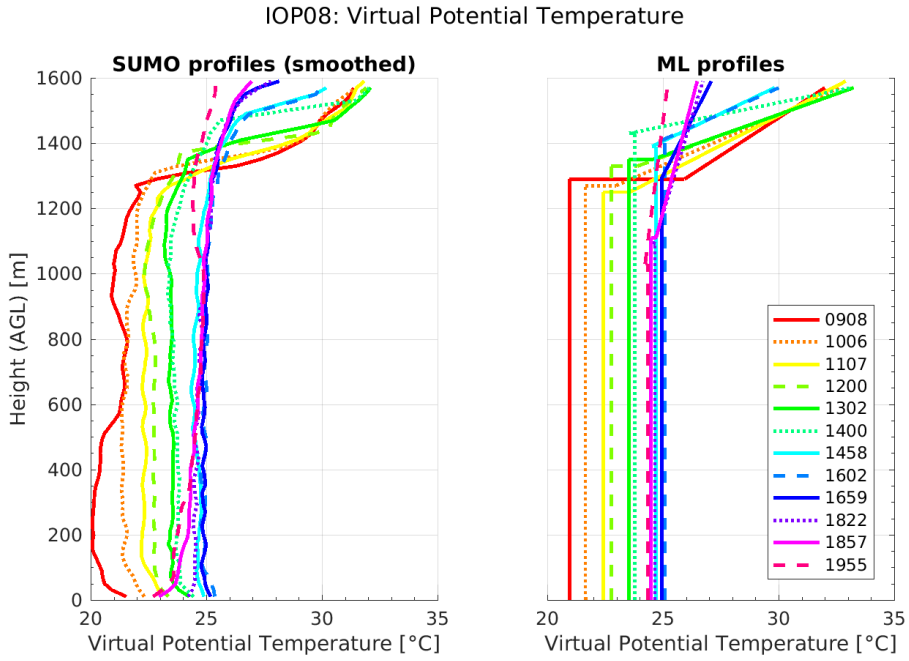

Figure 5.4: Virtual Potential Temperature profiles of IOP08 (30 June 2011). SUMO profiles on the left (with 3-point moving average applied), with ML approximations on the right.

height determination was associated with the RL, rather than any nocturnal SBL. In this case, that begins forming at 18:22 UTC (as evidenced by both the height of the BLH_{θ_V} criteria marker for IOP08 in Figure 5.2 and the SUMO profile in Figure 5.4 at this time). Comparisons of ML means for potential temperature and specific humidity also indicate that the CLASS simulation closely approximates observed values, with the smallest absolute values of RMSE and ME for each parameter, and high CORR. Overall, as advection and subsidence data from the MesoNH model was unavailable for this day, one of two deductions regarding IOP08 can be made:

- The role played by large-scale external forcings on IOP08 was **limited** compared to other IOPs.
- Or, the influence of large-scale external forcings was correspondingly **balanced by other processes**, such as areal extent of surface heterogeneity blending (Experiment 3)

5.2.2 IOP04 (Figure 5.1; Appendix C.2)

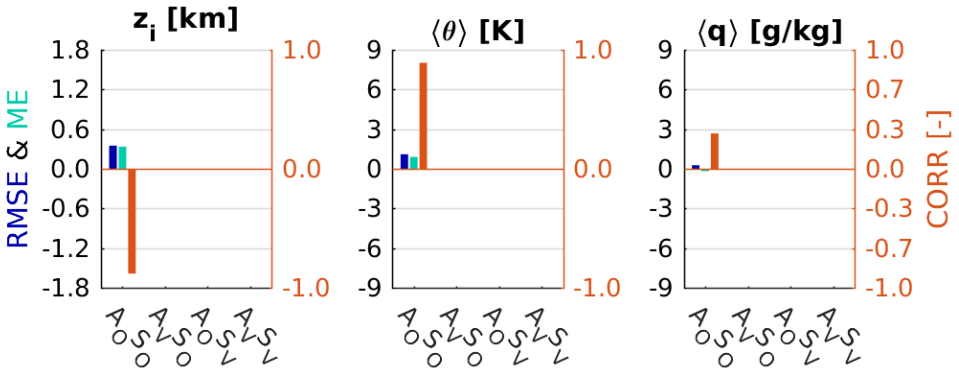

Figure 5.5: Statistical metrics for Experiment 1: IOP04

As previously mentioned, modelling of IOP04 produced BL heights closer to observed than most of the other IOP days. Comparisons of RMSE and

ME reveal that IOP04 has the second smallest values for these measures (see Figure 5.5), after IOP08. Additionally, though some spreading of criteria is also present for this day, maximum differences between best deemed height and the average criteria are smaller than compared to IOP08. If one were to look at profiles for IOP04 (Figure 5.6), one would see that the BL top has much better definition throughout the entire day, increasing the confidence in "BLH_{best}". This confidence also permeates over to observations of ML means, and correspondingly to statistical metrics. Prior to 15:00 UTC, the mean potential temperature from CLASS output was within 0.3 K of observed values. After this point, the temperatures diverge until the end of the

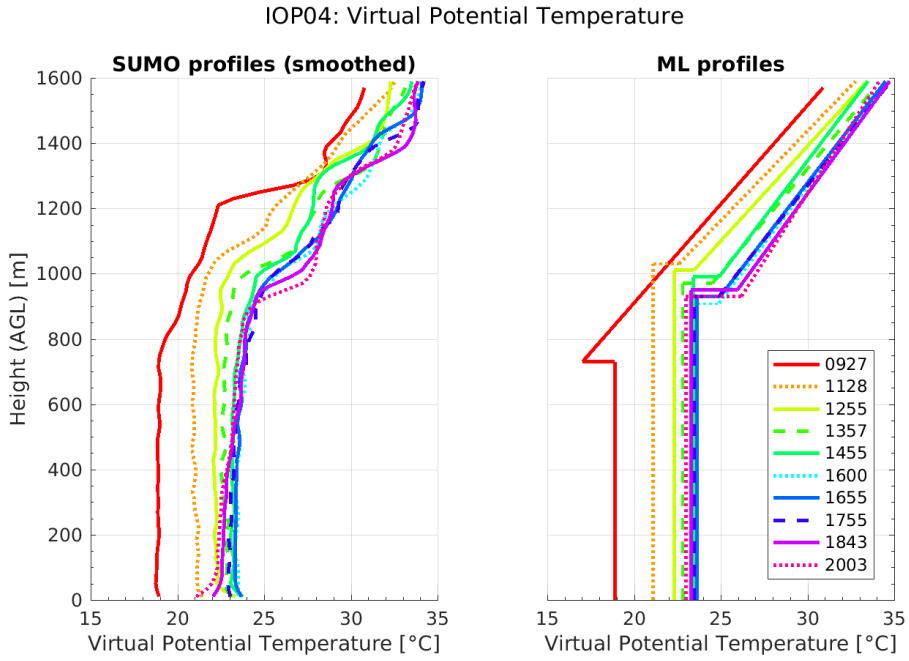

Figure 5.6: Virtual Potential Temperature profiles of IOP04 (24 June 2011). SUMO profiles on the left (with 3-point moving average applied), with ML approximations on the right.

simulation, reaching nearly 2 K at that time, though high CORR shows that the shapes of the two are alike. Though CLASS mean specific humidity only has a weak correlation with observations, with such low RMSE and ME, this CORR strength holds less meaning. So, one can reasonably arrive at the following for IOP04:

- Advection and subsidence have a **noticeable** effect on BL growth, while having a **limited** effect on ML means
- Or, similarly to IOP08, with MesoNH data unavailable for this day, it is possible that advection and subsidence were **significant and partially checked by other processes**, or, they were **limited and dominated by other processes**

5.2.3 IOP09 (Figure 5.2; Appendix C.4)

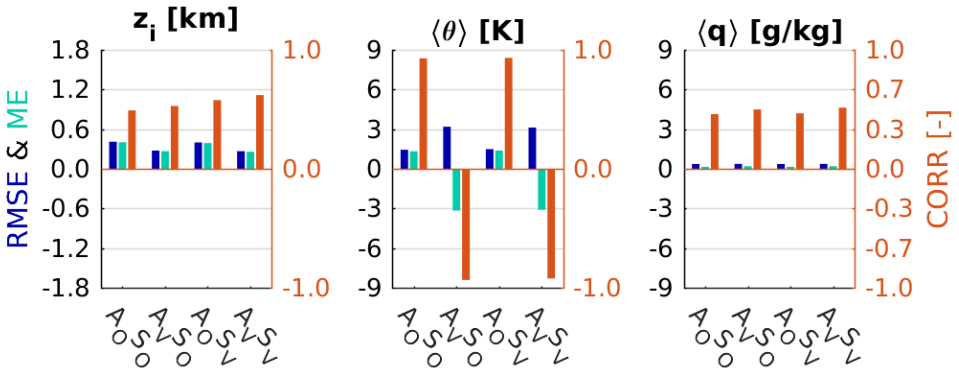

Figure 5.7: Statistical metrics for Experiment 1: IOP09

Just like IOPs 08 & 04, the advection and subsidence free CLASS run of IOP09 displayed less significant differences between modelled and observed BL heights, when compared to IOPs so far unmentioned. Though the difference does approach 470 m by 20:00 UTC, this departure from observation

is small compared to the almost 2000 m difference exhibited by the worst performer, IOP07. As well, ML means for potential temperature and specific humidity for the 'A-Off/S-Off' run of IOP09 approximate measured values, displaying high to mid-range CORR and below campaign average RMSE and ME.

Unlike IOPs 08 & 04, MesoNH data was available for IOP09. Upon introduction of this large-scale motion, BL heights improve for all three of the other runs. Despite having only having a mid-range CORR, 'A-Vary/S-Vary' has the second-lowest RMSE among IOPs with large-scale data. Improved ME over 'A-Off/S-Off' also indicates that the model run has less BL bias, drawing closer to observed BL heights. Unfortunately, such improvement can not be seen in the ML mean for potential temperature. Initially only displaying a 1.3 K bias, the model run with large-scale forcing now underestimates by 3 K, and has developed a strong anti-correlation. Showing neither improvement nor deterioration, ML mean specific humidity metrics remain largely unchanged across all runs.

Individual effects of advection and subsidence can be seen in 'A-Vary/S-Off' and 'A-Off/S-Vary', respectively. While 'A-Vary/S-Off' has a noticeable improvement on BL height estimates, 'A-Off/S-Vary' moreso seems to undulate about the red curve. This also causes little effect to ML means. Studying the subsidence evolution for this day (not shown), FA divergence oscillates with an average near to zero, essentially producing a null net effect. With subsidence playing such a small role, 'A-Vary/S-Off' must therefore generate the changes one can see in $\langle\theta\rangle$ and z_i. It is likely due to the fact that potential temperature advection is predominantly monotonic in time, increasing from strongly negative at first to eventually zero. This cooling diminishes BL growth by decreasing the buoyancy flux (Equation 5.4), which drives convective growth (Vilà-Guerau de Arellano et al. 2015, p.54).

$$\overline{w'\theta'_v} = \overline{w'\theta'} + 0.61(\langle\theta\rangle\overline{w'q'} + \langle q\rangle\overline{w'\theta'} + \overline{w'\theta'q'})$$
$$\overline{w'\theta'_v} \approx \overline{w'\theta'} + 0.61(\langle\theta\rangle\overline{w'q'}) \tag{5.4}$$

The consequences of this on the ML mean are substantial. 'A-Vary/S-Off' has the largest RMSE, strongest bias, and lowest CORR for $\langle\theta\rangle$ of the four runs. With this in mind, comparing metrics in Figure 5.7 leads to the following conclusions for IOP09:

- Advections and subsidence have a **limited** effect on BL growth, with advections contributing a larger impact
- And, these motions appear to have a **significant** impact on the development of the potential temperature ML mean, also mostly driven by the effects of advections

5.2.4 IOP11 (Figure 5.2; Appendix C.4)

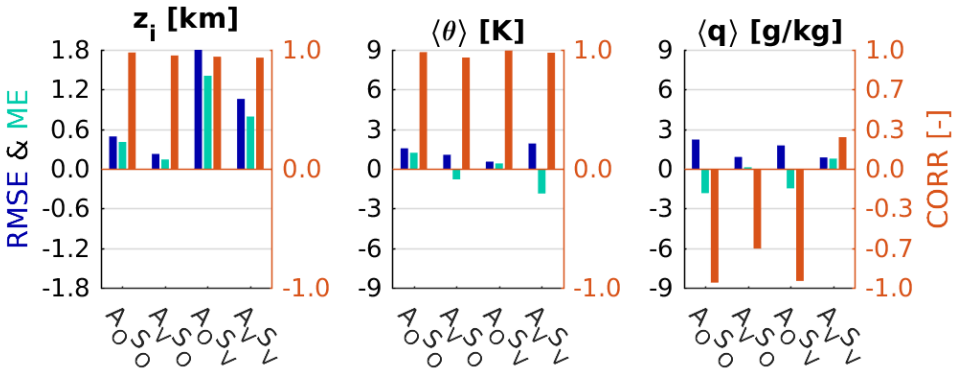

Figure 5.8: Statistical metrics for Experiment 1: IOP1

After IOPs 08, 04 & 09, the next best performing 'A-Off/S-Off' scenario is IOP11. Though RMSE is approaching 500 m and ME shows an overestimation, the CORR for this day is very high; the highest seen in Experiment 1.

While it is possible that this value may be inflated due to low sample size (5 flights), visual analysis of IOP11 in Figure 5.2 shows observed BL heights rising and the CLASS model rises to match. Even the inflection in curvature present at 10:29 UTC is reflected in the red curve. In fact, it is likely that the CORR for this curve could be even higher. Automatic criteria at 17:24 UTC for IOP11 in Figure 5.2 spreads, and the vertical profiles at this time (Figure 5.9) are similar to those seen in the evening hours of Figure 5.4 (IOP08), once again leaving determination of exact height up to interpretation. There is also a high correlation for potential temperature ML mean, with RMSE below campaign average for the same.

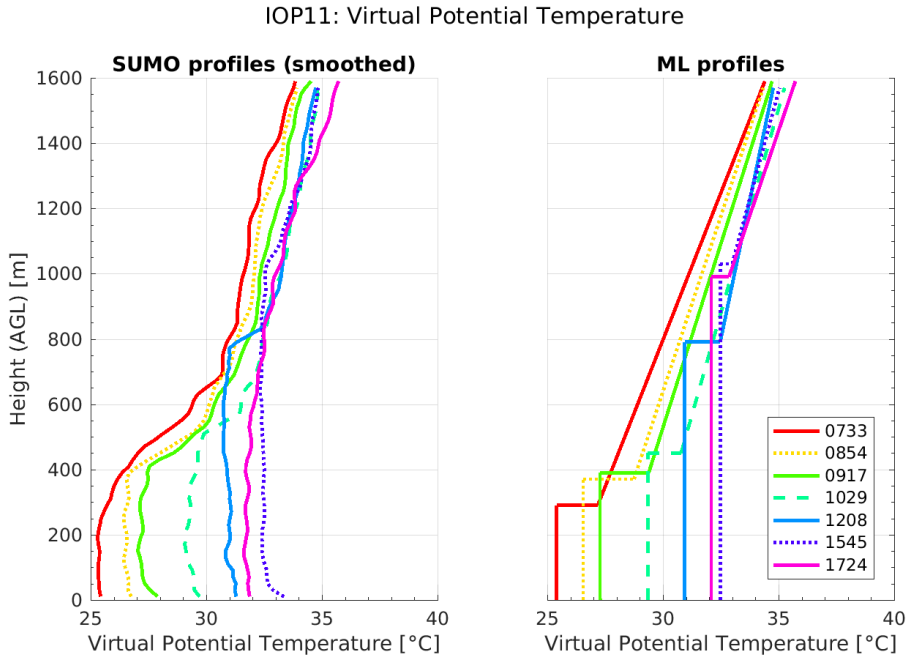

Figure 5.9: Virtual Potential Temperature profiles of IOP11 (05 July 2011). SUMO profiles on the left (with 3-point moving average applied), with ML approximations on the right.

With the introduction of subsidence, as IOP11 has mostly negative divergence throughout, BL growth is enhanced and the 'A-Off/S-Vary' run reaches a maximum height of 3.6 km, more than 3.5 times the maximum observed. Though BL height is grossly overestimated in this model run, ML mean potential temperature estimates have dropped, causing RMSE and ME to reach Experiment bests. The thicker layer allows energy to spread over a larger height (volume), a concept represented by Equation 5.5 (Vilà-Guerau de Arellano et al. 2015, p.25-26).

$$\frac{\partial\langle\theta\rangle}{\partial t} = \frac{(\overline{w'\theta'})_s - (\overline{w'\theta'})_e}{z_i} + \theta_{adv_{BL}} \tag{5.5}$$

Since in this run $\theta_{adv_{BL}} = 0$, as BL height, z_i, becomes larger, the tendency of $\langle\theta\rangle$ will decrease.

It is under these circumstances that a small, and yet very interesting, change in $\langle q\rangle$ occurs between 'A-Off/S-Off' and 'A-Off/S-Vary'. RMSE improves and underestimation also shrinks, an effect that is counter to what is seen in $\langle\theta\rangle$. To properly understand the process, the steps to the process must be broken down. Firstly, the BL is *uplifted with*, and not *through*, the FA. This uplifting enlarges z_i in Equation 5.5, decreasing the tendency of $\langle\theta\rangle$ (as $\theta_{adv_{BL}} = 0$). This diminished $\langle\theta\rangle$ acts to decrease the buoyancy flux through Equation 5.4 (as SH and LE are based on prescribed values). The buoyancy flux is proportional to the entrainment velocity, w_e, as it can be thought of as the strength of the large eddies, which drive entrainment (Vilà-Guerau de Arellano et al. 2015, p.44). Weaker eddies lead to less entrainment, therefore, less dry air is entrained into the ML and $\langle q\rangle$ increases. The same process also works upon $\langle\theta\rangle$, but to the opposite development (less warm air is entrained down, further decreasing the diminished $\langle\theta\rangle$.

However, when analysing results with only advections, $\langle\theta\rangle$ switches from over- to underestimated, as advection brings in cooler air for the entire simulation period. This cooler air reduces buoyancy and the effect of this can

be seen in the 'A-Vary/S-Off' BL height. This run approximates observed BL heights well, displaying a RMSE of only 225 m, the lowest amongst advection only runs. When time-dependency is applied for both subsidence and advection, the impacts of the two combine and an intermediary curve is produced; one which shows some influence from 'A-Vary/S-Off', but more closely parallels 'A-Off/S-Vary'. The outcomes of this combination are as follows:

- Advection and FA vertical motion have a **extremely significant** effect on BL growth, with the two contributing opposite tendencies, and uplifting dominating
- And, these motions have a **significant** impact on the development of ML variables means, mostly driven by the effects of advections
- As advection and subsidence act to underestimate these ML means, while **significantly** overestimating BL heights, other processes must be acting on the BL

5.2.5 IOP03 (Figure 5.1; Appendix C.2)

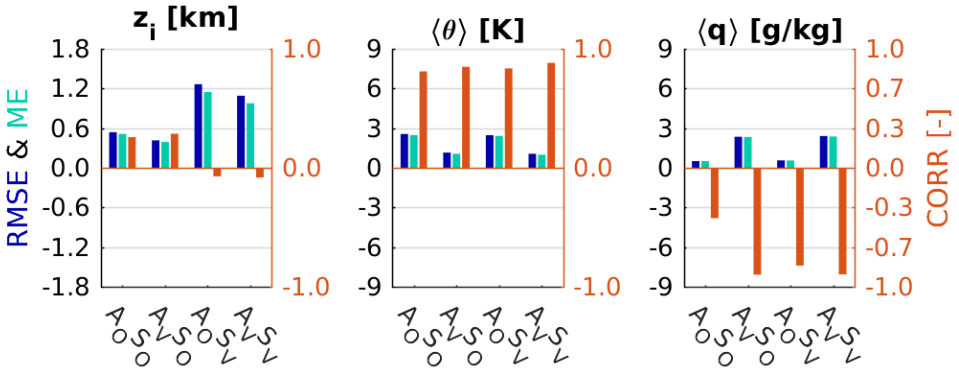

Figure 5.10: Statistical metrics for Experiment 1: IOP03

IOP03 'A-Off/S-Off' has BL height error metrics only slightly worse than IOP11, though with a much lower CORR. This discrepancy is due to observed IOP03 values exhibiting a much more diurnal pattern than IOP11, peaking at around 17:00 UTC before dropping back down. This pattern is not reflected in 'A-Off/S-Off', nor in any of the other three runs, especially due to the predominant negative divergence during this day. So with the introduction of subsidence, the 'A-Off/S-Vary' curve can be seen rising above and diverging from the red 'A-Off/S-Off' curve after 15:00 UTC. This increased overestimation in BL height only slightly differentiates $\langle\theta\rangle$ and $\langle q\rangle$ metrics in 'A-Off/S-Vary' from 'A-Off/S-Off', and in a very similar manner as described in IOP11.

ML mean metrics do change more significantly in the 'A-Vary/S-Off' setup. Prevalent cool air advection leads to the RMSE and ME of $\langle\theta\rangle$ decreasing while CORR improves, though the model run is still warmer than observations. Buoyancy in the BL is decreased by cool air advection (Equation 5.4), and is reflected as a lowering of BL height. With the strongest mean specific humidity advection occurring near the start of the simulation, $\langle q\rangle$ immediately rises, contrary to both observations and 'A-Off/S-Off'. Overestimated $\langle q\rangle$ may be explained by inspection of the MesoNH specific humidity advection timeseries (Figure 5.11). CLASS was initialised at 12:11 UTC and during this time, strong specific humidity advection is taking place in the upper BL. IOP03 can be summarized as:

- Large-scale vertical motion has an **extremely significant** effect on BL growth, with this uplifting overwhelming the effects of advection
- Advections produce a **noticeable** improvement in potential temperature ML mean, but also produce **significant** differences in the same for specific humidity
- Other processes must be working to cool, dry, and lower the BL

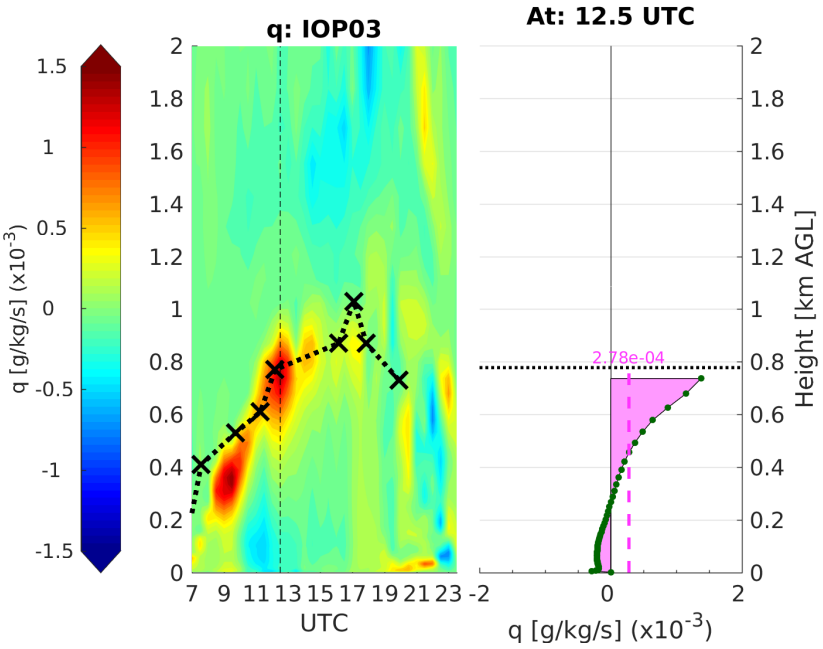

Figure 5.11: 3D Specific humidity advection evolution of IOP03 (20 June 2011) (left). Observed BL heights are indicated with ×, with linear interpolations between as dotted lines. Dashed line indicates time of vertical profile (right). Green dots are MesoNH model levels, and pink dashed line is the spatial average of the pink shaded area, over the model depth.

5.2.6 IOP10 (Figure 5.2; Appendix C.4)

With respect to BL height RMSE, IOP10 has the next best performing 'Off' scenario, though it is among the worse performing half of the IOPs. RMSE nears 600 m, with the red curve for IOP10 in Figure 5.2 increasing almost linearly, as observed BL heights show a diurnal pattern akin to that seen in IOP03. Such mismatch results in a very low CORR and a level of overestimation so-far unseen. Despite the large differences in BL height, errors in ML means for potential temperature and specific humidity are well below cam-

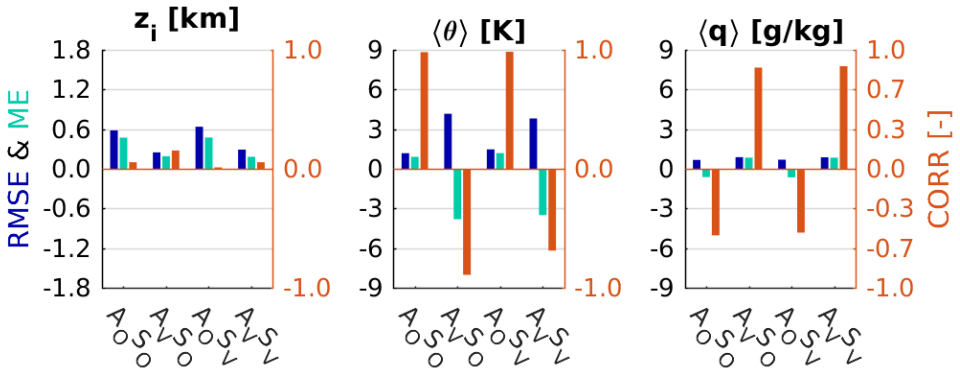

Figure 5.12: Statistical metrics for Experiment 1: IOP10

paign averages. BL height RMSE worsens when subsidence is introduced in 'A-Off/S-Vary', though ME remains almost unchanged. This small difference likely stems from the fact that the average of the daily subsidence evolution is on the order of -10^{-6}, about 5% of the maximum seen for the day, and small enough to explain such a small change as 3 m (see Appendix D.9). RMSE experiences a larger change, as undulations in subsidence take modelled BL height above 'A-Off/S-Off' towards the end of the simulation, just as observed BL heights are dropping, making the model run an even less accurate representation. Much more significant changes come about in 'A-Vary/S-Off'. BL height errors decrease substantially, as a weak CORR develops. Similarly to IOP09, this is due to the initially strong but then weakening advection of cold air. Cooler air reduces buoyancy and results in the lowered green curve. Unfortunately, this cooling lowers $\langle\theta\rangle$ well below observations, and switches a strong correlation to a strong anti-correlation. Activating moisture advection has the opposite effect, with underestimation turning into overestimation. When both advection and subsidence are implemented, the effects amalgamate to form a BL height estimate that appears similar to 'A-Off/S-Vary' oscillating about 'A-Vary/S-Off', while ML means differ little from 'A-Vary/S-Off'. Therefore, the following conclusions can be made

about IOP10:

- Advection and subsidence have a **noticeable** influence on BL growth, with advections contributing moreso
- Advections also have a **significant** impact on ML mean development, while changes due to subsidence are **limited**
- As advection and subsidence act to **significantly** underestimate $\langle\theta\rangle$, other processes **must** be acting on the BL

5.2.7 IOP05 (Figure 5.1; Appendix C.2)

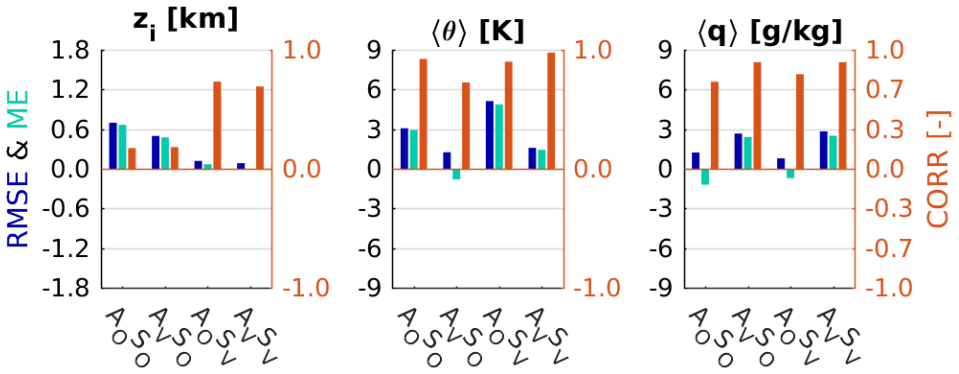

Figure 5.13: Statistical metrics for Experiment 1: IOP05

IOP05 is the first day that has RMSE and bias in 'A-Off/S-Off' exceeding the observed BL heights for the day. This base model run does not even capture the shape of the BL height evolution, as corroborated by a low CORR. RMSE and ME for potential temperature ML mean are also well above campaign averages, while those for specific humidity are on par. CORR for the two are robust, indicating that the trend in the evolution of $\langle\theta\rangle$ and $\langle q\rangle$ is represented, albeit with an over and under estimation, respectively. The addition of cool air advection in 'A-Vary/S-Off' improves RMSE

and ME metrics for potential temperature, with post-18:00 UTC differences keeping them from dropping further. Until this point, model estimates did not stray father than 0.3 K away from observations. This is due to a sharp intensification of cool air advection at 18:00 UTC (not shown), causing $\langle\theta\rangle$ to fall away from the observed trend. This cooling leads to a noticeable drop in BL height for this model run, however, this run also has $\langle q\rangle$ escalating well beyond observed values, as moisture advection is positive for almost the entire simulation.

'A-Off/S-Vary' seriously improves BL height reproduction over 'A-Off/S-Off', cutting the observed errors by 80%, and boosting CORR from almost insignificant to strong. This improvement comes from strong positive divergence throughout the entire simulation time, with particularly strong subsidence after 16:30 UTC. This BL height decrease raises the potential temperature ML mean above the 'A-Off/S-Off' curve, in the opposite manner as that described in IOP11. Interestingly, the compression is significant enough, and possibly the BL thin enough, to dominate the effects of enhanced dry air entrainment and $\langle q\rangle$ actually rises above 'A-Off/S-Off'. When both large-scale forcings are applied, $\langle\theta\rangle$ adopts the shape of 'A-Vary/S-Off', but is raised above it due to the effects of 'A-Off/S-Vary', although still below 'A-Off/S-Off'. Meanwhile, $\langle q\rangle$ is completely dominated by advection effects. The two work together to lower the BL height even closer to reality, reducing RMSE to within 100 m. Just as with $\langle\theta\rangle$ in 'A-Vary/S-Off', these metrics would be even better if only considering observation pre-18:00 UTC. This finding of large-scale forcings having a significant impact on BL development during IOP05 is corroborated by the conclusions of Pietersen et al. (2015). The outcomes for IOP05 can be summarized as:

- Advection and subsidence have a **significant** influence on BL growth, mainly driven by large scale divergence aloft

- The overall effect of large-scale forcings on potential temperature ML mean is **noticeable**
- Specific humidity ML mean is **significantly** overestimated by advection, in relation to both large-scale forcing free conditions and observed values

5.2.8 IOP02 (Figure 5.1; Appendix C.1)

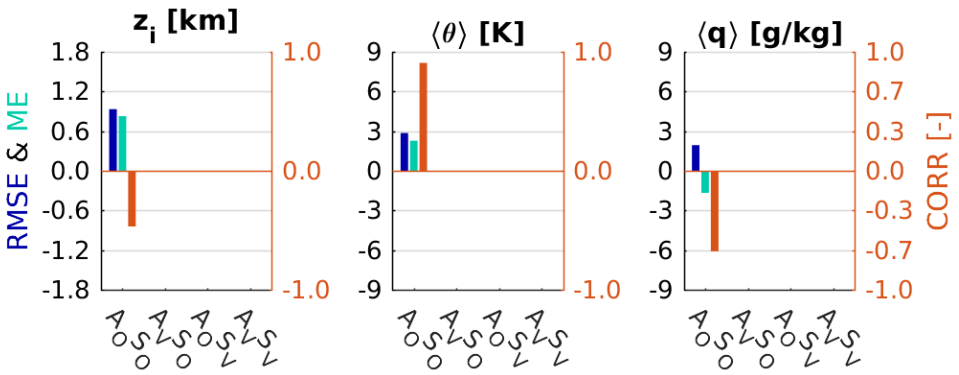

Figure 5.14: Statistical metrics for Experiment 1: IOP02

Errors in the 'A-Off/S-Off' runs of the as yet undiscussed IOPs quickly escalate. All six error metrics for IOP02 exceed campaign averages, with only potential temperature ML mean CORR displaying a favourable value. This only indicates that the general trend of the evolution is represented, but overestimates $\langle\theta\rangle$ while doing so. On the other hand, specific humidity ML mean is underestimated, while also being anti-correlated. But of the three parameters, BL height is the worst performer. From the starting height of 870 m, the modelled height rises near linearly to over 2000 m by the end of the simulation time. Overall, outcomes of IOP02 are:

- Advection and subsidence have a **significant** effect on BL growth, while having **noticeable** effect on ML means

- Or, it is possible that advection and subsidence were **extremely significant and partially checked by other processes**, or, they were **limited and other processes dominated** development and growth

5.2.9 IOP06 (Figure 5.1; Appendix C.3)

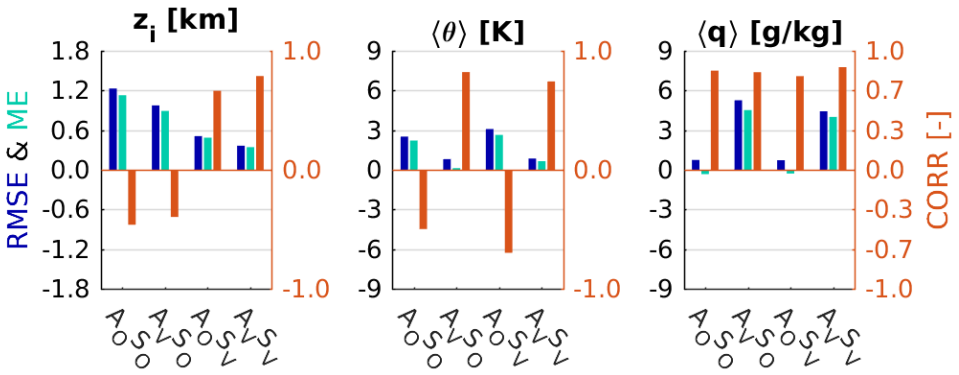

Figure 5.15: Statistical metrics for Experiment 1: IOP06

Though IOP06 has the second worst performing 'A-Off/S-Off' for BL height, the changes observed by including advection and subsidence are among the most interesting of all the IOPs studied. Initial inspection of 'A-Off/S-Off' BL height shows exactly what the RMSE and ME signify; an overinflated estimation, reaching almost 1900 m by the end of the simulation, well above the observed 230 m. ML mean potential temperature is also overestimated and with a mid-range anti-correlation, due to the fact that while this model run has $\langle\theta\rangle$ increasing in time, observed $\langle\theta\rangle$ actually drop. Specific humidity ML mean is the only parameter well-represented by CLASS, with a small negative bias and a RMSE well below campaign average. Unfortunately, adding advective effects in 'A-Vary/S-Off' nullifies this favourable representation of $\langle q\rangle$, resulting in the largest $\langle q\rangle$ RMSE of the campaign. Though, inclusion of advective forcings does result in improved metrics for

$\langle\theta\rangle$. Errors decrease and a strong CORR develops, as cool air is advected into the BL. This cooling reduces BL height errors, however not anywhere near the required levels as to be considered an accurate facsimile of observations.

However, 'A-Off/S-Vary' is the run that makes IOP06 so interesting. It is on this day that divergence achieves its maximum strength, on the order of $10^{-4}\,\mathrm{s}^{-1}$. Though BL height metrics do not impart any special significance to this run, visual analysis reveals an intriguing pattern. Despite only producing a mid-range CORR and still being overestimated, the CLASS model output produces a curve appearing very close to the pattern made by the observed heights, especially considering the 'uptick' after 19:00 UTC. Cause for this 'uptick' can be seen in Figure 5.16, as a yellow-red streak above the BL at around 20:00 UTC. Additionally, the strong subsidence occurring after 15:30 UTC also matches very well with observations. It is this subsidence, and subsequent lowering of the BL height, which raises $\langle\theta\rangle$ above the 'A-Off/S-Off' model run, slightly worsening its metrics. Metrics for $\langle q\rangle$ remain mostly unaffected, with minimal improvement in ME. This slight improvement is a result of the same process occurring in IOP05 'A-Off/S-Vary', where the effects of increased dry air entrainment are overpowered by the decrease in height (volume).

When the two forcings are combined, the ensuing modelled BL height curve retains the shape of 'A-Off/S-Vary', but is further lowered due to cool air advection. Though the errors for this curve are far from eliminated by this combination, the absolute reduction in RMSE is the largest of the campaign. ML means approximate the curves of 'A-Vary/S-Off'; a desirable outcome for $\langle\theta\rangle$, but less so for $\langle q\rangle$. Conclusions regarding IOP06 are:

- Large-scale forcings play a **significant** role in BL growth, with subsidence prevailing and advection supplementing
- Subsidence has a **limited** effect on both potential temperature and

specific humidity ML means, while advections have a **noticeable** and **significant** impact, respectively

- As ML means and BL heights are over-estimated, other processes, such as those at the surface, must be cooling, drying and lowering the BL

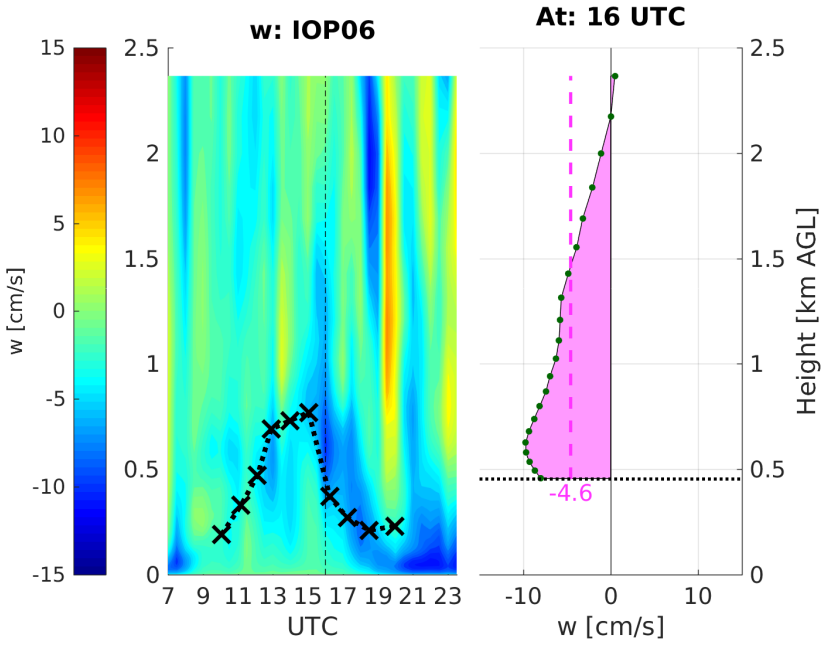

Figure 5.16: FA vertical motion evolution of IOP06 (26 June 2011) (left). Observed BL heights are indicated with $\times$, with linear interpolations between as dotted lines. Dashed line indicates time of vertical profile (right). Green dots are MesoNH model levels, and pink dashed line is the spatial average of the pink shaded area, from BL height to 2.37 km (model level just below 2.5 km).

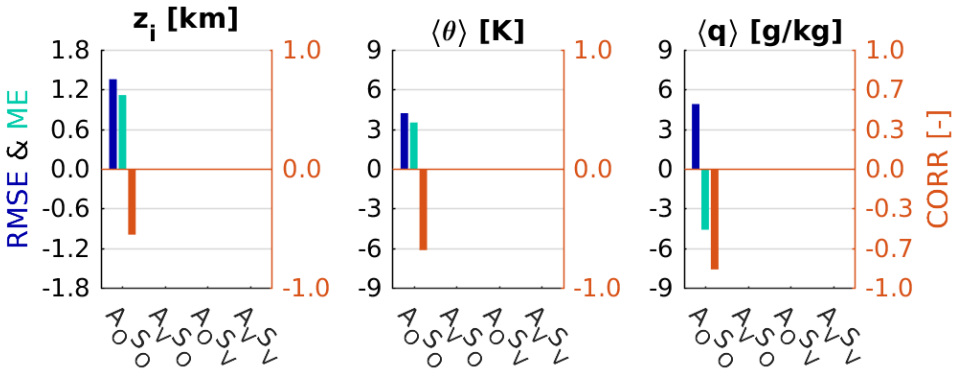

Figure 5.17: Statistical metrics for Experiment 1: IOP07

5.2.10 IOP07 (Figure 5.2; Appendix C.3)

And the worst performing 'A-Off/S-Off' of the study is IOP07. And though IOPs were covered in best-to-worst order of BL height RMSE, IOP07 would end the list for most of these metrics. BL height estimates fly far above measured values, doing nothing to reproduce the post-14:00 UTC decay observed, ending the simulation at near 2100 m. Potential temperature ML mean is also drastically overestimated, while specific humidity ML mean scarcely changes throughout the model run. Similarly to BL height, neither $\langle\theta\rangle$ nor $\langle q\rangle$ come close to sufficiently approximating observations. As such, deductions for IOP07 are:

- Advection and subsidence have a **significant** effect on BL growth and development
- Or, these forcings were **extremely significant and partially checked by other processes**
- While still possible, it is deemed unlikely that advection and subsidence played a limited role in BL growth and development for this day

5.3 Summary

As mentioned in Chapter 2, the MesoNH dataset has been assumed to match reality. CLASS model outputs using the dataset, such as those seen for subsidence and potential temperature advection on IOPs 05 & 06, are encouraging signs for the legitimacy of this assumption. However, introduction of MesoNH advection causes potential temperature on IOPs 09 & 10 to become anti-correlated and underestimated as compared with observations. Additionally, IOPs 03 & 11 have negative divergence in the FA, leading to BL lifting, a condition specifically not targeted by BLLAST. Utilizing prepared IOP summary documents (Blay-Carreras 2014, Nilsson 2011), the cause of this uplifting was investigated. Unfortunately, strong reasoning was not discovered, though since MesoNH is a mesoscale model, it is possible that subsynoptic scale influences, such as local effects from the Pyrenees Mountains (a theory corroborated by Pietersen et al. (2015)), led to the uplifting. It is also possible that IOPs 05 & 06 represent circumstances which MesoNH was able to recreate accurately, making them the exception and not the trend.

Furthermore, IOPs 03, 05 & 06 had substantial overestimations of ML mean specific humidity as compared to observations, with IOP06 ending up with almost double the moisture content by the end of the simulation. This over-moistening may be caused in part by a slight discrepancy between the best deemed BL height estimate using SUMO measurements, and those inherent in the MesoNH model. This mismatch is an example of one of the biggest challenges faced by integrating multiple datasets toward a common purpose; disagreement between boundary conditions. This conundrum can be summed up with a simple analogy: needing lemon juice, but only having limes to squeeze. Some may say they are so similar as to be interchangeable, but ultimately, their small differences could alter the final result. The resolution of this problem involves a non-trivial increase in complexity and

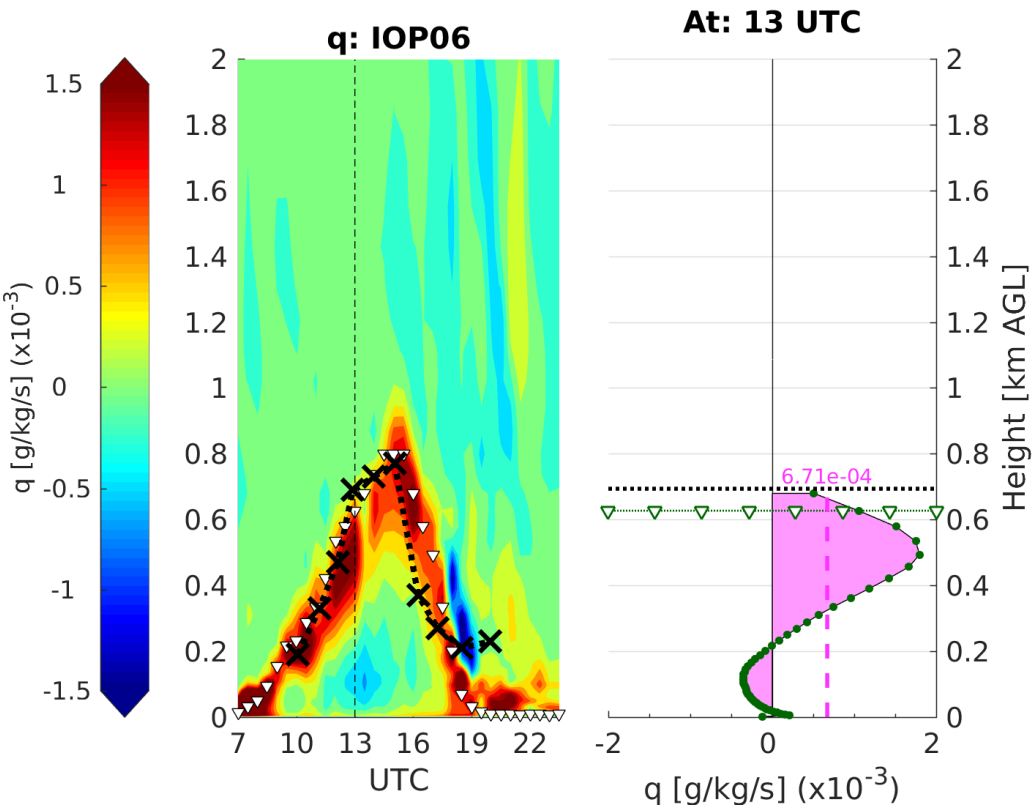

Figure 5.18: 3D Specific humidity advection evolution of IOP06 (26 June 2011) (left). Observed BL heights are indicated with ×, with linear interpolations between as dotted lines. Triangles denote BL height estimates found using virtual potential temperature profiles from MesoNH, and Criteria 2 (see Section 4.1.1). Dashed line indicates time of vertical profile (right). Green dots are MesoNH model levels, and pink dashed line is the spatial average of the pink shaded area, over the model depth. Triangle marked green line shows estimated BL height from MesoNH data.

effort, for what might be little gain. Figure 5.18 shows 3D specific humidity advection evolution for IOP06, as well as a vertical profile of the same at 13:00 UTC. Implementing Criteria 2 (see Section 4.1.1) on virtual potential temperature profiles calculated from the MesoNH dataset, it is revealed that while discrepancies do exist (one model level in Figure 5.18), their impact may be minimal. While the difference in the late afternoon transition may appear substantial, it should be taken into account that $\times$ represents the top of the RL. Ultimately, the calculation and confirmation of MesoNH BL heights was deemed outside of the scope of this study and advections were obtained using the best deemed BL height estimates found with SUMO.

5.4 Applying large-scale averages

As mentioned in Section 3.2, the standard version of CLASS only allows for application of constant subsidence and advection. Pietersen et al. (2015) implemented a time-dependent scheme for subsidence when studying IOP05, being derived from observations (Pietersen et al. 2015, p.4249), though this had limited temporal variability, and advections were still treated as constants. With the availability of the MesoNH dataset, and a finer resolution of advection and subsidence information, this project was able to create a more detailed evolution. Earlier versions of this thesis involved analyses focused between model runs with averaged large-scale forcings, 'Const', and varying runs, 'Vary'. It was revealed that BL height (ML means) would approximate one another if subsidence (advections) oscillated about the average, minimizing the overall net effect. Additionally, for all six IOPs with large-scale data, 'Const' and 'Vary' BL heights would end reasonably close to one another by the end of the simulation.

Distinct differences would manifest only if these forcings were predominantly monotonic (as in Figure 5.19), and of sufficient strength. In regard to

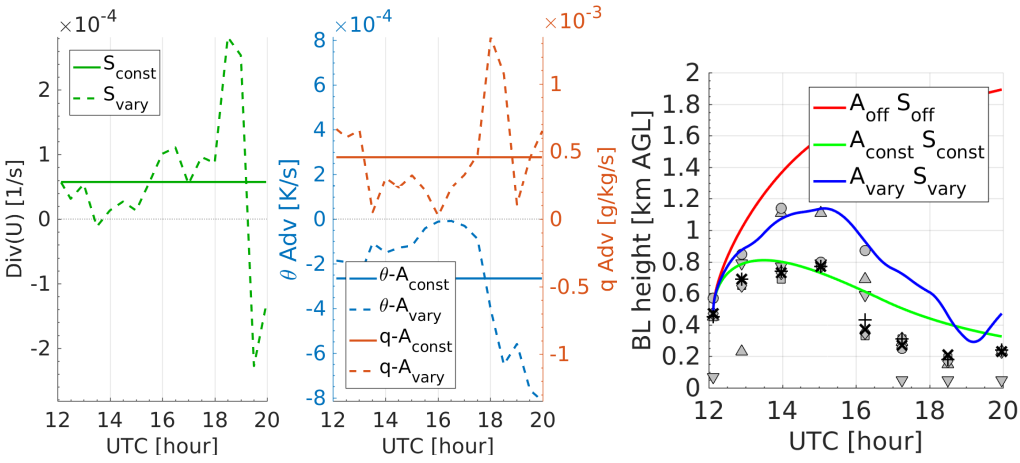

(a) Subsidence and advection evolutions (b) CLASS model output

Figure 5.19: (a) Comparisons between constant and time-dependent divergence (i.e. subsidence) (left) and potential temperature and specific humidity advections (right), from the MesoNH outputs, for IOP06 (26 June 2011) (b) CLASS model output with 'Const' run having constant averaged values for subsidence and advection applied

BL height, IOP06 is the most distinct of the six MesoNH IOPs. 'Const' and 'Vary' runs for this day differed up to 430 m between 15:00 and 15:30 UTC, highlighting the impact that differences between the two setups have in the early afternoon. These comparisons emphasise the significance of introducing detailed time-dependency.

6 Experiment 2: Sensitivity to Initial Conditions

An important aspect of the analyses was to investigate how sensitive the CLASS initialisation was to the use of information from different SUMO flights. How well BL heights, and ML means of potential temperature and specific humidity converge across multiple initialisation times can help to give an indication of the quality of the large-scale advection and subsidence data, as well as the representativeness of the selected SUMO profile for an appropriate initialisation. As the differences between the first choice run ("#1"; red curve in Figure 6.1) and observations have already been discussed in Experiment 1, this chapter focuses moreso on the differences between the runs initialised by SUMO profiles at different times. Run #1 was designated as a control run, and was subsequently subtracted from the two test runs initialised by different SUMO profiles ("#2", green curve and "#3", blue curve). The differences were then analysed for BL heights (Figure 6.1), and ML means of potential temperature and specific humidity (Appendix E).

The model results for the six investigated IOPs were, for an objective analysis of the comparison, grouped into the separate categories of "convergent", "paralleling", or "divergent". These categories were based off of the following criteria:

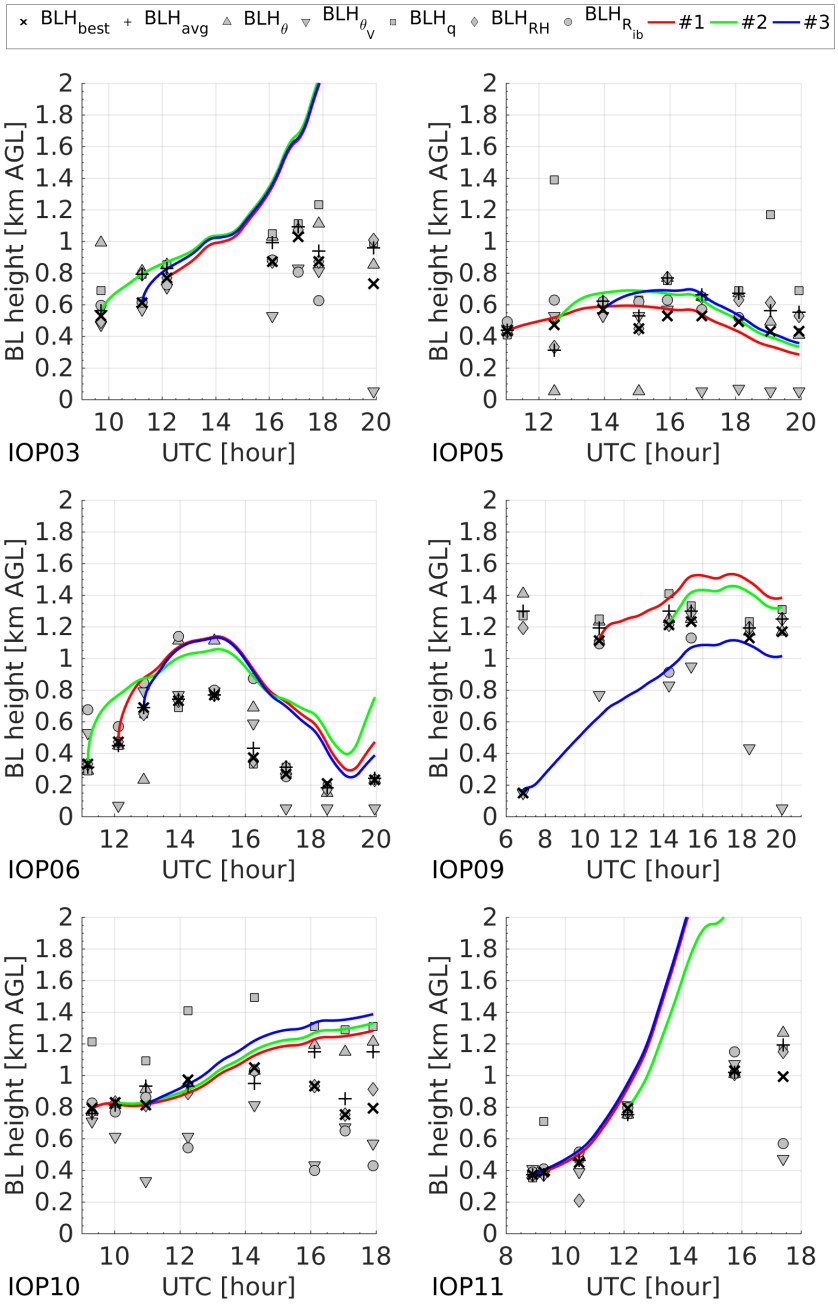

Figure 6.1: CLASS model runs for Experiment 2. Legend entries for lines correspond to choices in Table 4.3 in Section 4.2.2. (Jump to: IOP03, IOP05, IOP06, IOP09, IOP10, IOP11)

Convergent If a run is within $50\,\mathrm{m}/0.5\,\mathrm{K}/0.5\,\mathrm{g\,kg^{-1}}$ of the control by the end of the simulation time

Paralleling Though criteria for convergence is not met, the derivative of the difference between run and control becomes near zero, for the latter half of the simulation time

OR

a run with a non-zero derivative works to reduce differences, for the latter half of the simulation time, but still falls outside defined thresholds for convergence

Divergent A run is neither convergent nor paralleling.

Once the individual performance of each parameter was gauged, an overall classification was assigned to each IOP.

6.1 Discussion

6.1.1 IOP03 (Figure 6.1; Appendix E.1)

Almost all runs across all parameters on IOP03 converge, with only the #2 run just barely failing to meet the criteria for convergence, ending up 64 m away from the control by the simulation endtime. Even then, this run parallels the control for the majority of the run. Having multiple parameters converge, or nearly converge, can infer that both model initialisations and large-scale forcings are consistent with one another. This means that the advections and subsidence generated by MesoNH help to modify the BL development, so as to guide model estimates towards the observations at later initialisation times. The ML means for IOP03 in Appendix E.1 exemplify this point. The green curves pass through the initialisation points of the blue curves, which both in turn pass very close to the initialisation points of the

red curves. The #2 specific humidity curve even deflects downward around 11:00 UTC to match better with the control starting value. Such alignment is not present in BL height estimates, though both test runs are paralleling the control by 15:00 UTC.

It is worth noting here that the word "convergent" is being used slightly modified from its conventional definition, which would be that the difference between test and control is decreasing with time (i.e. test and control are

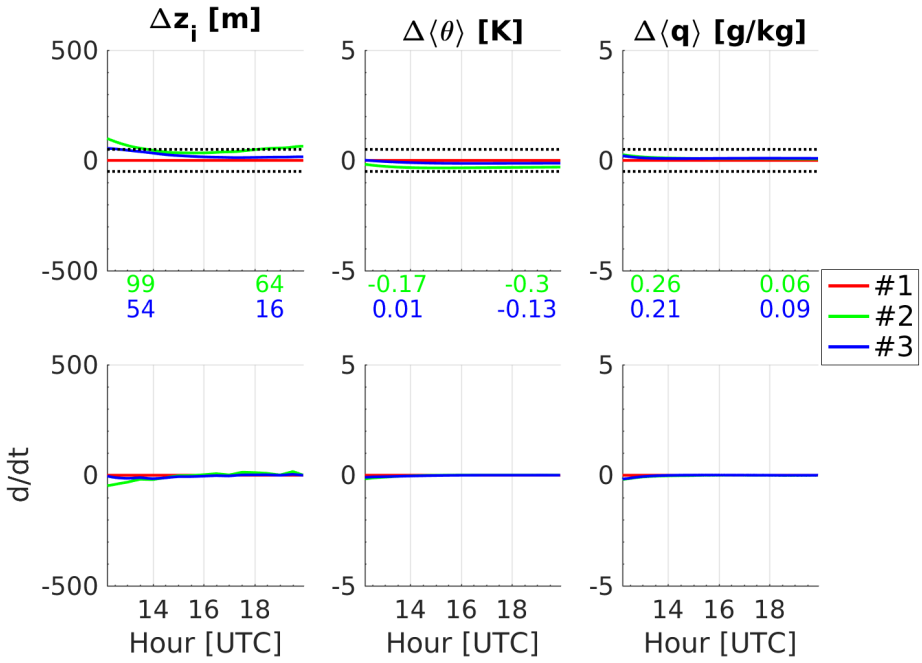

Figure 6.2: (Upper) Differences between test and control runs for BL heights, and ML means of potential temperature and specific humidity on IOP03. Text along bottom left of figures indicate differences between runs at start, while bottom right has the same at end, in matching colours. Threshold values for convergence criteria are dotted black lines above and below red control. (Lower) First derivatives of differences to test for paralleling criteria.

closer at the end than at the start). By this definition, BL heights for both #2 and #3 runs are convergent, as can be seen in Figure 6.2. However, the same definition would classify #3 $\Delta\langle\theta\rangle$ as divergent, simply because it's hardly possible to get any closer, and unrealistic to expect it to do so. Though this Experiment does focus on the sensitivity of CLASS to the choice of SUMO initialisation profiles, it is not a true sensitivity analysis, whereby a small perturbation/change is introduced to a single parameter. Initial displacements to any one of the three parameters are not perturbations to the initialisation, as the other two measures are able to change. It is for this reasoning that, for the purposes of this Experiment, convergent be redefined as the criteria in Section 6.1, and #2 Δz_i be classified as paralleling. Though this run does have the positive attribute of ending within the convergent threshold of #3 Δz_i, its classification is unaltered, since a consistent "ruler" (#1 aka "Vary" in Experiment 1) must be maintained. However, this extraneous result does help to reinforce the assertion that IOP03 is modelled under a well-balanced initialisation and evolves under stable large-scale forcings.

As IOP03 is one of the two days to develop under mostly negative FA divergence, it is possible that the enlarged BL is damping the generation of differences. This is especially possible for those that might arise in $\langle\theta\rangle$ or $\langle q\rangle$, as tendencies of these are inversely proportional to z_i (Equation 5.5, for example).

6.1.2 IOP05 (Figure 6.1; Appendix E.2)

Whereas IOP03 #2 BL height was the only parameter to not converge, the same parameter for IOP05 is the sole converger, and only just by 1 m. Neither $\Delta\langle q\rangle$ runs converge, despite #2 being very close, though both can be described as paralleling the control run, as can $\Delta\langle\theta\rangle$ runs. These last two are within the convergent threshold of each other, an encouraging sign as to

Table 6.1: Differences between test run and control, at start and at end for measured parameters, for IOP05

Test	Δz_i [m]		$\Delta\langle\theta\rangle$ [K]		$\Delta\langle q\rangle$ [g/kg]	
run	Start	End	Start	End	Start	End
#2	87	49	-0.64	-1.13	-0.25	-0.52
#3	14	72	-1.24	-1.55	-1.13	-1.41

the stability of this particular day. #3 Δz_i fails to meet the definition for convergence, though differences between run and control are ever decreasing from 17:00 UTC onwards. This non-zero rate disqualifies the run from fulfilling the first test for paralleling, however, it does pass the second test. This second test was designed with runs such as this one in mind, as given a longer simulation it is possible the run would achieve convergence. So to describe such a run as divergent would be counter-productive to the purpose of this experiment.

With 5 out of 6 parameters paralleling, and the shapes present in Figure 6.1 and Appendix E.2, it can be said that even though natural BL development and large-scale forcings create initial displacements, these displacements are not sufficiently large enough to accumulate and begin to feedback upon themselves. Of course, there are more parameters than just Δz_i, $\Delta\langle\theta\rangle$ and $\Delta\langle q\rangle$, where differences between the model runs may exist. Strengths of temperature and moisture inversions ($\Delta(\Delta\theta)$ and $\Delta(\Delta q)$) may also vary between runs, as can $\Delta\langle u\rangle$ and $\Delta\langle v\rangle$. However the previous assessment of ML profiles and large-scale forcings creating a stable configuration across all of IOP05, still stands.

6.1.3 IOP06 (Figure 6.1; Appendix E.2)

Of IOPs included in Experiment 2, IOP06 shows the most sensitivity to initialisation. As can be seen in Figure 6.3, only the blue #3 $\Delta\langle q\rangle$ run surpasses the convergence threshold, and it does so just within the last hour of the simulation. All other runs and parameters diverge, doing so decisively (see Figure 6.3). #2 $\Delta\langle q\rangle$ does intersect the control run, however it quickly spreads away and ends outside of the convergent threshold. The lead up to this undershooting, and overshooting in #2 $\Delta\langle\theta\rangle$ and Δz_i, begins between 18:30-19:00 UTC, corresponding with a weakening of subsidence, eventually turning to uplifting. Though all runs are experiencing the same FA forcings, the unique configuration of parameters, even those beyond the three in Figure 6.3, results in an entrainment velocity peak 3 times greater than what is

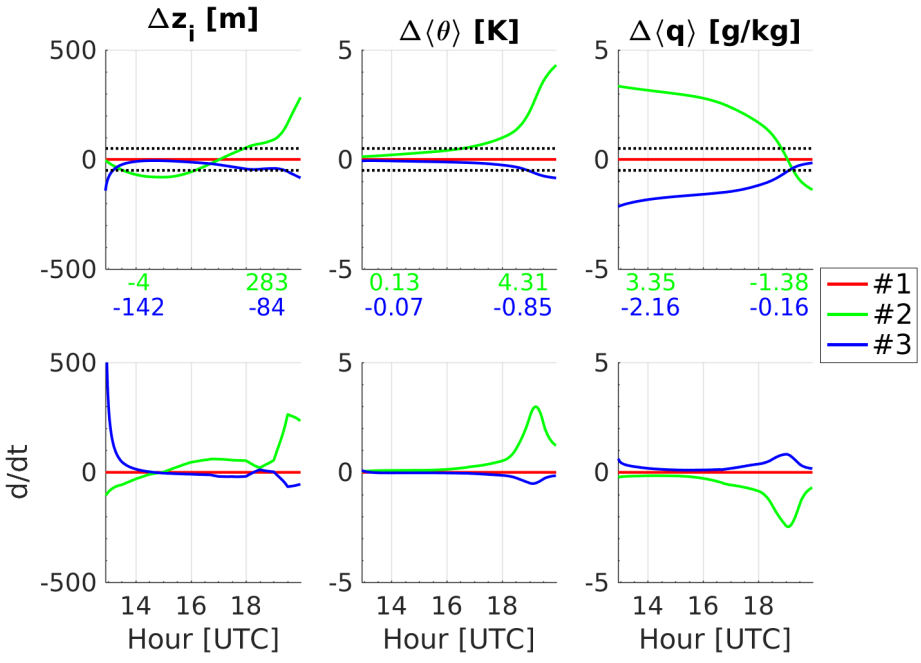

Figure 6.3: As in Figure 6.2, but for IOP06.

present in the control run. Entrainment velocity is representative of the exchange rate between FA and BL (Vilà-Guerau de Arellano et al. 2015, p.28). Higher exchange rates pull down more warm, dry air from aloft, and mix it into the BL, exactly as is seen in Figure 6.3 and Appendix E.2. A hotter BL means increased buoyancy, which enables the BL height to grow even faster, as is seen in Figure 6.1 and Figure 6.3. #2 seems to be an unstable regime of large-scale forcing and ML initialisations in CLASS, with initial differences growing on one another, and eventually leading to divergence.

#3 does not exhibit the same degree of instability, with one measured parameter achieving convergence, while the other two diverge, though to a lesser extent than #2. Overall, it is thought that the strength of the large-scale forcings, which are among the most extreme of the MesoNH IOPs, is causing separate initialisations to diverge from one another.

6.1.4 IOP09 (Figure 6.1; Appendix E.2)

Table 6.2: Differences between test run and control, at start and at end for measured parameters, for IOP09

Test	Δz_i [m]		$\Delta\langle\theta\rangle$ [K]		$\Delta\langle q\rangle$ [g/kg]	
run	Start	End	Start	End	Start	End
#2	-166	60	2.69	2.74	-0.02	0.22
#3	-443	-369	1.28	1.91	1.37	1.18

IOP09 includes the largest difference between initialisation times, spanning almost 7.5 hours. Despite this, the #2 $\Delta\langle q\rangle$ run still manages to reach convergence, though as can been seen in Appendix E.2, convergence involves maintaining near constant moisture. The #2 Δz_i run comes close to convergence, but is ultimately classified as paralleling. Three other runs are classified as paralleling: #2 $\Delta\langle\theta\rangle$, #3 $\Delta\langle q\rangle$, and #3 Δz_i. The #3 run is

characterized by the largest Δz_i displacements of the Experiment, approximately 400 m lower than the control run. This underestimation is due to strong FA divergence aloft and cold air advection in the morning around 07:00 UTC, both of which work to inhibit BL growth.

The only divergent run of IOP09 is #3 $\Delta\langle\theta\rangle$, which eventually runs near parallel with the control, but only for the last 2 hours of the simulation time. When compared to observations (Appendix E.2), however, the run has much better statistical metrics than the control, which has an anti-correlation with observations. The higher than control temperatures present in #3 $\Delta\langle\theta\rangle$ are likely due to the lower BL heights present in this run, increasing tendency of $\Delta\langle\theta\rangle$ (Equation 5.5). Though this improvement is noted, its presence does not alter its classification in this Experiment.

6.1.5 IOP10 (Figure 6.1; Appendix E.3)

Table 6.3: Differences between test run and control, at start and at end for measured parameters, for IOP10

Test	Δz_i [m]		$\Delta\langle\theta\rangle$ [K]		$\Delta\langle q\rangle$ [g/kg]	
run	Start	End	Start	End	Start	End
#2	15	48	0.68	0.56	-0.55	-0.36
#3	-3	105	1.92	1.38	-0.67	-0.12

The #2 run converges or nearly converges across all three measured parameters, with $\Delta\langle\theta\rangle$ falling 0.06 K outside the criteria threshold. The #3 run for the same is further outside the threshold, but as its displacement from the control run is ever-decreasing over the course of the simulation, it is classified as paralleling. As can be seen in Appendix E.3, $\Delta\langle\theta\rangle$ runs evolve with limited variability in temperature, as do $\Delta\langle q\rangle$ runs, which converge with the

control run. And though #3 Δz_i does not converge, the run does parallel the control for the latter half of the simulation.

In a similar fashion as IOP05, the large-scale forcings and ML initialisations neither seriously enhance nor substantially reduce initial displacements.

6.1.6 IOP11 (Figure 6.1; Appendix E.3)

Table 6.4: Differences between test run and control, at start and at end for measured parameters, for IOP11

Test	Δz_i [m]		$\Delta\langle\theta\rangle$ [K]		$\Delta\langle q\rangle$ [g/kg]	
run	Start	End	Start	End	Start	End
#2	-133	-327	1.90	2.11	-1.30	-0.93
#3	-30	17	-0.69	-0.76	0.79	0.92

IOP11 FA uplifting is comparable to that present in IOP03. But the fact that only one measured parameter (#3 Δz_i) converges, indicates that the combination of the large-scale forcings and the natural development of the BL are not as balanced as for IOP03. This is especially poignant, as the #3 test run only precedes the control run by less than half an hour, and yet $\Delta\langle\theta\rangle$ and $\Delta\langle q\rangle$ simply parallel the control. The same is true for $\Delta\langle\theta\rangle$ and $\Delta\langle q\rangle$ of the #2 test run. #2 Δz_i is the sole diverger, ending the simulation more than 300 m below the control. This divergence is strongest in the first half of the simulation, as growth of the control is outpacing the growth of #2. This can be explained with Equation 6.1, which describes the BL height growth rate.

$$\frac{\partial z_i}{\partial t} = w_e + w_s = w_e - Div(U_{FA})z_i \tag{6.1}$$

As $Div(U_{FA})$ is negative for the entire day, and initial w_e and z_i are both smaller in #2, the growth rate is inhibited, and hence the run diverges from the control and #3 run.

6.1.7 Summary

Of the six IOPs with subsidence and advection data, four (IOPs 05, 09, 10 & 11) show mostly **neutral** reactions to changes to initialisation, where measured differences **parallel** each other, or may even slowly improve. Three of these days display mostly linear evolutions of ML means, with the exception of IOP05, which impressively has all three runs paralleling each other, despite the non-linear nature of their development (see Appendix E.2).

Similarly, IOP03 has **convergence** across non-linear growth, though some initial displacements barely exceed the convergence threshold. Additionally, it is possible that uplifting present on this day suppressed the growth of differences, though comparable uplifting did not produce the same results for IOP11. Nevertheless, IOP03 exhibits **stable** reactions to changing initial conditions.

Alternatively, IOP06 shows signs of **instability** when differences in initial conditions are introduced. Due to the significant large-scale forcings present on this day, it is thought that these work to amplify small differences in initialisations, causing a cascade of changes which culminate in **divergence** by the end of the simulation.

7 Experiment 3: Areal Averaging Effects

While large-scale forcings can exert great impact on BL growth and development, surface processes can have extensive effects as well. The SH and LE fluxes and their relative importance are key variables for the convective growth. Surface horizontal land use and surface characteristics have a large influence on the magnitude of these fluxes. An asphalt parking lot will have very different diurnal fluxes as compared to an irrigated corn field. This influence becomes particularly important when modelling over an area of heterogeneous surface types, as this heterogeneity can induce secondary circulations which are superimposed on the BL scale circulation.. As MLMs assume no horizontal gradients in the BL, inhomogeneous surfaces pose a painstaking problem. One approach involves averaging the different fluxes of various surfaces in a particular area, thereby blending the various magnitudes into a representative value for SH, or LE, to pass to CLASS. However, this approach seems to address one problem, while simultaneously creating another: how large should the area be?

Answering such a question is no small task. The effects of heterogeneity *size* on the BL have been investigated by van Heerwaarden et al. (2014), and BLLAST heterogeneity has been treated as an advective process by Cuxart et al. (2016). However this chapter will not explicitly concentrate

on the size or shape of any one heterogeneity, nor transform their influence into advection, but moreso focus on how far the heterogeneity was from the launch site of the profiler. Figure 7.1 provides a basic illustration of this concept. Staying on a completely homogeneous surface (red field), fluxes do not vary across the same surface. When a profiler, such as a SUMO, is launched (white dot), one central question arises: How large must the distance (d) from a differing surface (blue field) be, for that surface to not influence the profile obtained? The axis units in Figure 7.1 emphasise this. Whether the differing surface was on the order of 20 m or 20 km away would affect the certainty of one's answer. The question can be rephrased to, given an area centred around a profile site, how does the proportion of surface type included in that area relate to its effect on the profile?

Such a question invokes thoughts of the "flux footprint", a concept whereby flux measurements taken at a point are not only affected by the surface immediately underneath the sensor, but also different surfaces upwind of the sensor. As Burba & Anderson (2010) succinctly summarize, "it is the area

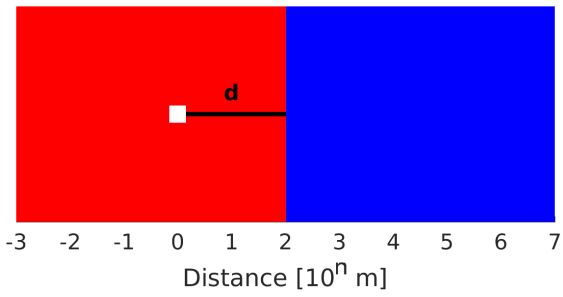

Figure 7.1: Simple example illustrating two surface types (red and blue), profile launch site (white dot) and distance between launch site and blue surface (d, black line). Units are of any single order of magnitude (e.g. 10^3 = km or 10^0 = m).

'seen' by the [measuring] instrument". Different approaches to calculating the size of this footprint have been taken (e.g. Schuepp et al. 1990, Wilson 2015), but generally they are dependent on the height of the sensor, wind speed, and wind direction. Given that a SUMO aircraft, or any profiler, is an ever-rising measurement platform, and the wind information obtained by SUMO is hourly at best, such a calculation involving heights and winds would prove complicated and ultimately likely inaccurate.

The method applied in this Experiment detaches from such dependency, and utilizes the "well-mixed" property of the MLM. By removing the possibility of horizontal gradients within the ML, the inclusion of all surface types, and associated heat fluxes, within a particular domain size will blend together and incorporate into a representative value for that domain. By changing the domain size over which fluxes were averaged, the effects of land surfaces further away from the launch site could be examined.

7.1 Experiment 3a: Coarse Areal Averaging Effects

7.1.1 Results

Figures 7.2 and 7.3 show the CLASS model estimates of BL height for this Experiment (Appendix F contains ML means). As evidenced by the position of the red or purple curves, BL heights for all days reach their maximums in the 4 km or 10 km runs. While differences between the runs do exist, they occur while still mostly preserving the shape of the day. IOPs 02, 04, 07 & 08 compare changes of areal averages in the 'A-Off/S-Off' model run, while the other IOPs utilize the 'A-Vary/S-Vary' scenario. Though it is an average over a 10 km $\times$ 10 km domain, the MesoNH data was also taken to be representative of large-scale forcings in the smaller domains for these days.

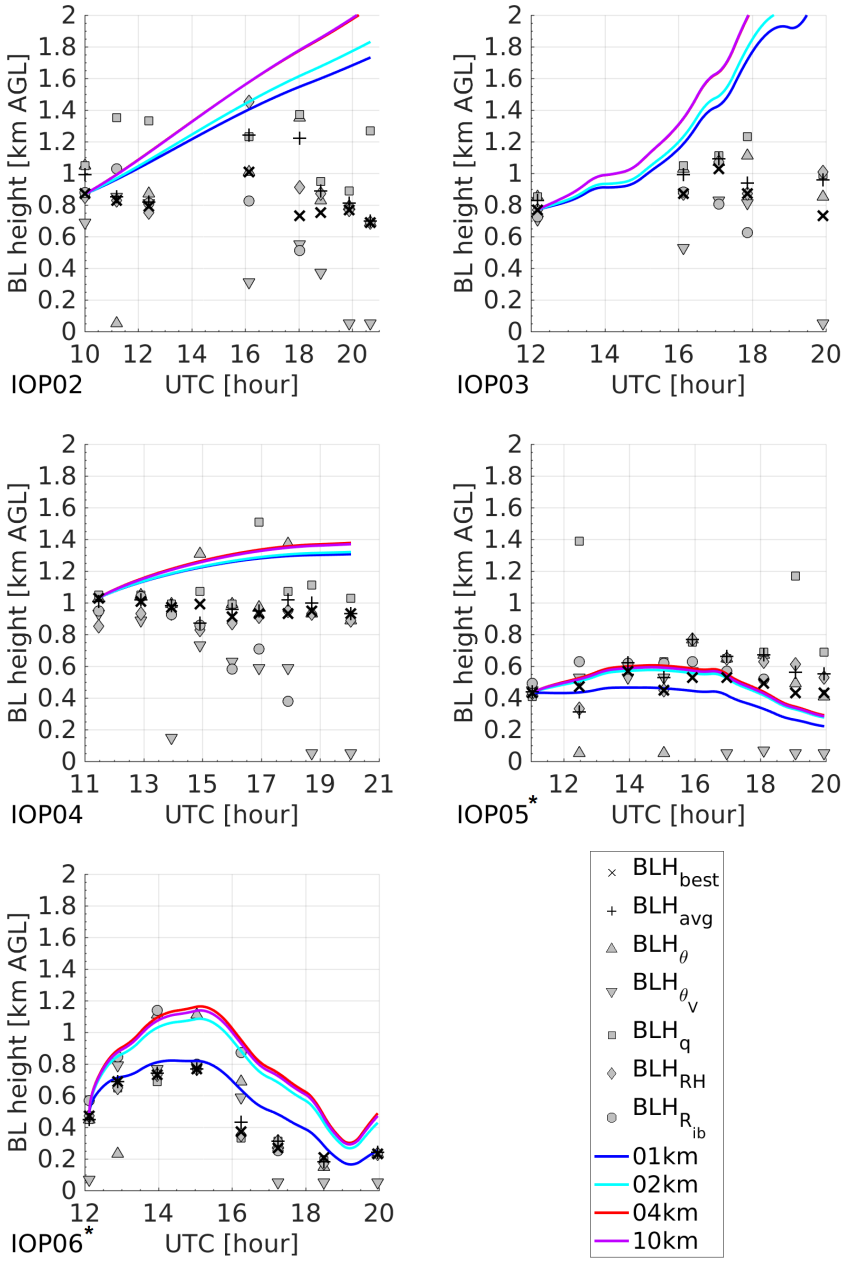

Figure 7.2: CLASS model runs for Experiment 3, IOPs 02-06. Later IOPs and description continued in Figure 7.3. IOPs marked with "*" indicate Site #2. (Jump to: Site #1: IOPs 02-04 & 08-11, Site #2: IOPs 05-07)

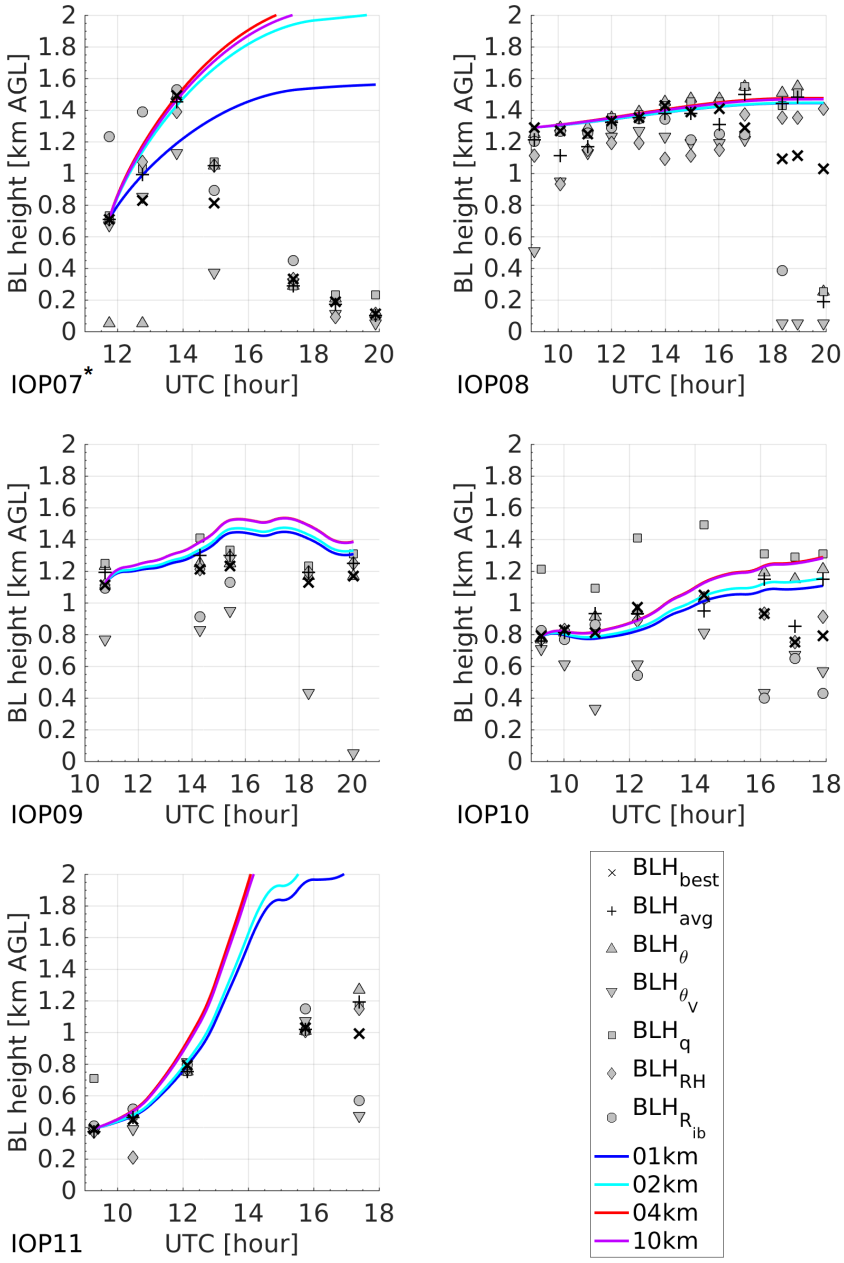

Figure 7.3: CLASS model runs for Experiment 3, IOPs 07-11. Legend entries for lines refer to the side lengths of the averaging box (domain), centred on the launch site, for that particular run. IOPs marked with "*" indicate Site #2. (Jump to: Site #1: IOPs 02-04 & 08-11, Site #2: IOPs 05-07)

7.1.2 Discussion

Recalling from Table 2.1, SUMO flights on IOPs 05, 06 & 07 were launched from Site #2, while the other IOPs launched from Site #1. The two sites are separated by approximately 4.5 km, leading to the potential for distinctly different surface proportions between the two sites, in particular at small domain sizes; Figure 7.4 shows the location of the two sites relative to the city of Lannemezan and each other. As smaller domains are characterised by higher levels of homogeneity, the effects will be discussed in the order of increasing domain size, starting with the 1 km scale, and ending with the 10 km run for continuity with respect to Experiments 1 & 2. As the surface heat flux maps use 30 m resolution, and therefore do not always divide evenly into the averaging domain sizes, actual domain sizes can differ by ±20 m. In order to properly evaluate the effects of area averaging, this discussion will

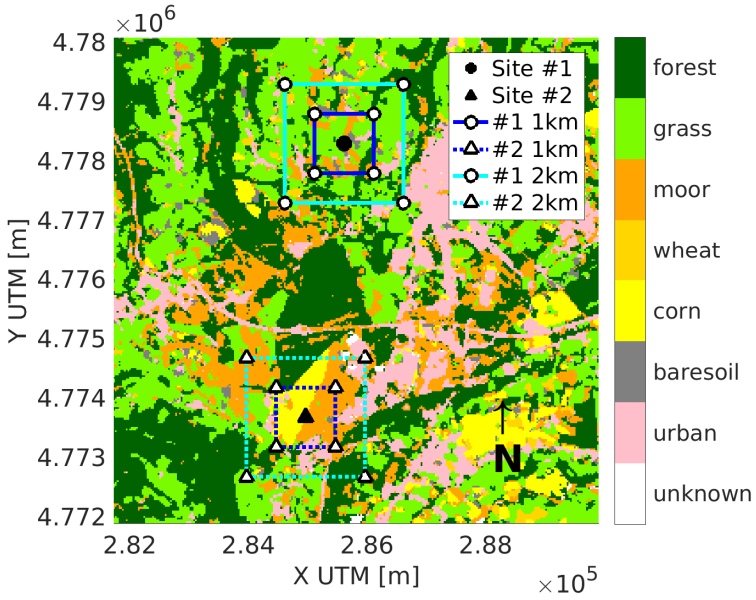

Figure 7.4: Site locations and surrounding land uses. The city of Lannemezan is the large pink area east of the sites.

separate focus into IOPs of Site #1 and those of Site #2, rather than each IOP day individually as was done for Experiments 1 & 2.

Site #1: IOPs 02-04 & 08-11 (Figures 7.2 & 7.3; Appendix F.1-F.3)

Site #1 is situated to the northwest of Lannemazan, immediately surrounded by predominantly grassland, moor and forest. As can be seen in Figure 7.5, the vast majority of IOPs have the largest SH flux over forest, while grass and moor are among the lowest and are of similar magnitude (Hartogensis 2015*b*). These last two make up about 76% of the 1 km box, whereas forest contributes only 10%. Figure 7.6 shows land use proportions across the four domains.

Expanding outwards to a 2 km domain, grass and moor proportions drop

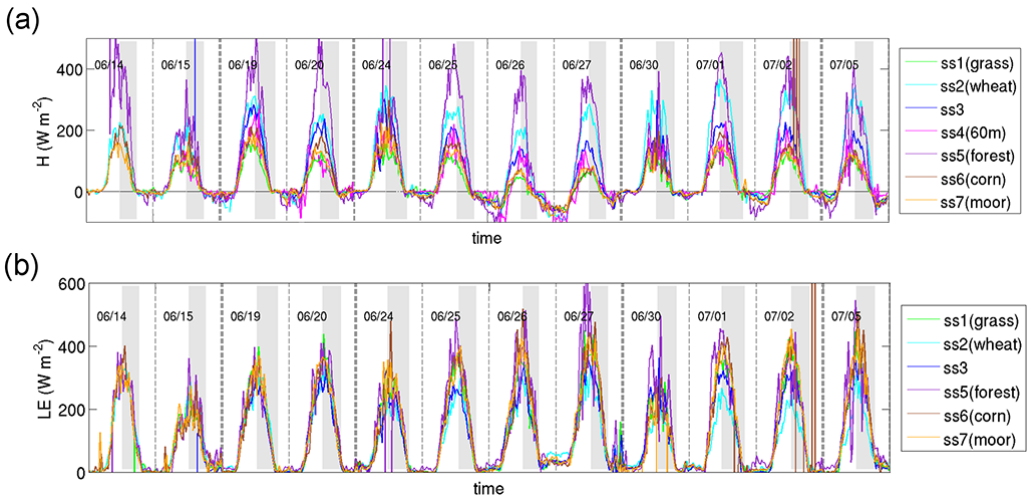

Figure 7.5: Evolutions of (a) sensible heat flux, H, and (b) latent heat flux, LE, measured over several surfaces at the different sites for IOPs 00-11 (left-right) (modified from (Lothon et al. 2014, p.10945))

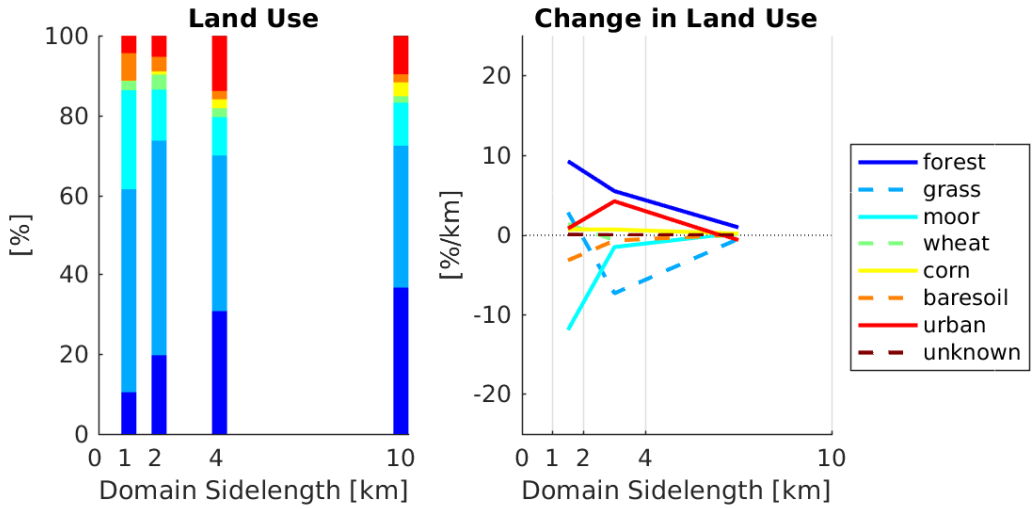

Figure 7.6: (Left) Land use proportions of Site #1. (Right) Rate of change of land use between domain sizes. Colours in legend apply to both figures.

to 67%, while forest has risen to 20%, its largest rate of increase across the four domains. With other surface type distributions remaining mostly the same, this approximately 10% switch to a higher SH flux can be seen as a small increase in BL height in Figures 7.2 & 7.3 (for Site #1 IOPs). Though this change in proportion is also applied to LE fluxes, there is less variability in this flux among the surface types; the exception being urban surfaces (not shown in Figure 7.5), which is consistently no more than half the magnitude of the other surface types.

Additionally, going from a 1 km box to a 2 km causes ML means (Appendix F) for potential temperature to increase, while specific humidity decreases. This is true across all Site #1 IOPs, apart from IOP08, where the converse occurs. IOP08 was characterised by cloudy sky conditions (Lothon et al. 2014, p.10943), resulting in less incoming solar radiation reaching the ground, as compared to the other IOPs. As well, rain was received during

the two days prior to IOP08, allowing for ample availability of surface moisture. When one compares the ratio of maximum LE to the sum of SH and LE, aka. the Evaporative Fraction (EF) (Figure 7.7a), IOP08 is the only IOP to show an increase from a 1 km to a 2 km domain. So of the reduced incoming solar radiation that did make it to the surface, more was being partitioned to LE. This dual effect can be seen in Figure 7.5 for IOP08 (06/30), with reduced forest SH. While the inclusion of more forest surface typically acted to raise the mean SH on other days, inclusion of the wetted woods and other surrounding area on IOP08 actually decreased the mean SH (effectively switching blue and cyan curves in Figure 7.7b), resulting in a lowered $\langle\theta\rangle$. Despite the reduced SH, BL heights stayed largely the same, even slightly increasing. The tendency of BL height is dependent on the entrainment velocity (recall Equation 6.1), which is proportional to the buoyancy flux,

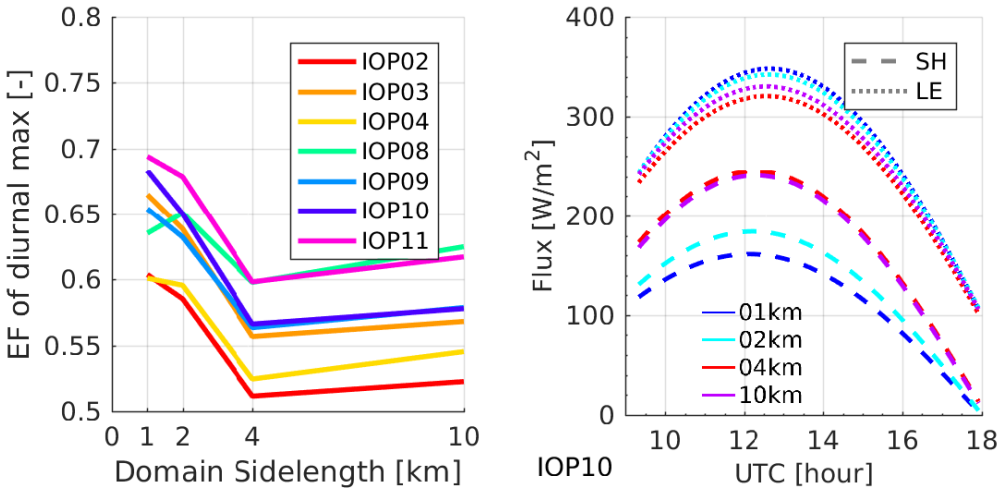

(a) EF of Site #1 IOPs

(b) Surface Heat Fluxes of IOP10

Figure 7.7: (a) EF of the diurnal maximum as a function of domain sidelength (b) An example of averaged surface heat flux evolutions over changing domain size.

$\overline{w'\theta'_v}$. The buoyancy flux is determined by both SH and LE (recall Equation 5.4). This signifies that the reduction in SH ($\approx$3.5 W m^{-2}) is more than compensated by the increase in LE ($\approx$10 W m^{-2}).

Increasing domain once again, to 4 km, the urban surface proportion shows its largest increase, up to 14%, along with forest (now at 31%), while grass and moor continue dropping (down to 49%). The cumulative effect of these relatively high SH surfaces causes the most rapid decrease of the EF across all IOPs, due to both large increases of SH and diminishing LE. Figure 7.7b shows the typical changes (IOP08 notwithstanding) in diurnal maximums of surface heat fluxes for Site #1 IOPs; notice the large jump in SH from 2 km to 4 km. SH reaches maximum values in the 4 km run while simultaneously achieving minimum LE. ML means for potential temperature and specific humidity follow accordingly, increasing and decreasing, respectively.

However, the degree of change in SH and LE are not equal, with SH increasing faster than LE is decreasing. This net increase in buoyancy flux leads to BL heights in the 4 km run being higher than in the 2 km, sometimes substantially, with mean differences between the two of up to 150 m and maximum differences of up to almost 300 m. When compared to observations, the 4 km model run contains most of the worst performing error metrics for z_i and $\langle\theta\rangle$ (see Figure 7.7a), as well as EF minimums across all model runs (see Figure 7.7). This EF minimum can help to explain the errors in modelled BL height, which was almost entirely overestimated in Experiment 1. As the combined energy from SH and LE stays mostly steady with the jump to the 10 km domain, falling EF would be due to increased partitioning to SH, which would result in a larger buoyancy flux, as its contribution to the flux is more significant than LE. A larger buoyancy flux means an even greater overestimation at 4 km. Though this difference from 10 km is small and 4 km BL heights can be thought of as approximate to the 10 km heights.

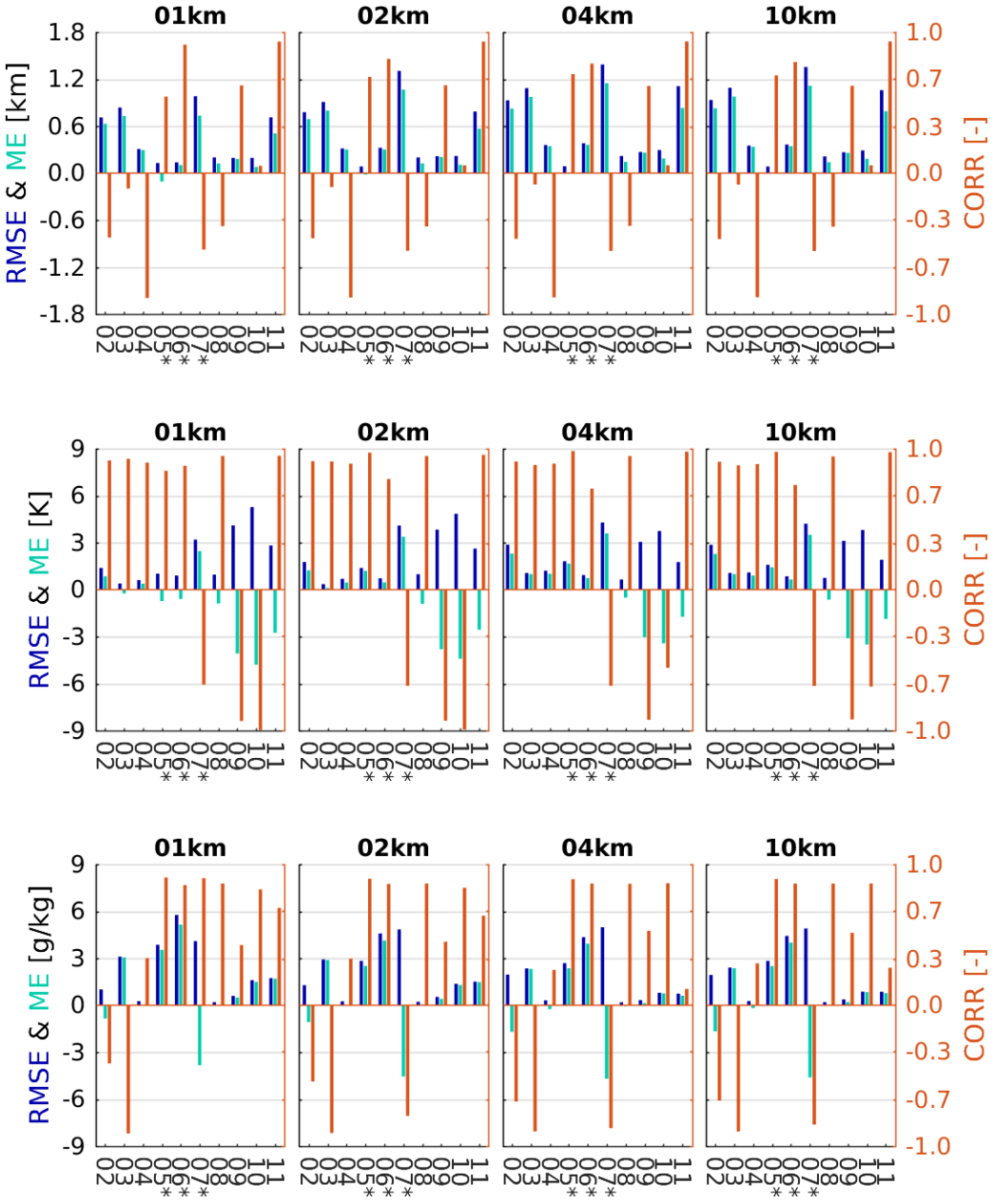

Figure 7.8: Statistical metrics for Experiment 3. X-Axis in each figure is IOP number. (Upper) z_i, (Middle) $\langle\theta\rangle$, and (Lower) $\langle q\rangle$. IOPs with profiles conducted at Site #2 are marked with "*".

To try and understand why BL heights remain generally steady from 4 km to 10 km domains, one must again analyse land use proportions and their rates of change between domain sizes. Most derivatives (Figure 7.6 (left)) approach zero, except for grass, forest and urban. By expanding well into the countryside to the northwest and completely engulfing the forest to the south and west, forest increases to 37% of the total area and becomes the dominant surface type. At the same time, urban land decreases to 9%, causing a cancellation between two of the largest sources of SH. Owing to its low SH, the slight changes occurring in grass proportions are insignificant, compared to forest and urban, and there is little net change. This observation is not only true for BL height, but also for $\langle\theta\rangle$ and $\langle q\rangle$.

Site #2: IOPs 05-07 (Figures 7.2 and 7.3; Appendix F.4)

Site #2 is situated to the southwest of Lannemazan, with immediate surroundings consisting mostly of moor, corn and urban lands. Moor makes up 55% of the 1 km box, while corn is 31% (see Figure 7.9). For Site #2 IOPs, SH of moor and corn are of similar magnitudes. Along the edges of the domain, urban surfaces contribute about 8%. While urban makes up less than a tenth of the total land area, the peak of its diurnal SH curve is on the order of 10 times that of moor/corn. Therefore its inclusion has a significant effect on the mean SH.

When increasing the domain to 2 km, jumps in BL height can be seen in Figures 7.2 and 7.3. Breaking down land usage, moor and corn percentages have dropped substantially to 32% and 16%. Meanwhile, urban has increased to 14%, while inclusion of surrounding wooded areas has caused forest representation to surge from 3% to 24%. This incorporation of surfaces with higher magnitude SH causes the mean SH to increase by more than 50% compared to the 1 km domain, while LE decreases slightly (Figure 7.10b). IOPs 06 & 07 actually show a doubling of SH peak from 1 km to 2 km, and

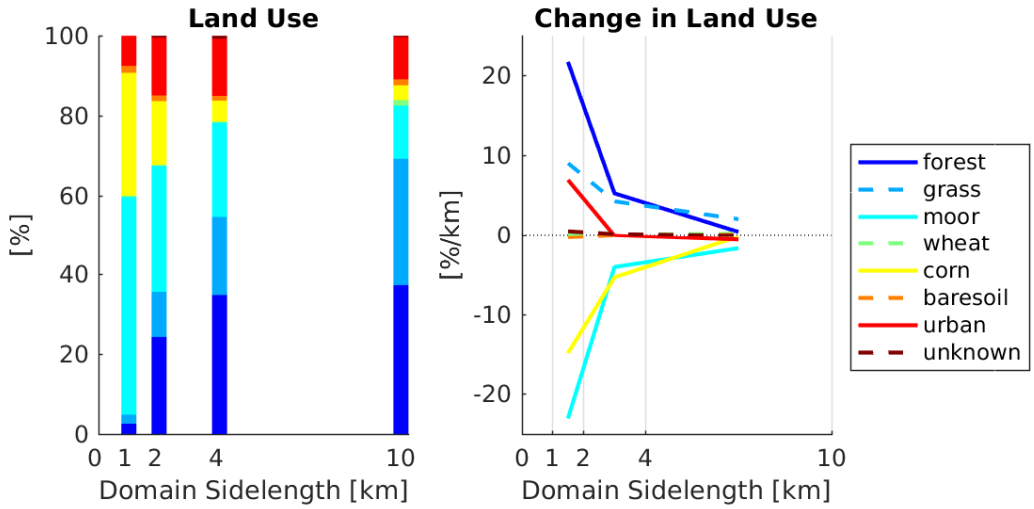

Figure 7.9: (Left) Land Use proportions of Site #2. (Right) Rate of change of Land Use between domain sizes. Colours in legend apply to both figures.

a more significant drop in LE, as compared to IOP05. This causes a steeper decline in EF (Figure 7.10a). And though all three curves in Figure 7.10a match in shape, IOPs 06 & 07 are elevated above IOP05, indicating more partitioning to LE. Whereas EF abnormalities in IOP08 could be explained by the possibility of changing ground conditions induced by the precipitation of the day before which provided ample moisture for LE, these three IOPs are on consecutive days, with no precipitation reported between (Nilsson 2011, Blay-Carreras 2014). However, IOPs 06 & 07 are distinguishable in a different regard: the highest observed temperatures of the campaign (see Appendix F.4). Using the bulk aerodynamic formula for SH (Equation 7.1) (Hartmann 1994, p.101), the strength of SH is dependent on the difference between the temperature of the surface (T_s) and the temperature of the ML (T_a).

$$SH = \rho c_p C_{DH} U (T_s - T_a) \tag{7.1}$$

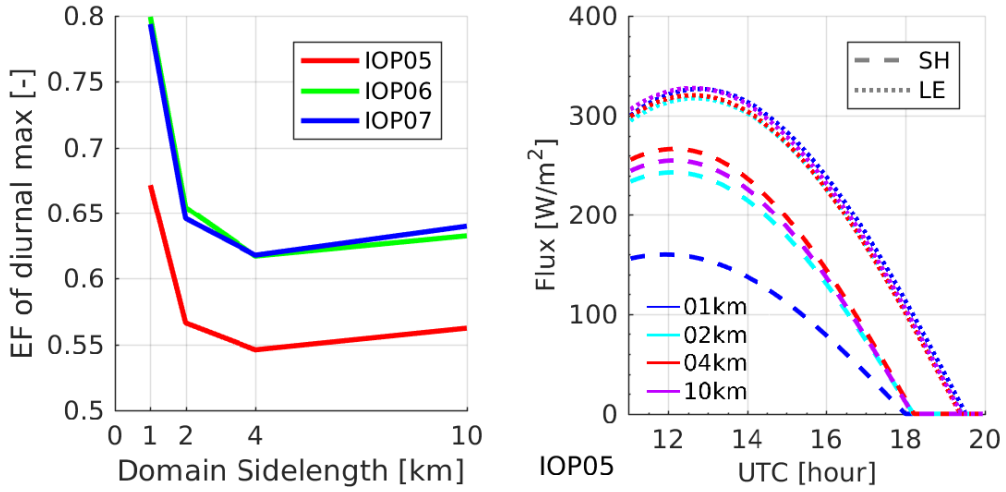

(a) EF of Site #2 IOPs

(b) Surface Heat Fluxes of IOP05

Figure 7.10: (a) EF of the diurnal maximum as a function of domain sidelength (b) An example of averaged surface heat flux evolutions over changing domain sidelength.

With increased T_a, the gradient between land and atmosphere decreases, and SH drops. So the raised EF for these days is driven by changing SH, rather than by LE, as was the case on IOP08.

Despite this dissimilarity in EF, all three days possess ML mean potential temperature acting accordingly with the increase of SH from 1 km to 2 km, climbing 1 K on average. While the decrease in LE is less substantial, $\langle q \rangle$ still decreases by around $0.5\,\mathrm{g\,kg^{-1}}$, as enhanced buoyancy and BL growth have entrained more dry air from aloft; the warming seen by $\langle \theta \rangle$ is also enhanced by this process. While such drying is beneficial for aligning the model run closer with observations on IOPs 05 & 06, decreasing $\langle q \rangle$ on IOP07 only further distances the model run from reality.

These same increases and decreases occur at the 4 km domain, although less dramatically, as forest proportions rise to 35% and urban stays level

at 14%. Spreading further into rural areas to the southwest, grassland has increased to 20%, and moor has dropped to 24%. These changes in proportion culminate to once again drive up the SH, pushing BL heights and $\langle\theta\rangle$ further from observations. As LE stays approximately the same as in the 2 km domain, the EF bottoms out during the 4 km model run, a commonality shared with Site #1. In fact, while some differences do exist between 4 km and 10 km runs, these changes are minor and the effects of increasing domain size to 10 km can be considered limited.

7.2 Experiment 3b: Fine Areal Averaging Effects

Expanding upon the results of Experiment 3a, an analysis with higher resolution was conducted across different domain sizes. The introduction of a finer grid interval was motivated by the goal of capturing at exactly which domain size the changes observed in Experiment 3a occurred. Starting with the 10 km domain, the box size was decreased by increments of 250 m, all the way down to 250 m.

In Experiment 3a, IOPs were differentiated between Site #1 or Site #2, which is the general vicinity from which they were launched. However, the average location of the daily SUMO profiles could vary slightly between IOPs at the same site, up to 250 m for Site #1. As the average flux calculation can be sensitive to the exact location used, especially at small box sizes, the particular location of each individual IOP was used as the center of areal averaging. The proportions reported in Experiment 3a are averages from between IOPs of each respective site, which only vary by 1 % to 2 %, and can be thought of being representative of the site when at the 1 km box size or larger.

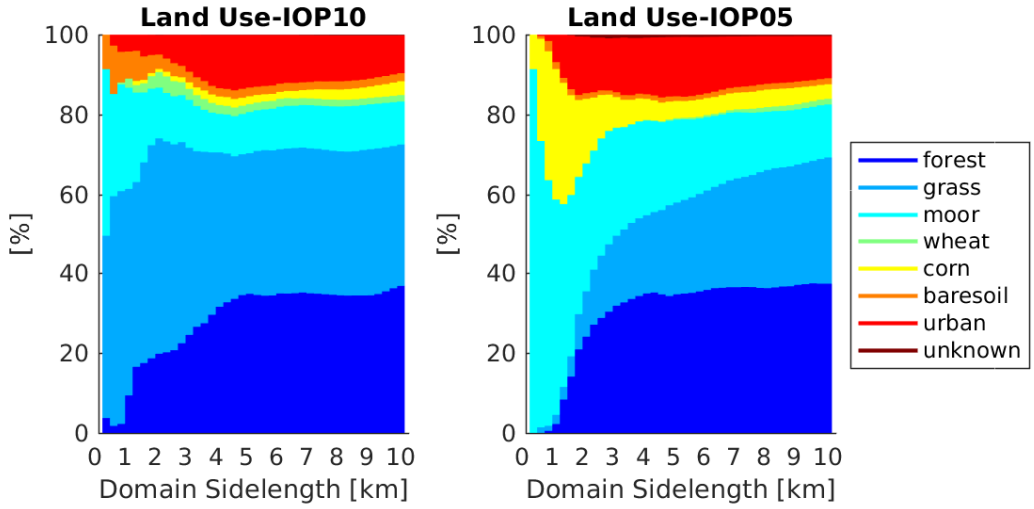

Figure 7.11: (Left) Land use proportions for IOP10 (Site #1). (Right) The same for IOP05 (Site #2).

Figure 7.11 shows how land use proportions change at the finer resolution for IOPs 10 & 05, corresponding to Sites #1 and #2, respectively. In addition to capturing the general features presented in Experiment 3a (Figures 7.6 & 7.9), this finer resolution allows one to study these changes in detail. Both IOPs (sites) display considerable variations in proportions at domain sizes smaller than 5 km, however rates of change are more pronounced for IOP05 (Site #2). The rapidly changing land use proportions directly impact the calculation of areal averaged surface heat fluxes, as shown in Figure 7.12a. Correspondingly, modelled BL heights react accordingly to those variations in fluxes, via the buoyancy flux (recall Equations 5.4 & 5.5). Figure 7.12b illustrates the effects on BL height evolution for IOP05, for all 40 model runs of Experiment 3b.

Though colours of the runs range from dark blue to dark red, the majority of variation occurs in the blue range, representing smaller domain sizes. However in Figure 7.12b, it appears as though domain sizes beyond 2 km are

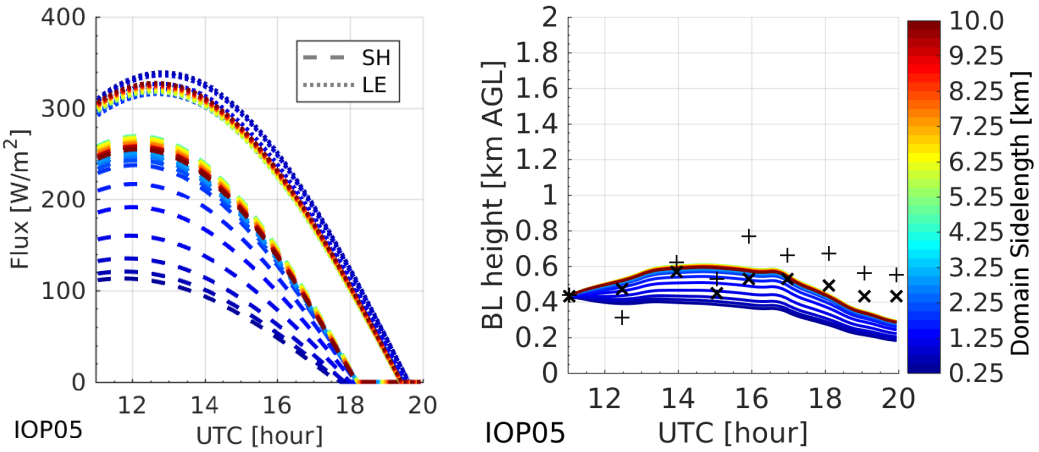

(a) Surface heat fluxes of IOP05 (b) BL height estimates of IOP05

Figure 7.12: (a) Surface heat fluxes of IOP05, and (b) CLASS outputs of IOP05 for Experiment 3b. Curve colours correspond to the matching domain sidelength on the colourbar.

overlaying on top of each other. Figure 7.13 provides an alternative visualisation, and better emphasises the differences between model runs. Coloured contours indicate the linearly interpolated difference between CLASS model BL height estimates and observed values, divided by the observed value at that time, referred to as the "relative difference" (Equation 7.2).

$$relative\ difference = \frac{z_{i,CLASS} - z_{i,OBS}}{z_{i,OBS}} \tag{7.2}$$

Red areas indicate CLASS overestimation, while blue areas are underestimation. The dashed contours indicate the ratio between domain sidelength and observed BL height at that time, providing a spatial aspect ratio, relating the horizontal extent of the domain size to the vertical depth of the BL. Finally, the solid line marks the time when the SH flux became zero in the CLASS simulations.

This visualisation can be related back to Figure 7.12b. Representing the

smallest domain sizes, the dark blue curves in Figure 7.12b are reflected in the steep gradient at the bottom of Figure 7.13, whereby small changes in domain size result in large changes of relative difference (i.e. BL height). These contours, mostly horizontal at small domain sizes in Figure 7.13, gradually begin to turn towards vertical at larger domain sizes. This begins around the 2 km domain, but is fully established by the 4 km mark. This better shows what was implied, but obscured by subsequent runs in Figure 7.12b;

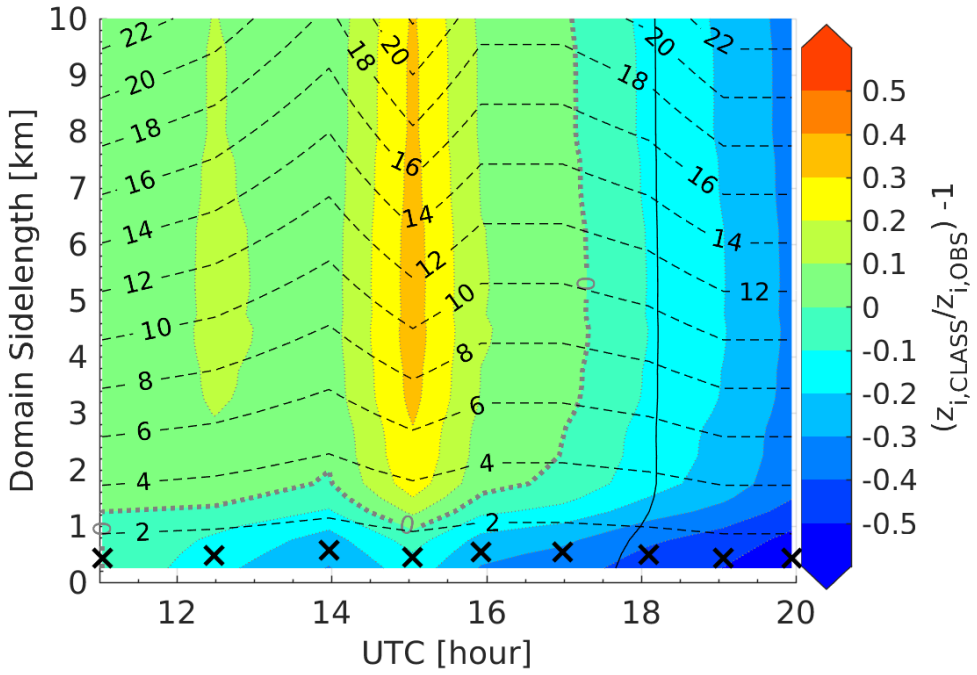

Figure 7.13: IOP05: (Coloured contours) Difference between modelled BL height and observations, divided by observed BL height. The zero contour is emphasised in bold. (Dashed contours) Ratio of domain sidelength to observed BL height. The solid vertical line indicates the time when SH approaches zero. × denote observed BL height (in km) and SUMO profile times.

namely, that relative differences develop independence from domain size at larger domain sizes. To see this domain size independence developing, one can take the derivative of the relative difference with respect to domain size (Figure 7.14). Rates of change peak between 1 km to 1.5 km, with small local maxima thereafter, before eventually settling near zero at 4.5 km. Similar patterns develop for the other IOPs, though IOPs launched from Site #1 have a second peak at 3 km, but also then approximate zero around 4.5 km or 5 km.

This distance can be thought of as a "MLM blending length-scale", specific to the BLLAST campaign area, where extents and flux characteristics of heterogeneities are sufficiently mixed so as to approximate a homogeneous surface. This is not to say that land use proportions remain steady across all domain sizes, as can be seen in Figure 7.11 (right), with grass and moor proportions continuously exchanging with one another all the way up to the maximum domain size. Rather, the surfaces involved change proportions while maintaining similar flux evolutions (Figure 7.12a), which in this case is due to grass and moor having very similar SH and LE (Figure 7.5).

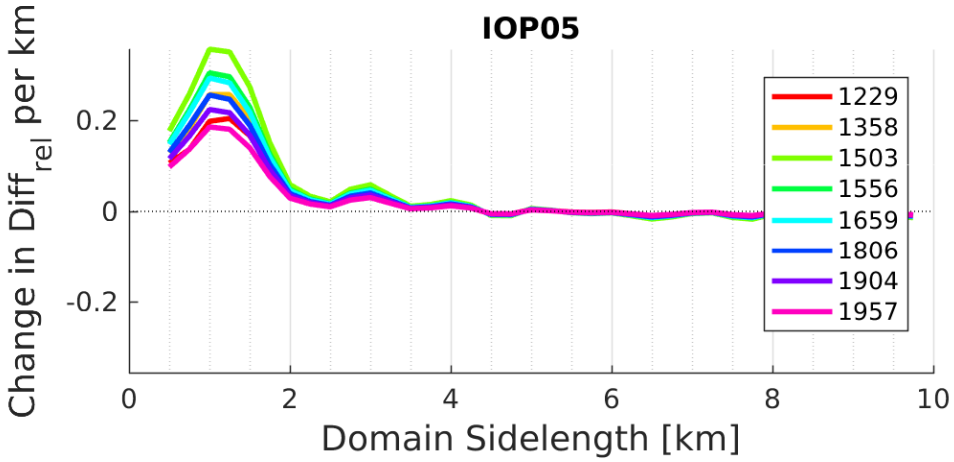

Figure 7.14: Rate of change of relative difference for IOP05

Figure 7.13 also showcases an interesting relationship between aspect ratio and the zero contour of relative difference. This contour remains between the 2:1 and 4:1 aspect ratio isolines for most of the simulation, only exceeding this threshold and turning to domain independence approximately an hour before the SH flux reaches zero. This contour can be interpreted as the evolution of the optimal domain sidelength, or the conceptual size of domain "felt" by the BL height. As contour lines are interpolations based on BL height differences between CLASS and observations, when the zero contour intersects the time of a SUMO profile, an optimal domain sidelength can be associated with the profile. Though IOP05 possesses the best and most examples of this intersection, three other IOPs present with at least one occurrence (Figure 7.15). However, examination of the direct relationship between BL height and optimal domain sidelength (left) reveals little in the way of a definitive trend across all occurrences. This is especially true for IOPs 05 & 06, two consecutive days with highly different trends.

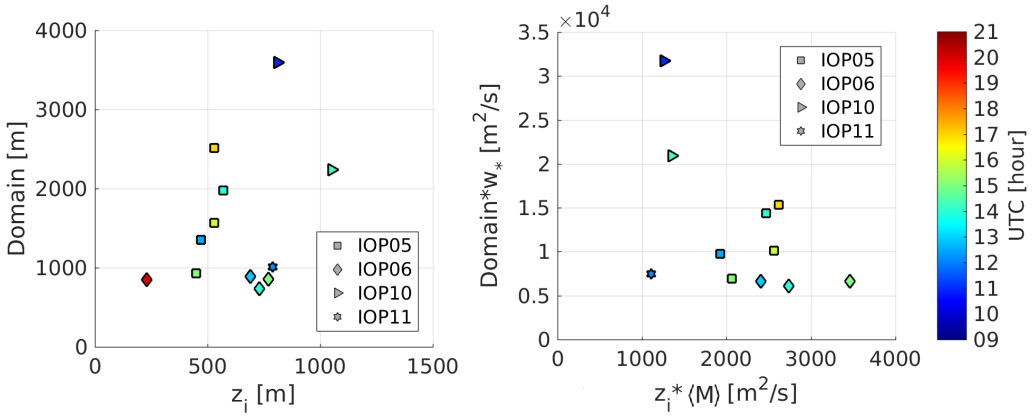

Figure 7.15: (left) z_i versus optimal domain size, (right) z_i multiplied by ML wind speed ($\langle M \rangle$) versus optimal domain size mulitiplied by the convective velocity scale (w_*). Marker colours denote time of the day.

Similarly to the flux footprint method, dependence on wind speed (but not direction) was introduced into further analysis via the convective distance, X^{ML} (Equation 7.3) (Stull 1988, p.484).

$$X^{ML} = \frac{Domain * w_*}{z_i \langle M \rangle} \qquad w_* = \left(\frac{g z_i}{\langle \theta_v \rangle} (\overline{w'\theta'_v})_s \right)^{\frac{1}{3}} \tag{7.3}$$

where $\langle M \rangle$ is the ML wind speed, and w_* is the convective velocity scale, which was found via interpolation of $(\overline{w'\theta'_v})_s$ between fine resolution grid points. Figure 7.15 (right) shows the relationship between the numerator and denominator of X^{ML}. Though no overall pattern emerges, a more favourable trend has developed for IOP05, indicating that inclusion of 3D motion (wind speed and convection) acted to better organise the data. And while such a result is encouraging, even with a more substantial trend amongst all IOPs, a direct expression for optimal domain size would still be unattainable in practical application, as $(\overline{w'\theta'_v})_s$, and therefore w_*, is a function of domain size.

7.3 Summary

Despite changing land use proportions in the areas surrounding Sites #1 & #2 combining with changes in ground and atmospheric conditions, surface heterogeneities achieve a "MLM blending length-scale" by 5 km during the BLLAST campaign. Beyond this size, areal averages of surface heat fluxes from the heterogeneities level out and show little variation up to 10 km. Although, flux magnitudes at these sizes act to overestimate BL heights for most days studied, with the best results occurring for smaller domain sizes.

While the outcomes presented for the "optimal domain size" focus on IOP05, this day is not typical for the IOPs studied, and represent one of the best cases of this Experiment. Overall, the "optimal domain size" appears in only four of the ten days studied, IOPs 05, 06, 10, & 11. The BL heights

are entirely overestimated for the other six days, seeming to imply that the optimal side length be an area smaller than 250 m. Given that many of these other six days have BL heights higher than 800 m, the implication that such a small area of land, with approximately a 1:3 horizontal-to-vertical ratio, would serve as the foundation of a developing BL seems unlikely. As well, four of those six (IOPs 02, 04, 07, & 08) do not have any large-scale forcings included. Additionally, the IOP03 BL is uplifted far above observations, while IOP09 has significantly underestimated ML mean potential temperature approximations, both of which draw the legitimacy of large-scale forcings into question. The same statements can be applied to IOPs 11 & 10, respectively, as even though each display some form of optimal size, occurrences are limited. And of the two remaining days with multiple instances of optimal size, IOPs 05 & 06, only IOP06 shows sensitivity with respect to initialisation. This leaves IOP05 as the sole non-divergent example, where introduction of large-scale forcings does not create anti-correlations of $\langle\theta\rangle$, nor induce uplifting which contradicts observations.

With such a modest sample size, definitive evidence of the optimal domain size concept can not be acquired. It is possible that this absence of evidence will eventually prove to be contributory evidence of absence, and the results of IOP05 are coincidental. Nevertheless, this can only be achieved with further research.

8 Conclusions & Outlook

This study utilized multiple datasets from the BLLAST campaign, and the CLASS model, to identify the effects of large-scale atmospheric and surface forcings on the development of the BL. To facilitate the extraction of BL properties from SUMO flights and the subsequent generation of ML profiles, a specially designed, and mostly autonomous, program was created. Once generated, the program passes initialisation profiles to CLASS, as well as time-dependent large-scale forcings, if so configured. In this way, a consistent methodology was applied to the analysis of almost all of the BLLAST IOPs, a previously unexplored line of research. This study draws from the past experience of Blay-Carreras et al. (2014) and Pietersen et al. (2015). While these works focused on an in-depth analysis and investigation of individual IOPs, this study has aimed to provide fundamental information regarding large-scale forcings for nearly all of the IOPs, in order to expedite further research. This has been accomplished through the categorization of IOPs into groups, depending on the influence of the underlying large-scale forcings. This categorization is extended by an analysis of the sensitivity of the corresponding CLASS simulations on the initialisation profiles (Table 8.1).

After investigating and describing the role played by large-scale forcings, and determining the sensitivity on the time of initialisation, the effects of surface heterogeneity were subject to deeper analysis. This was done via the introduction of areal averaging of surface heat fluxes, consolidating fluxes of

Table 8.1: Summary of large-scale forcing influence and sensitivity for each IOP. IOPs marked with "*" indicate those days for which MesoNH data was unavailable. Influences for these IOPs are then compared to observations, whereas other days compare "A-Off/S-Off" runs with "A-Vary/S-Vary". IOPs marked with "†" exhibited uplifting from MesoNH.

IOP	Calendar	Influence of Large-scale forcings			Sensitivity to
Date	Date	z_i	$\langle\theta\rangle$	$\langle q\rangle$	Initial Conditions
IOP02	19-Jun	Significant*	Noticeable*	Noticeable*	-
IOP03	20-Jun	Very Significant†	Noticeable	Significant	Convergent
IOP04	24-Jun	Noticeable*	Limited*	Limited*	-
IOP05	25-Jun	Significant	Noticeable	Significant	Paralleling
IOP06	26-Jun	Significant	Noticeable	Significant	Divergent
IOP07	27-Jun	Significant*	Significant*	Significant*	-
IOP08	30-Jun	Limited*	Limited*	Limited*	-
IOP09	01-Jul	Limited	Significant	Limited	Paralleling
IOP10	02-Jul	Noticeable	Significant	Noticeable	Paralleling
IOP11	05-Jul	Very Significant†	Significant	Significant	Paralleling

all incorporated land types into a single flux evolution that was representative of the area and day. Through this novel method, a "MLM horizontal blending length-scale" of around 5 km was discovered for all IOPs, suggesting that surface heat flux averages over areas larger than this produce similar MLM results as those at 5 km. This can have implications for future modelling efforts, providing potential validation for smaller domains at higher resolutions.

While the outcomes of this study are intriguing, it has not been without challenges. Even a simple concept such as determination of BL height elicits a multitude of criteria, each possibly giving different results. Visual estimates underwent multiple revisions for some IOPs, sometimes invoking non-trivial

differences. For IOPs with BL heights upwards of 1200 m, a 20 m (one height interval of SUMO profile) change to BL height could substantially change FA lapse rates, as SUMO profiles only reached 1600 m, leaving 400 m or less for calculating linear trends. Additionally, ML profiles passed to CLASS require a specific BL height, with no room for ambiguity. In the absence of a well-defined capping inversion, the exact determination of BL height was open to some subjectivity, and its precise placement would modify both lapse rate calculations and inversion strengths. Ultimately, the chosen BL height estimates were attempts at balancing automatic criteria, and visual cues; a fusion between science and skill.

Further research would be best served by the implementation of a robust, perhaps as-of-yet undiscovered BL height criteria, or the combination of multiple existing criteria, similar to the "BLH_{avg}" used in this study. Such research could also expand upon the results of this study, through the use of a circular area average of surface heat fluxes, rather than a simple square shape, thereby including only those surfaces equidistant to the profile site in the areal average calculation. The use of a square box size was deemed suitable in this study, as its use was moreso a proof of concept. And though the assumption of MesoNH large-scale forcings matching reality is a keystone of this thesis, it may not be the case for all IOPs. It may be that MesoNH is adept at recreating circumstances occurring during some IOPs, while failing to represent all processes occurring during others. Researching what these processes might be, could reveal a great deal about some of the complex interactions going on in the development of the BL.

Overall, the initial results from IOPs 05 & 06 demonstrate that their evolutions are well represented by MLM governing equations upon incorporation of MesoNH large-scale forcings and Hartogensis (2015*b*) surface heat flux maps. And it is through the use of time-dependent large-scale forcings that BL development for these two days is better recreated, though special treat-

ment should be given to IOP06 as it displayed sensitivity to initialisation. As well, despite not having large-scale forcing data, IOP08 development is also well represented under an advection and subsidence free regime. Therefore, while all IOPs in the BLLAST dataset are ripe for continued study, with the availability of the current MesoNH dataset it is believed that these three days are prime candidates for further MLM research.

Appendices

Appendix A:

CLASS Modification details

Working with the FORTRAN research version of CLASS, two logical inputs were introduced into the NAMOPTIONS initialization file (see Appendix B): `lvarying_wsls` and `lvarying_adv`. When set to `true`, these switches create a 1D array of length equal to `time` divided by `dtime`. In the FORTRAN environment, this is known as the `runtime`, which represents the number of timesteps executed by CLASS. After allocation, CLASS then reads an external file, generated at the same time as NAMOPTIONS, with `runtime` number of entries (see Section 4.1.4 for information regarding file generation). Finally, during the main `do` loop in CLASS, if the logic switch is set to `true`, then the constant value listed in NAMDYN is rewritten to the appropriate time varying value of the 1D array. The example code block below corresponds to time-dependent subsidence, but the same principles apply to potential temperature and specific humidity advections, as well as for time varying incoming solar radiation in the NAMRAD field of NAMOPTIONS.

```
  real, dimension(:), allocatable :: wsls_changing
    ...
! option for the dynamics
  namelist/NAMDYN/ &
```

```
    lvarying_wsls, &
    wsls, &
    ...

! Time-dependent subsidence
  if (lvarying_wsls) then
    allocate ( wsls_changing(runtime) )
    open(2,file = 'subsidence')
    read(2,*) wsls_changing
    close(2)
    write (*,*) 'wsls is varying in time'
  endif
    ...

do t=1, runtime
    ...

  if (lvarying_wsls) then
    wsls = wsls_changing(t)
  endif

! subsidence velocity (large-scale advection)
  ws=-wsls*zi(1)
```

Appendix B:

CLASS NAMOPTIONS example

```
&NAMRUN
!ML_props generated at: 18-Mar-2017 22:59:13
outdir               = 'IOP06-1207_A-vary_S-vary_MESONH_10km'
time                 = 28260
dtime                = 1
atime                = 60
atime_vert           = 1800
h_max                = 4000
latt                 = 43.0839
long                 = 0.35854
day                  = 177
hour                 = 12.1167
/

&NAMDYN
zi0                  = 470
beta                 = 0.2
lenhancedentrainment = .true.
lvarying_wsls        = .true.
wsls                 = 5.2e-05
lfixedlapserates     = .false.
c_fluxes             = .false.
pressure             = 950
wthetasmax           = 0.1765
thetam0              = 309.6
dtheta0              = 0.5
gamma                = 2.3e-03
lvarying_adv         = .true.
advtheta             = -2.9e-04
```

```
wqsmax                = 0.1346
qm0                   = 9.5
dq0                   = -2.8
gammaq                = 1.6e-04
advq                  = 3.7e-04
lencroachment         = .false.
!ladvecFT             = .false.
c_ustr                = .false.
z0                    = 0.433
uws0                  = 0.1284
vws0                  = -0.0172
um0                   = -4.2
vm0                   = 0.6
ug                    = -2.5
vg                    = -0.7
gammau                = 6.7e-03
gammav                = -7.4e-04
!lscu                 = .false.
!lrelaxdz             = .false.
!tau                  = 0
/

&NAMFLUX
offset_wt             = 0
offset_wq             = 0
function_wt           = 2
function_wq           = 2
starttime_wt          = -17188
endtime_wt            = 16496
starttime_wq          = -22128
endtime_wq            = 22823
/

&NAMSURFLAYER
lsurfacelayer         = .true.
z0m                   = 0.433
z0h                   = 0.433
/

&NAMRAD
lradiation            = .true.
!cc                   = 0.0
lvarySwin             = .true.
S0                    = 1376
albedo                = 0.2
/

&NAMSURFACE
```

```
llandsurface          = .false.
/
```

Appendix C:

Experiment 1: Advection & Subsidence Influence - ML means

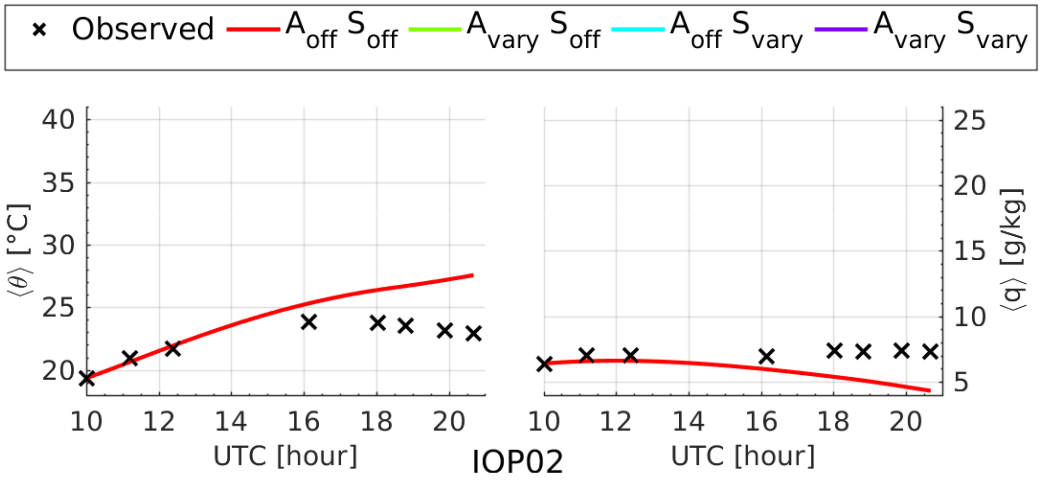

Figure C.1: Jump to: IOP02

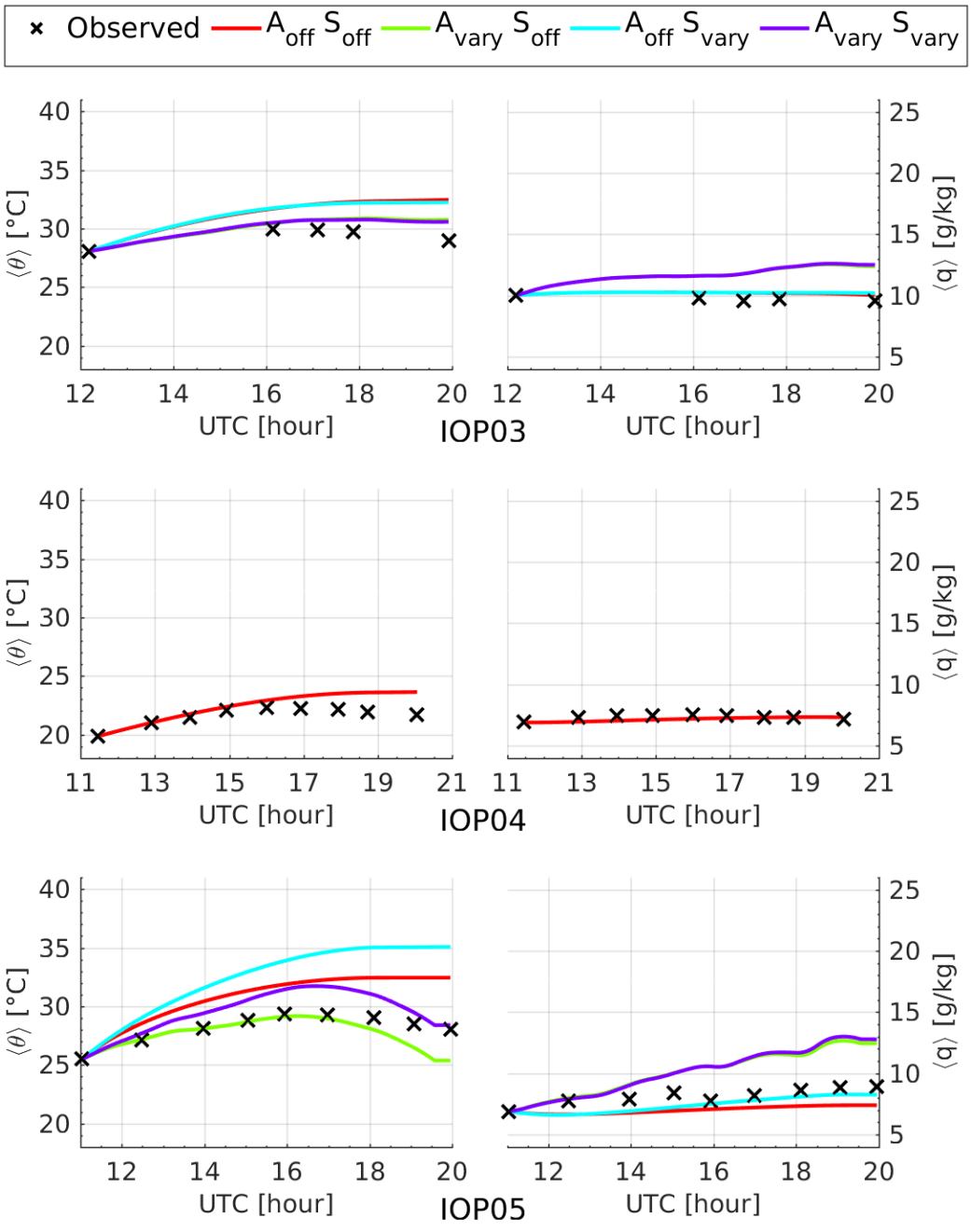

Figure C.2: Jump to: IOP03, IOP04, IOP05

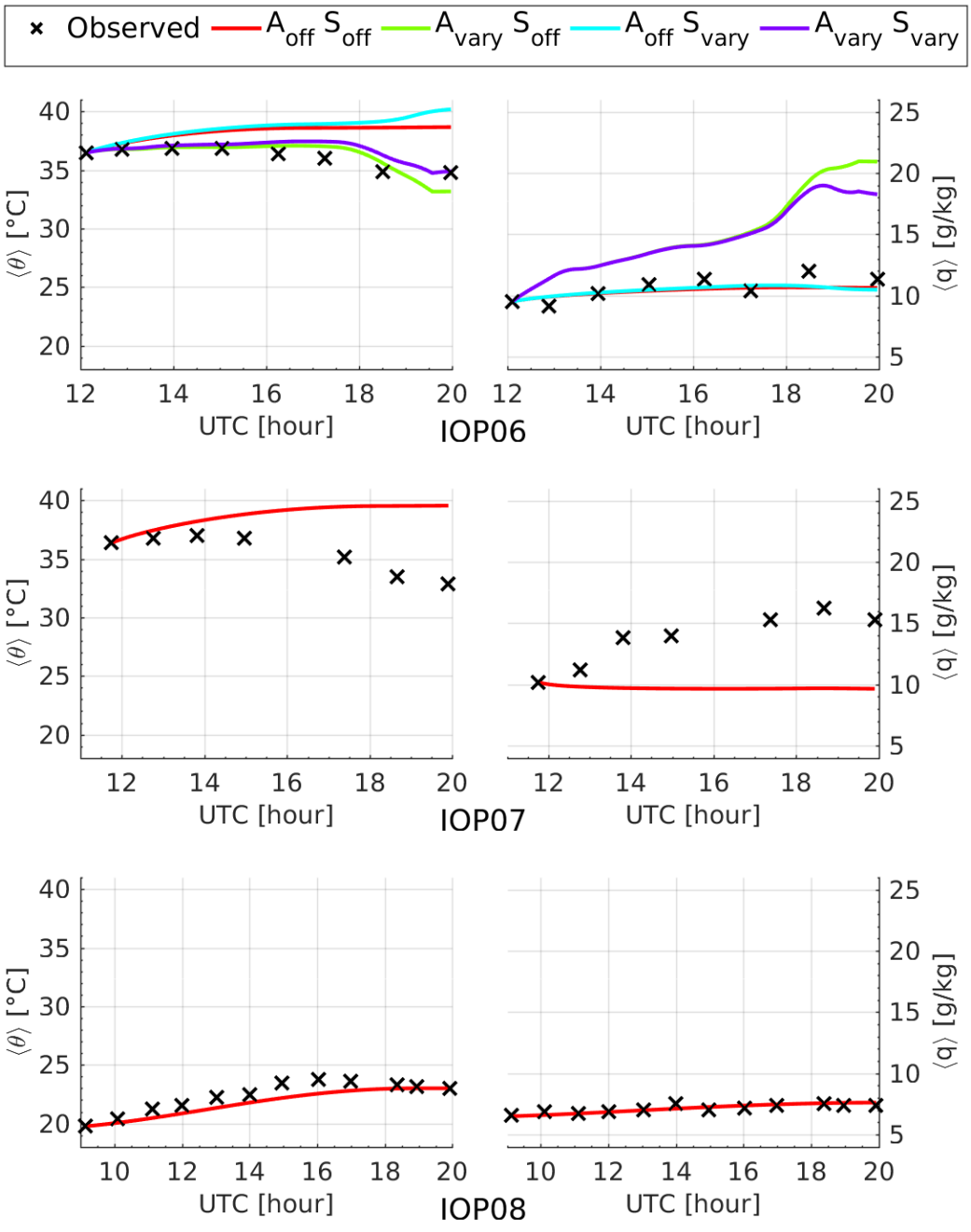

Figure C.3: Jump to: IOP06, IOP07, IOP08

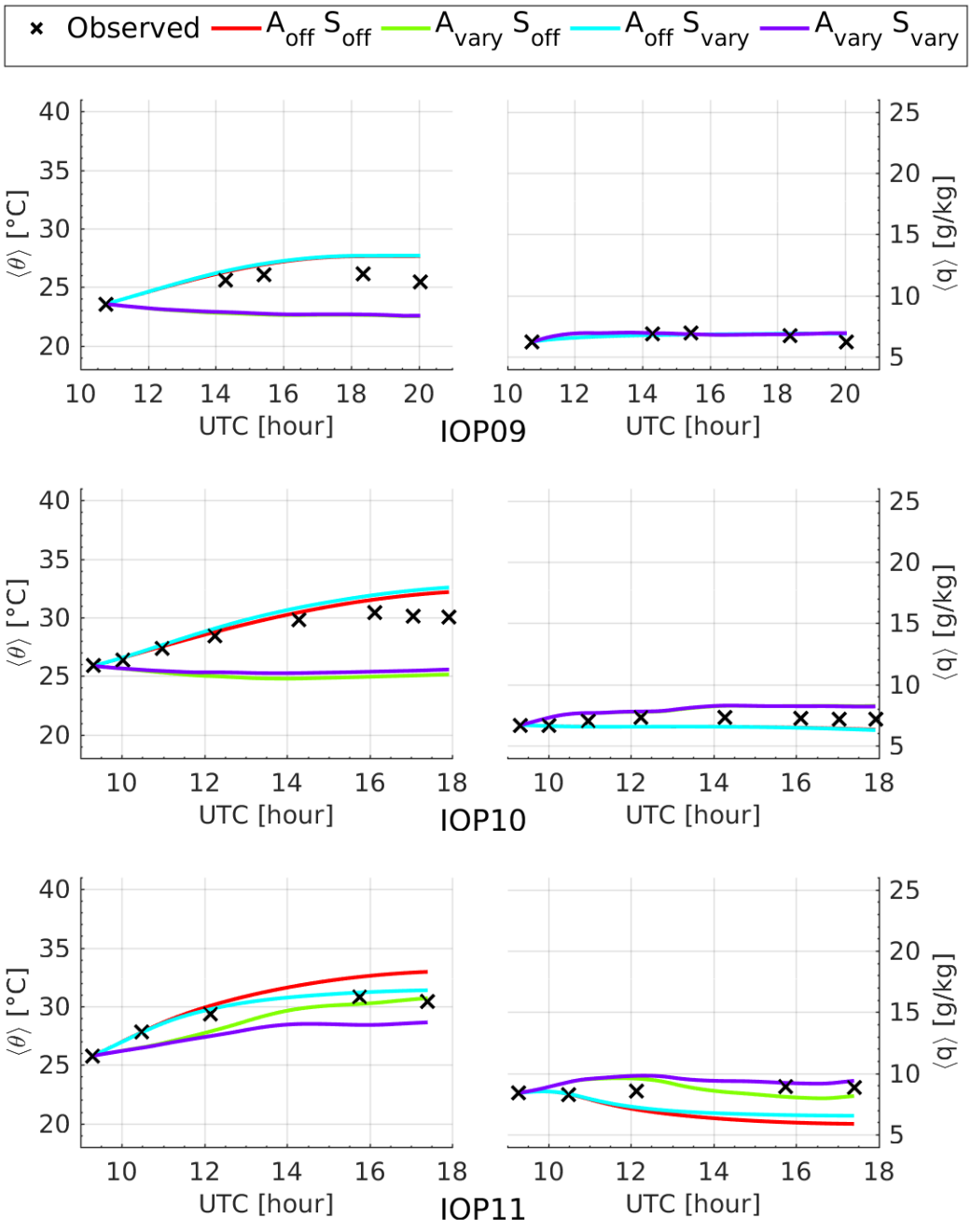

Figure C.4: Jump to: IOP09, IOP10, IOP11

Appendix D:

Experiment 1: Advection & Subsidence Influence - Statistical Metrics

Table D.1: Statistical metrics for Experiment 1: IOP02. Jump to: IOP02

	A-Off/S-Off		
	RMSE	ME	CORR [-]
z_i [m]	933	827	-0.468
$\langle\theta\rangle$ [K]	2.86	2.28	0.907
$\langle q\rangle$ [g/kg]	1.94	-1.67	-0.676

Table D.2: Statistical metrics for Experiment 1: IOP03. Jump to: IOP03

	RMSE	ME	CORR [-]	RMSE	ME	CORR [-]
	A-Off/S-Off			A-Vary/S-Off		
z_i [m]	538	514	0.258	415	391	0.286
$\langle\theta\rangle$ [K]	2.56	2.48	0.810	1.15	1.06	0.849
$\langle q\rangle$ [g/kg]	0.51	0.51	-0.423	2.35	2.33	-0.898
	A-Off/S-Vary			A-Vary/S-Vary		
z_i [m]	1264	1146	-0.072	1090	977	-0.0.82
$\langle\theta\rangle$ [K]	2.47	2.41	0.836	1.06	0.99	0.882
$\langle q\rangle$ [g/kg]	0.56	0.55	-0.822	2.40	2.37	-0.896

Table D.3: Statistical metrics for Experiment 1: IOP04. Jump to: IOP04

	A-Off/S-Off		
	RMSE	ME	CORR [-]
z_i [m]	351	336	-0.881
$\langle\theta\rangle$ [K]	1.10	0.90	0.891
$\langle q\rangle$ [g/kg]	0.27	-0.18	0.297

Table D.4: Statistical metrics for Experiment 1: IOP05. Jump to: IOP05

	RMSE	ME	CORR [-]	RMSE	ME	CORR [-]
	A-Off/S-Off			A-Vary/S-Off		
z_i [m]	696	666	0.174	498	475	0.182
$\langle\theta\rangle$ [K]	3.07	2.94	0.923	1.25	-0.80	0.726
$\langle q\rangle$ [g/kg]	1.23	-1.20	0.732	2.67	2.40	0.896
	A-Off/S-Vary			A-Vary/S-Vary		
z_i [m]	120	69	0.733	85	-6	0.693
$\langle\theta\rangle$ [K]	5.13	4.87	0.900	1.59	1.43	0.977
$\langle q\rangle$ [g/kg]	0.79	-0.71	0.795	2.83	2.50	0.896

Table D.5: Statistical metrics for Experiment 1: IOP06. Jump to: IOP06

	RMSE	ME	CORR [-]	RMSE	ME	CORR [-]
	A-Off/S-Off			A-Vary/S-Off		
z_i [m]	1231	1129	-0.462	975	891	-0.396
$\langle\theta\rangle$ [K]	2.51	2.21	-0.498	0.81	0.13	0.822
$\langle q\rangle$ [g/kg]	0.74	-0.33	0.834	5.26	4.52	0.821
	A-Off/S-Vary			A-Vary/S-Vary		
z_i [m]	510	487	0.664	364	343	0.788
$\langle\theta\rangle$ [K]	3.08	2.64	-0.698	0.85	0.65	0.743
$\langle q\rangle$ [g/kg]	0.73	-0.28	0.787	4.43	4.00	0.863

Table D.6: Statistical metrics for Experiment 1: IOP07. Jump to: IOP07

	A-Off/S-Off		
	RMSE	ME	CORR [-]
z_i [m]	1355	1116	-0.553
$\langle\theta\rangle$ [K]	4.21	3.50	-0.683
$\langle q\rangle$ [g/kg]	4.90	-4.61	-0.846

Table D.7: Statistical metrics for Experiment 1: IOP08. Jump to: IOP08

	A-Off/S-Off		
	RMSE	ME	CORR [-]
z_i [m]	213	139	-0.380
$\langle\theta\rangle$ [K]	0.75	-0.64	0.945
$\langle q\rangle$ [g/kg]	0.20	0.02	0.863

Table D.8: Statistical metrics for Experiment 1: IOP09. Jump to: IOP09

	RMSE	ME	CORR [-]	RMSE	ME	CORR [-]
	A-Off/S-Off			A-Vary/S-Off		
z_i [m]	410	401	0.491	275	267	0.528
$\langle\theta\rangle$ [K]	1.44	1.32	0.928	3.18	-3.16	-0.934
$\langle q\rangle$ [g/kg]	0.36	0.15	0.460	0.37	0.20	0.499
	A-Off/S-Vary			A-Vary/S-Vary		
z_i [m]	400	390	0.578	267	258	0.620
$\langle\theta\rangle$ [K]	1.49	1.38	0.932	3.12	-3.10	-0.921
$\langle q\rangle$ [g/kg]	0.36	0.15	0.467	0.37	0.20	0.514

Table D.9: Statistical metrics for Experiment 1: IOP10. Jump to: IOP10

	RMSE	ME	CORR [-]	RMSE	ME	CORR [-]
	A-Off/S-Off			A-Vary/S-Off		
z_i [m]	580	471	0.055	249	190	0.154
$\langle\theta\rangle$ [K]	1.18	0.91	0.981	4.16	-3.81	-0.891
$\langle q\rangle$ [g/kg]	0.67	-0.63	-0.559	0.88	0.84	0.851
	A-Off/S-Vary			A-Vary/S-Vary		
z_i [m]	636	474	0.012	290	182	0.055
$\langle\theta\rangle$ [K]	1.47	1.19	0.984	3.81	-3.50	-0.688
$\langle q\rangle$ [g/kg]	0.69	-0.64	-0.536	0.87	0.84	0.863

Table D.10: Statistical metrics for Experiment 1: IOP11. Jump to: IOP11

	RMSE	ME	CORR [-]	RMSE	ME	CORR [-]
	A-Off/S-Off			A-Vary/S-Off		
z_i [m]	489	406	0.978	225	142	0.953
$\langle\theta\rangle$ [K]	1.55	1.22	0.981	1.06	-0.80	0.935
$\langle q\rangle$ [g/kg]	2.21	-1.84	-0.957	0.90	0.12	-0.670
	A-Off/S-Vary			A-Vary/S-Vary		
z_i [m]	1802	1408	0.943	1058	791	0.934
$\langle\theta\rangle$ [K]	0.54	0.41	0.994	1.91	-1.87	0.976
$\langle q\rangle$ [g/kg]	1.77	-1.48	-0.943	0.86	0.77	0.266

Appendix E:

Experiment 2: Sensitivity to Initial Conditions - ML means

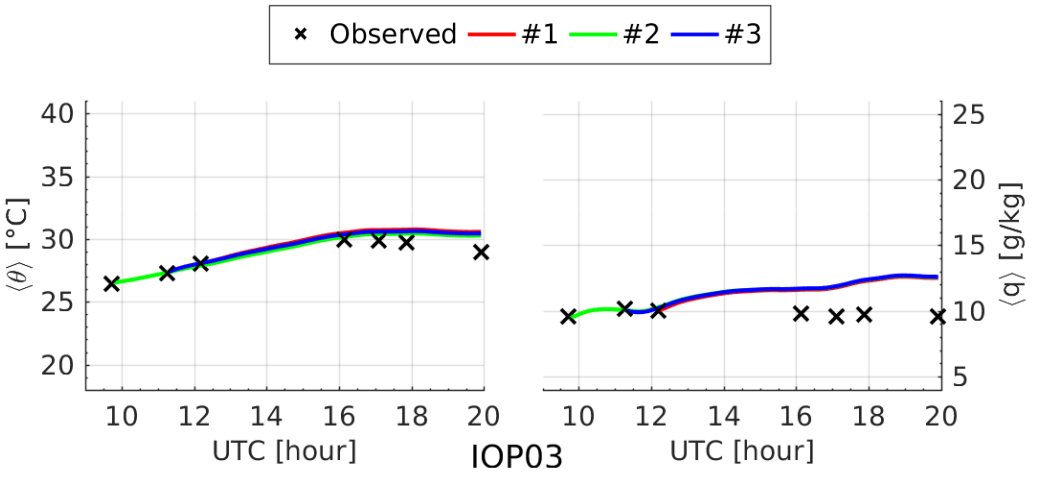

Figure E.1: Jump to: IOP03

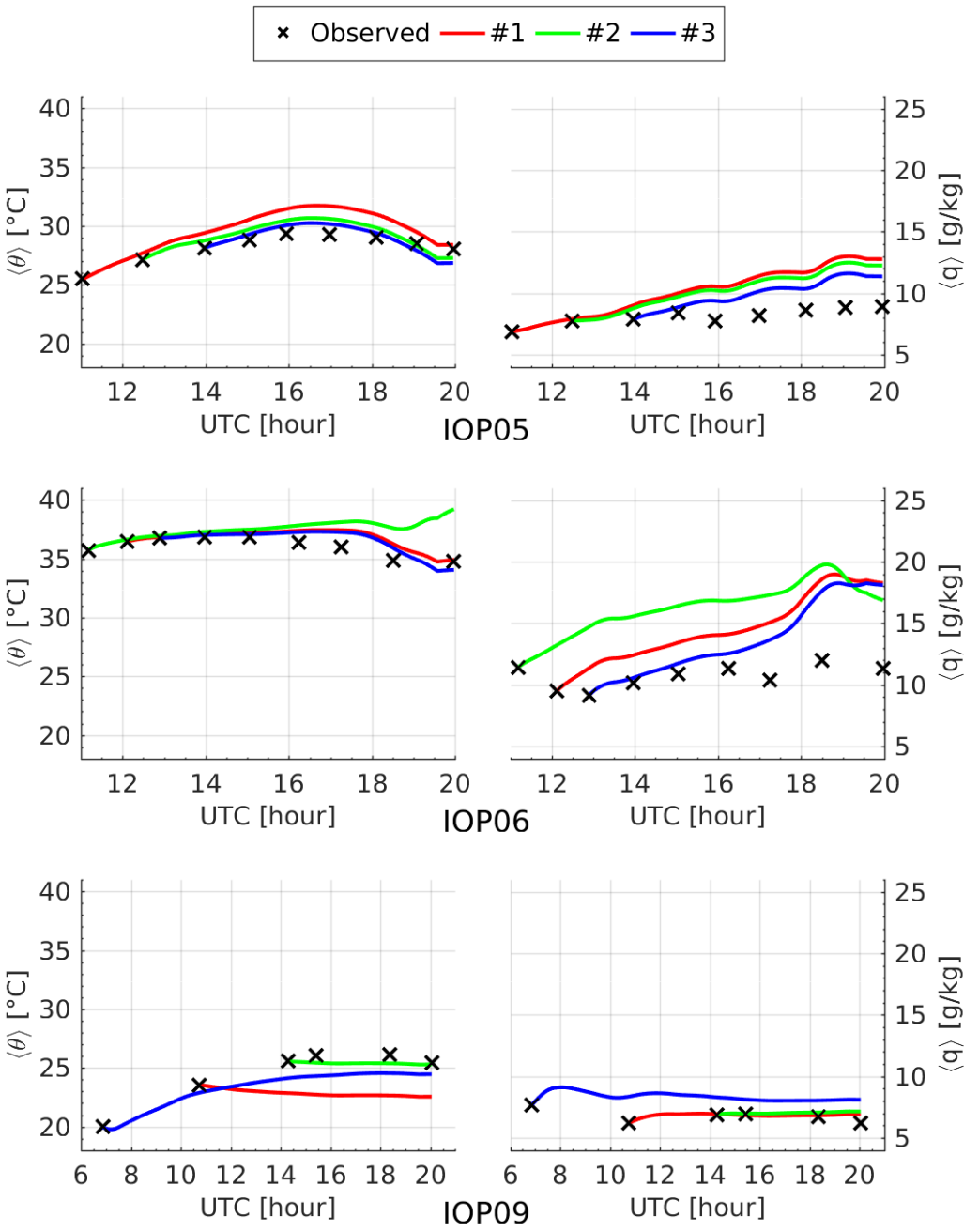

Figure E.2: Jump to: IOP05, IOP06, IOP09

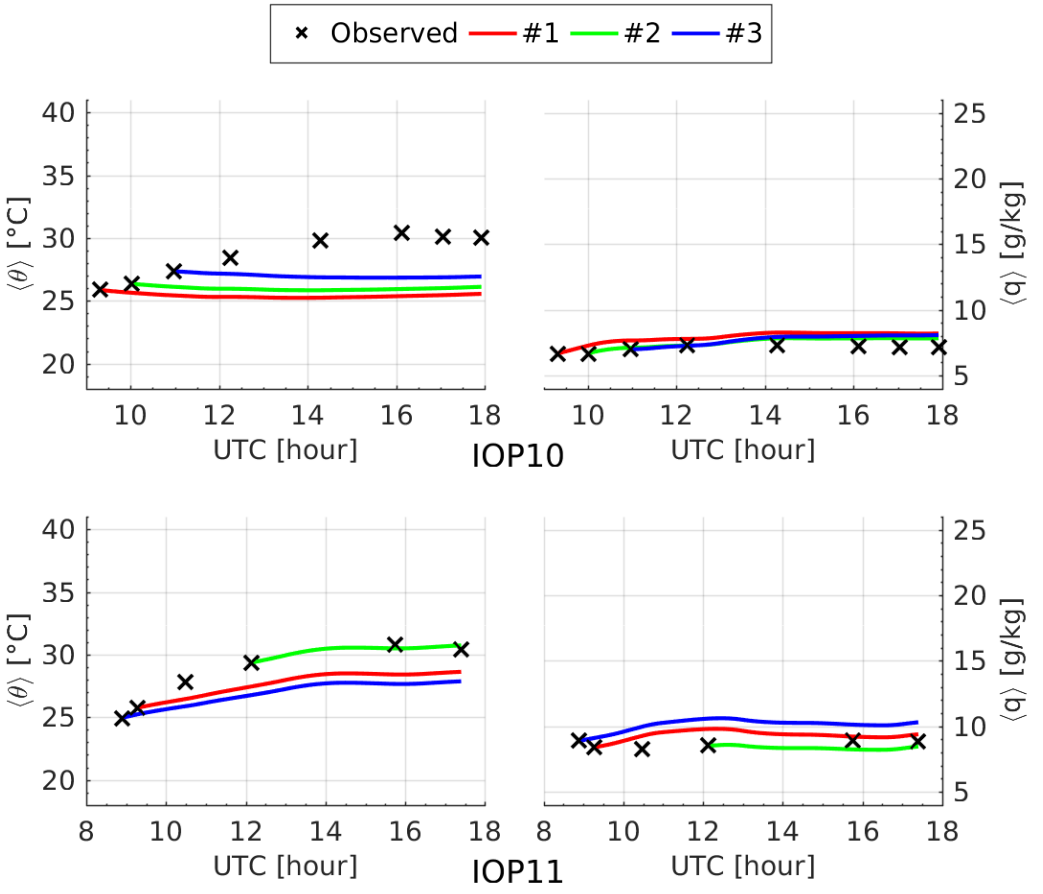

Figure E.3: Jump to: IOP10, IOP11

Appendix F:

Experiment 3a: Coarse Areal Averaging Effects - ML means

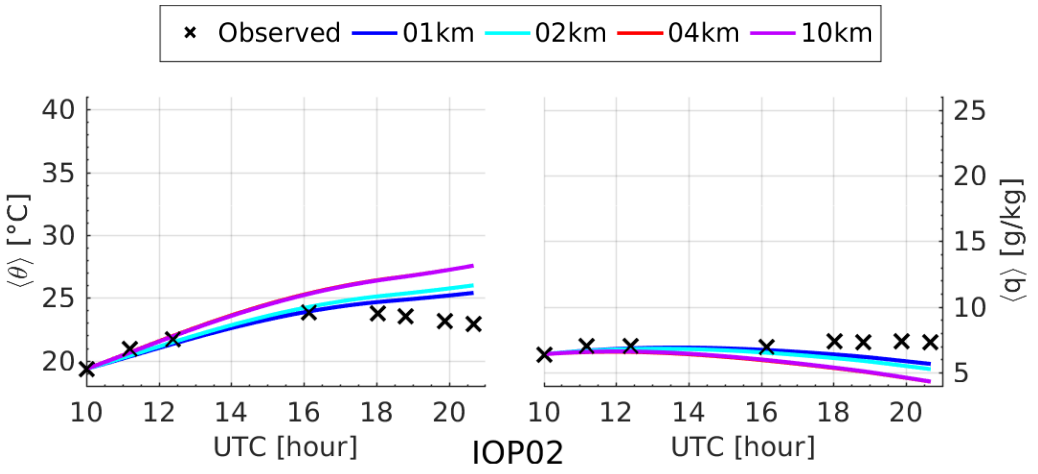

Figure F.1: Jump to: Site #1: IOPs 02-04 & 08-11

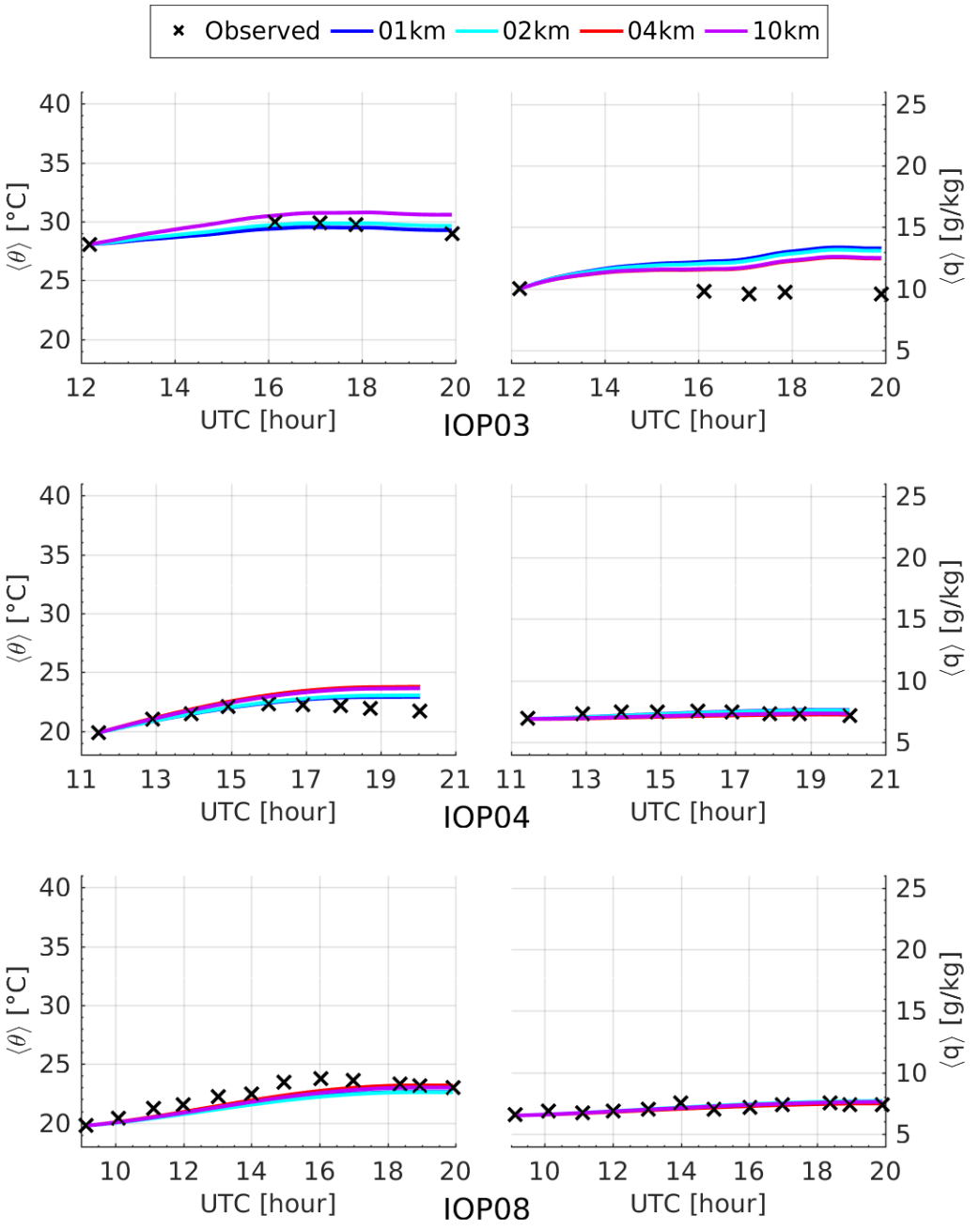

Figure F.2: Jump to: Site #1: IOPs 02-04 & 08-11

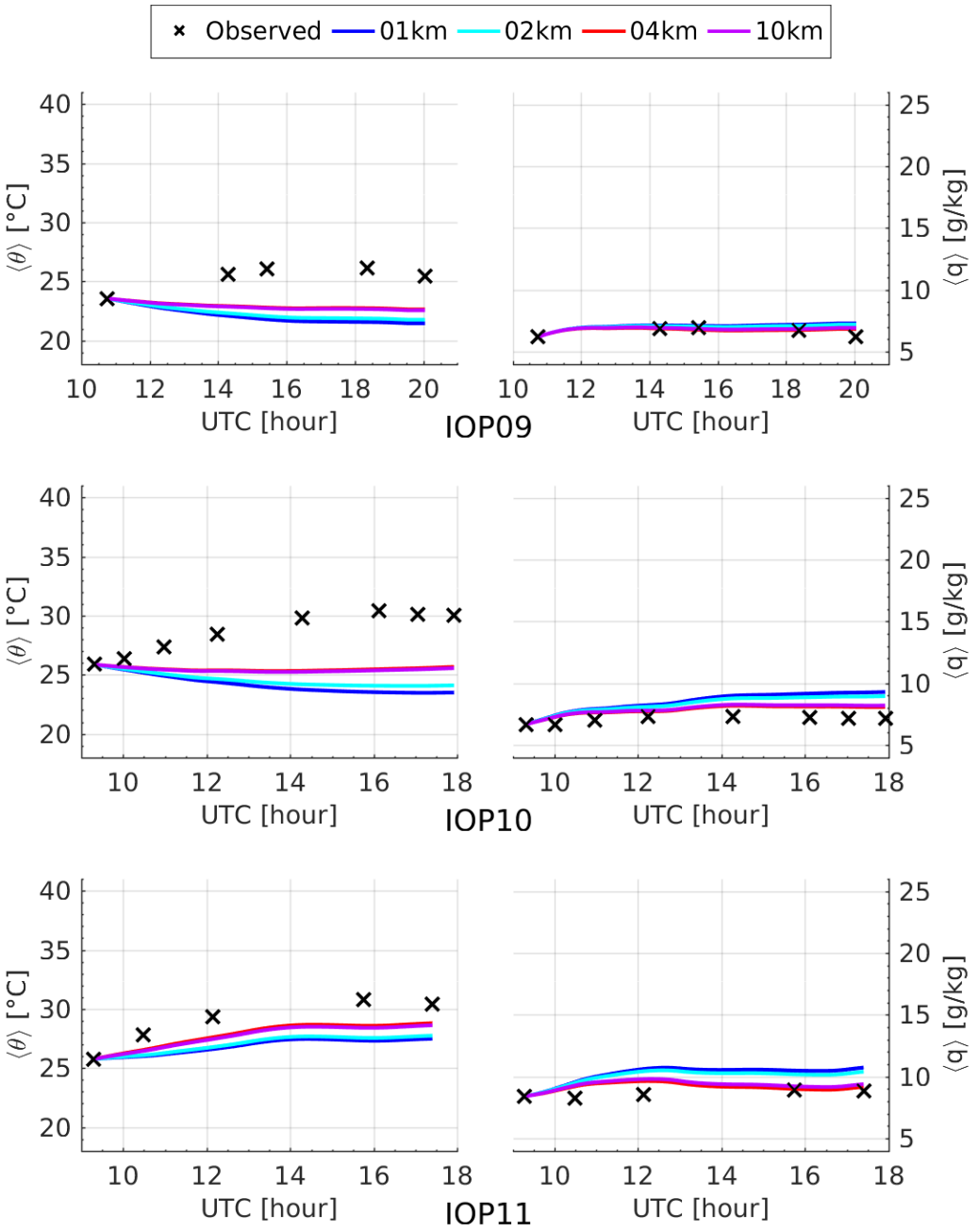

Figure F.3: Jump to: Site #1: IOPs 02-04 & 08-11

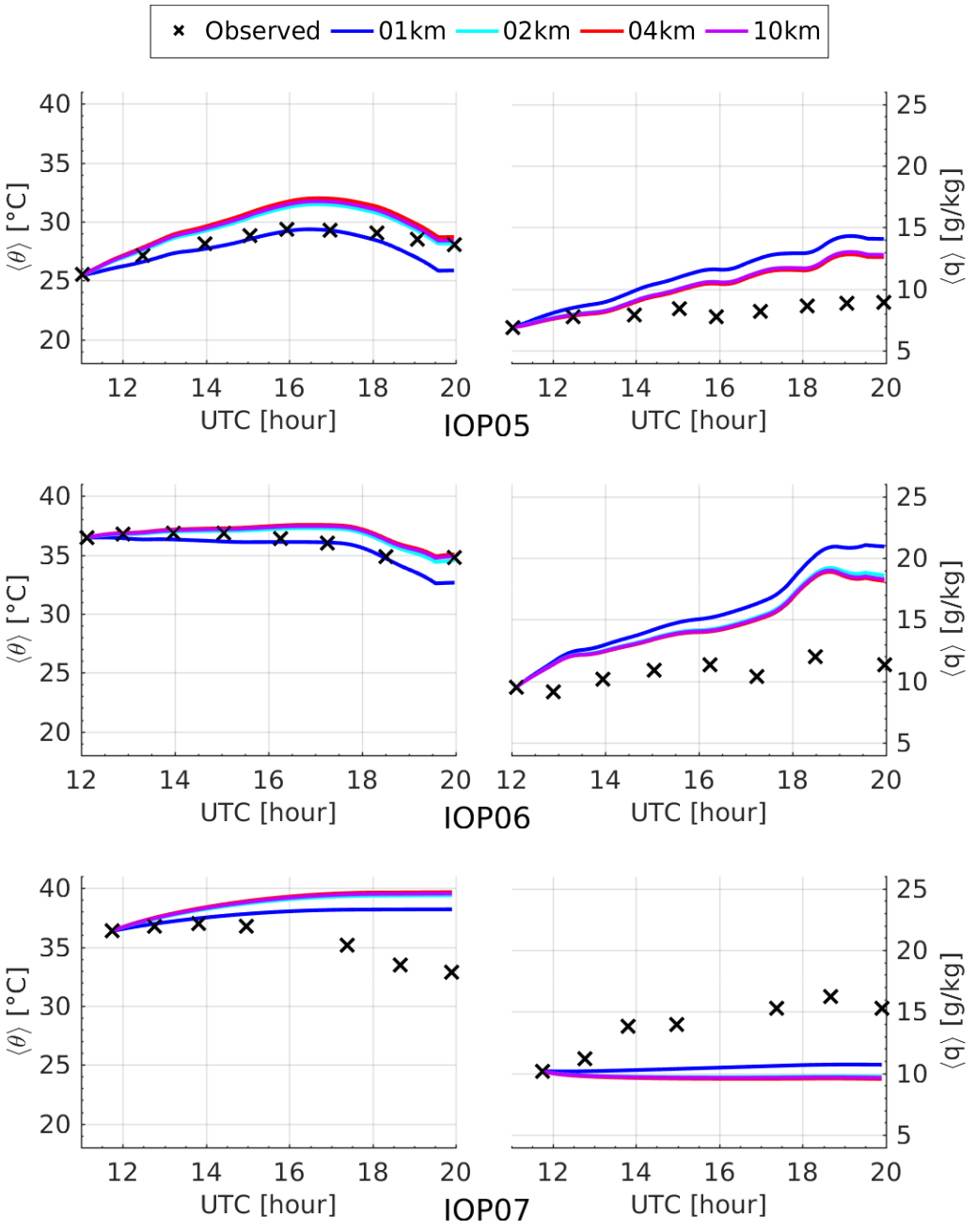

Figure F.4: Jump to: Site #2: IOPs 05-07

Bibliography

Båserud, L. (2013), Investigating the potential of turbulence measurements with the RPAS SUMO, Master's thesis, Geophyical Institute, University of Bergen, Norway.

Blay-Carreras, E. (2014), Transisitonal Periods of the Atmospheric Boundary Layer, Phd thesis, Universitat Politècnica de Catalunya.

Blay-Carreras, E., Pino, D., Vilà-Guerau De Arellano, J., Van De Boer, A., De Coster, O., Darbieu, C., Hartogensis, O., Lohou, F., Lothon, M. & Pietersen, H. (2014), 'Role of the residual layer and large-scale subsidence on the development and evolution of the convective boundary layer', *Atmospheric Chemistry and Physics* **14**(9), 4515–4530.

Burba, G. & Anderson, D. (2010), *A Brief Practical Guide to Eddy Covariance Flux Measurements: Principles and Workflow Examples for Scientific and Industrial Applications*, LI-COR Biosciences.

Couvreux, F. (2012), 'Dataset Edition: estimation of boundary-layer height from SUMO profiles'.
URL: *http://bllast.sedoo.fr/database/source/displayDataset.php?repertoire=../data/AUTH/Boundary-layer_height/In_Situ/&fichier=estimationofboundary-layerheightfromSUMOprofiles.xml*

Cuxart, J., Wrenger, B., Martínez-Villagrasa, D., Reuder, J., Jonassen, M. O., Jiménez, M. A., Lothon, M., Lohou, F., Hartogensis, O., Dünnermann, J., Conangla, L. & Garai, A. (2016), 'Estimation of the advection effects induced by surface heterogeneities in the surface energy budget', *Atmospheric Chemistry and Physics* **16**(14), 9489–9504.

Hansen, F. V. (1993), Surface roughness lengths, Technical Report August, DTIC Document.

Hartmann, D. L. (1994), *Global Physical Climatology*, first edn, ACADEMIC PRESS.

Hartogensis, O. (2015*a*), BLLAST Flux maps, *in* 'BLLAST Workshop - Barcelona', Barcelona, pp. 1–32.
URL: *http://bllast.sedoo.fr/database/source/displayDataset.php?repertoire=../data/AUTH/Area-averaged_surface_flux_maps/&fichier=Documentation.xml*

Hartogensis, O. (2015*b*), 'Surface flux maps'.
URL: *http://bllast.sedoo.fr/database/source/displayDataset.php?repertoire=../data/AUTH/Area-averaged_surface_flux_maps/&fichier=Surfacefluxmaps.xml*

Jiménez, M. A. (2016), Large-scale temperature and humidity advections seen by the MesoNH model (IOPs 3,5,6,9,10,11).

Jiménez, M. A. & Cuxart, J. (2014), 'A study of the nocturnal flows generated in the north side of the Pyrenees', *Atmospheric Research* **145-146**, 244–254.

Jonassen, M. O. (2008), The Small Unmanned Meteorological Observer (SUMO) - Characterization and test of a new measurement system for at-

mospheric boundary layer research, Master's thesis, Geophyical Institute, University of Bergen, Norway.

Lothon, M., Lohou, F., Pino, D., Couvreux, F., Pardyjak, E. R., Reuder, J., Vilà-Guerau De Arellano, J., Durand, P., Hartogensis, O., Legain, D., Augustin, P., Gioli, B., Lenschow, D. H., Faloona, I., Yagüe, C., Alexander, D. C., Angevine, W. M., Bargain, E., Barrié, J., Bazile, E., Bezombes, Y., Blay-Carreras, E., Van De Boer, A., Boichard, J. L., Bourdon, A., Butet, A., Campistron, B., De Coster, O., Cuxart, J., Dabas, A., Darbieu, C., Deboudt, K., Delbarre, H., Derrien, S., Flament, P., Fourmentin, M., Garai, A., Gibert, F., Graf, A., Groebner, J., Guichard, F., Jiménez, M. A., Jonassen, M., Van Den Kroonenberg, A., Magliulo, V., Martin, S., Martinez, D., Mastrorillo, L., Moene, A. F., Molinos, F., Moulin, E., Pietersen, H. P., Piguet, B., Pique, E., Román-Cascón, C., Rufin-Soler, C., Saïd, F., Sastre-Marugán, M., Seity, Y., Steeneveld, G. J., Toscano, P., Traullé, O., Tzanos, D., Wacker, S., Wildmann, N. & Zaldei, A. (2014), 'The BLLAST field experiment: Boundary-Layer late afternoon and sunset turbulence', *Atmospheric Chemistry and Physics* **14**(20), 10931–10960.

Mayer, S., Hattenberger, G., Brisset, P., Jonassen, M. & Reuder, J. (2012), 'A 'no-flow-sensor' Wind Estimation Algorithm for Unmanned Aerial Systems', *International Journal of Micro Air Vehicles* **4**(1).

Moeng, C.-H. (1984), 'A Large-Eddy-Simulation Model for the Study of Planetary Boundary-Layer Turbulence', *Journal of the Atmospheric Sciences* **41**(13), 2052–2062.

Moeng, C. H. & Sullivan, P. P. (2015), NUMERICAL MODELS: Large-Eddy Simulation, *in* G. R. North, J. Pyle & F. Zhang, eds, 'Encyclopedia of Atmospheric Sciences (Second Edition)', second edi edn, Academic Press, Oxford, pp. 232–240.

Moin, P. & Mahesh, K. (1998), 'DIRECT NUMERICAL SIMULATION: A Tool in Turbulence Research', *Annual Review of Fluid Mechanics* **30**(1), 539–578.

Nilsson, E. (2011), Synoptic weather analysis of every day during BLLAST experiment, Technical report.
URL: *http://bllast.sedoo.fr/documents/*

Pietersen, H. P., De Arellano Vilà-Guerau, J., Augustin, P., Van De Boer, A., De Coster, O., Delbarre, H., Durand, P., Fourmentin, M., Gioli, B., Hartogensis, O., Lohou, F., Lothon, M., Ouwersloot, H. G., Pino, D. & Reuder, J. (2015), 'Study of a prototypical convective boundary layer observed during BLLAST: Contributions by large-scale forcings', *Atmospheric Chemistry and Physics* **15**(8), 4241–4257.

Pino, D., de Arellano, J. V. G. & Kim, S. W. (2006), 'Representing sheared convective boundary layer by zeroth- and first-order-jump mixed-layer models: Large-eddy simulation verification', *Journal of Applied Meteorology and Climatology* **45**(9), 1224–1243.

Rai, M. M. & Moin, P. (1993), 'Direct Numerical Simulation of Transition and Turbulence in a Spatially Evolving Boundary Layer', *Journal of Computational Physics* **109**(2), 169–192.

Reuder, J., Båserud, L., Jonassen, M. O., Kral, S. T. & Müller, M. (2016), 'Exploring the potential of the RPA system SUMO for multipurpose boundary-layer missions during the BLLAST campaign', *Atmospheric Measurement Techniques* **9**(6), 2675–2688.

Reuder, J., Brisset, P., Jonassen, M., Müller, M. & Mayer, S. (2009), 'The Small Unmanned Meteorological Observer SUMO: A new tool for atmo-

spheric boundary layer research', *Meteorologische Zeitschrift* **18**(2), 141–147.

Reuder, J., Jonassen, M. & Ólafsson, H. (2012), 'The Small Unmanned Meteorological Observer SUMO: Recent developments and applications of a micro-UAS for atmospheric boundary layer research', *Acta Geophysica* **60**(5), 1454–1473.

Schuepp, P. H., Leclerc, M. Y., MacPherson, J. I. & Desjardins, R. L. (1990), 'Footprint prediction of scalar fluxes from analytical solutions of the diffusion equation', *Boundary-Layer Meteorology* **50**(1-4), 355–373.

Stull, R. B. (1988), *An Introduction to Boundary Layer Meteorology*, Springer Netherlands, Dordrecht.

Tennekes, H. (1973), 'A Model for the Dynamics of the Inversion Above a Convective Boundary Layer', *Journal of the Atmospheric Sciences* **30**(4), 558–567.

Tennekes, H. & Driedonks, A. G. M. (1981), 'Basic entrainment equations for the atmospheric boundary layer', *Boundary-Layer Meteorology* **20**(4), 515–531.

van Heerwaarden, C. C., Mellado, J. P. & de Lozar, A. (2014), 'Scaling Laws for the Heterogeneously Heated Free Convective Boundary Layer', *Journal Of The Atmospheric Sciences* **71**(11), 3975–4000.

Vilà-Guerau de Arellano, J., van Heerwaarden, C. C., van Stratum, B. J. & van den Dries, K. (2015), *Atmospheric Boundary Layer: Integrating Chemistry and Land Interactions*, Cambridge University Press.

Wilson, J. D. (2015), 'Computing the Flux Footprint', *Boundary-Layer Meteorology* **156**(1), 1–14.

Zhang, Y., Gao, Z., Li, D., Li, Y., Zhang, N., Zhao, X. & Chen, J. (2014), 'On the computation of planetary boundary-layer height using the bulk Richardson number method', *Geoscientific Model Development* **7**(6), 2599–2611.